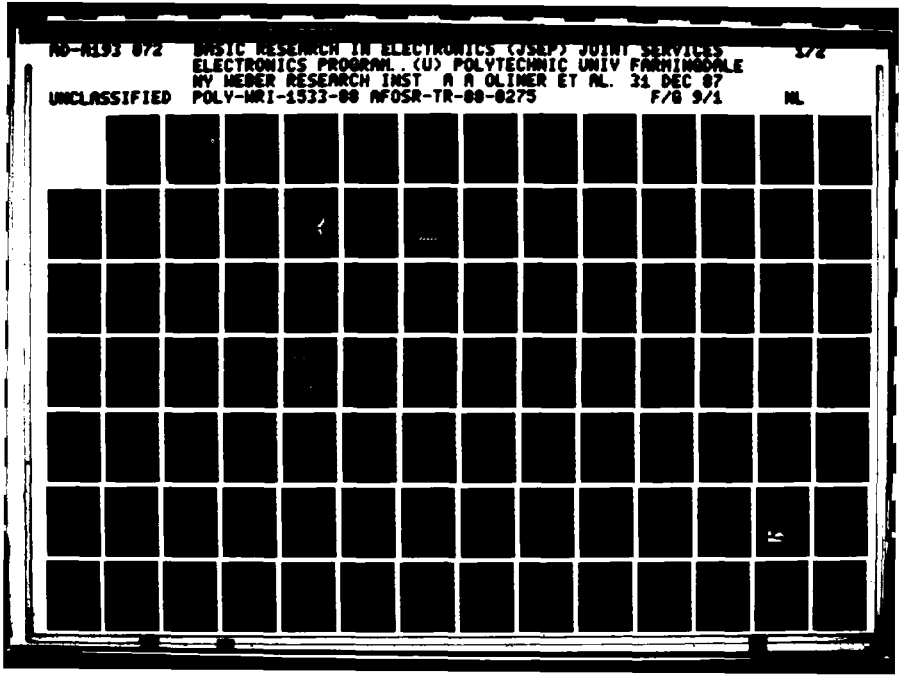
AD-A193 872 BASIC RESEARCH IN ELECTRONICS (JSEP) JOINT SERVICES 1/2
ELECTRONICS PROGRAM..(U) POLYTECHNIC UNIV FARMINGDALE
NY WEBER RESEARCH INST A A OLINER ET AL. 31 DEC 87
UNCLASSIFIED POLY-WRI-1533-88 AFOSR-TR-88-0275 F/G 9/1 NL

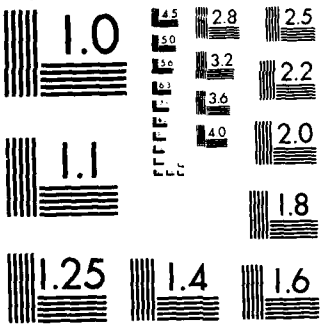

(1)

AFOSR-TR-88-0275

31 December 1987
POLY-WRI-1533-88

ANNUAL REPORT
on
BASIC RESEARCH IN ELECTRONICS (JSEP)

CONTRACT NO. F49620-85-C-0078
JANUARY 1, 1987 TO DECEMBER 31, 1987

POLYTECHNIC UNIVERSITY
WEBER RESEARCH INSTITUTE
FARMINGDALE, NEW YORK 11735

UNCLASSIFIED
SECURITY CLASSIFICATION OF THIS PAGE

ADA192072

REPORT DOCUMENTATION PAGE

Form Approved OMB No. 0704-0188

1a. REPORT SECURITY CLASSIFICATION	1b. RESTRICTIVE MARKINGS
2a. SECURITY CLASSIFICATION AUTHORITY: Unclassified	3. DISTRIBUTION/AVAILABILITY OF REPORT: Approved for public release; distribution unlimited.
2b. DECLASSIFICATION/DOWNGRADING SCHEDULE	
4. PERFORMING ORGANIZATION REPORT NUMBER(S): POLY-WRI-1533-88	5. MONITORING ORGANIZATION REPORT NUMBER(S): AFOSR-TR-88-0275
6a. NAME OF PERFORMING ORGANIZATION: Weber Research Institute, Polytechnic University / 6b. OFFICE SYMBOL (If applicable)	7a. NAME OF MONITORING ORGANIZATION: Air Force Office of Scientific Research/NE
6c. ADDRESS (City, State, and ZIP Code): Route 110, Farmingdale, New York 11735	7b. ADDRESS (City, State, and ZIP Code): Bolling Air Force Base, Washington, DC 20332
8a. NAME OF FUNDING/SPONSORING ORGANIZATION: Air Force Office of Scientific Research/NE / 8b. OFFICE SYMBOL (If applicable): NE	9. PROCUREMENT INSTRUMENT IDENTIFICATION NUMBER: F49620-85-C-0078
8c. ADDRESS (City, State, and ZIP Code): Bolling Air Force Base, Washington, D. C. 20332	10. SOURCE OF FUNDING NUMBERS: PROGRAM ELEMENT NO. 61102F / PROJECT NO. 2301/~~A9~~ / TASK NO. A1 / WORK UNIT ACCESSION NO.
11. TITLE (Include Security Classification): Basic Research in Electronics (JSEP) (Unclassified)	
12. PERSONAL AUTHOR(S): Arthur A. Oliner and Erich E. Kunhardt, Co-Directors	
13a. TYPE OF REPORT: ANNUAL REPORT / 13b. TIME COVERED: FROM Jan. 1987 TO Dec. 1987 / 14. DATE OF REPORT (Year, Month, Day): 87 December 31 / 15. PAGE COUNT	
16. SUPPLEMENTARY NOTATION	

17. COSATI CODES			18. SUBJECT TERMS (Continue on reverse if necessary and identify by block number)
FIELD	GROUP	SUB-GROUP	Electromagnetics, microwaves, millimeter waves, waveguides and antennas, optics, x-rays, solid state interactions and materials, information electronics, image restoration.

19. ABSTRACT (Continue on reverse if necessary and identify by block number)

This report presents a summary of the scientific progress and accomplishments on research projects by the Joint Services Electronics Program (JSEP) for the contract periods from 1 January 1987 through 31 December 1987. It does not contain information regarding accomplishments on research projects funded in other ways.

The Joint Services Electronics Program at the Polytechnic is the core of interdisciplinary research in electronics encompassing programs in the Department of Electrical Engineering, Physics, and Chemistry under the aegis of the Weber Research Institute. The research encompassed by this program is grouped under three broad categories: Electromagnetics, Solid State Electronics, and Information Electronics. The detailed projects (research units) comprising the complete program are listed in the Table of Contents.

20. DISTRIBUTION/AVAILABILITY OF ABSTRACT: ☒ UNCLASSIFIED/UNLIMITED ☐ SAME AS RPT. ☐ DTIC USERS	21. ABSTRACT SECURITY CLASSIFICATION: Unclassified
22a. NAME OF RESPONSIBLE INDIVIDUAL: ~~Erich E. Kunhardt, Director~~	22b. TELEPHONE (Include Area Code): ~~516/260-4250~~ / 22c. OFFICE SYMBOL: NE

DD Form 1473, JUN 86 — Previous editions are obsolete. SECURITY CLASSIFICATION OF THIS PAGE UNCLASSIFIED

Dr Wittman 202 767-4984

TABLE OF CONTENTS

DIRECTOR'S OVERVIEW

This report presents a summary of the scientific progress and accomplishments on research projects funded by the Joint Services Electronics Program (JSEP) for the contract period from 1 January 1987 through 31 December 1987. It does not contain information regarding accomplishments on research projects funded in other ways.

The Joint Services Electronics Program at Polytechnic University is the core of interdisciplinary research in electronics encompassing programs in the Departments of Electrical Engineering, Physics and Chemistry under the aegis of the Weber Research Institute. The research encompassed by this program is grouped into three broad categories: Electromagnetics, Solid State Electronics and Information Electronics. The detailed projects (research units) comprising the complete program are listed in the Table of Contents.

Following our previous practice, Section 2 of every research unit contains a short *summary* of the recent progress. Further details regarding that progress are contained in Section 3, State of the Art and Progress Details.

Each of the research units described in this report is designated, for example, as EM7-1, SS7-1 or IE7-1, corresponding to the category, year (1987), and number within the category. These numbers follow the numbers given in our annual proposal dated December 31, 1986, with two exceptions. In accord with instructions of the Technical Coordinating Committee we phased out the Information Electronics unit referenced in the proposal as IE7-1 before the start of the period covered by this report. Consequently, we have renumbered the other two Information Electronics units. The numbers were reduced by one: the proposed IE7-2 is reported here as IE7-1; and the proposed IE7-3 is reported here as IE7-2.

Following this Overview, we present the *Report on Significant Scientific Accomplishments,* which highlights a few of our more important contributions this year.

REPORT ON SIGNIFICANT ACCOMPLISHMENTS

(December 31, 1987)

1. Focus Wave Mode Causality Dilemma

   Professors E. Heyman and L.B. Felsen
   Unit EM7-3

2. Conductor-Backed Lines: Dangers and Full Wave Analysis

   Professor A.A. Oliner
   Unit EM7-1

3. Optical Multistability of Anistropic Microparticles

   Professor K.M. Leung
   Unit SS7-2

1. FOCUS WAVE MODE CAUSALITY DILEMMA

Professors E. Heyman and L. B. Felsen

Efficient transfer of electromagnetic energy in space has motivated the study of time-dependent wave fields that propagate in missile-like fashion without diffusion or dispersion. Among new wave functions addressing these objectives, the focus wave modes (FWM) have received major attention [1,2]. These wave objects are exact solutions of the time-dependent source-free field equations, and they have infinite energy. They travel through space at the speed of light with undistorted profiles that match the focal region of a well-collimated beam. These features are highly desirable for directed energy transfer.

A major question has been whether and how the FWM can be excited by causal source distributions in a physical aperture. Through several alternative studies involving Green's function and spectral techniques, we have been able to show that backward propagating wave phenomena are dominant in the synthesis of a forward propagating FWM [3,4]. While this behavior is compatible with the source-free regime, it can not be established by causal initial conditions in an aperture plane. This important conclusion has led to a reassessment of the role, if any, to be played by the FWM in physical pulsed beam propagation.

REFERENCES

1. J. N. Brittingham, "Focus Wave Modes in Homogeneous Maxwell's Equations: Transverse Electric Mode," J. Appl. Phys., Vol. 54, 1983, pp. 1179-1189.
2 R. W. Ziolkowski, "Exact Solutions of the Wave Equation with Complex Source Locations," J. Math. Phys., Vol. 26, 1985, pp 861-863.
3. E. Heyman, B. Z. Steinberg and L. B. Felsen, "Spectral Analysis of Focus Wave Modes," J. Opt. Soc. Am. A, Vol. 4, 1987, pp. 2081-2091.
4 E. Heyman, "Focus Wave Modes: A Dilemma with Causality," submitted to IEEE Trans. Antenna & Propagat

2. CONDUCTOR-BACKED LINES: DANGERS AND FULL WAVE ANALYSIS

Professor Arthur A. Oliner

In millimeter-wave integrated circuits and in monolithic microwave circuits (MMICs), it is a common complaint that components that work well separately fail when combined together. The most common cause of such failure is that unexpected and unwanted radiation is produced that results in cross talk and other deleterious effects. These ill effects occur in pronounced fashion when certain transmission lines, such as slot lines and coplanar waveguides, are

conductor backed.

It is very tempting to introduce such conductor backing because such backing has many advantages, such as a lower Z_o, reduced dispersion, better mechanical strength, and so on. Raytheon is planning to employ conductor-backed coplanar waveguide in its MMICs because of easier fabrication and lower cost, in addition to these advantages. However, there are also certain important dangers, or serious potential problems, that are introduced by the use of conductor backing. They include leakage of power into surface waves or into the dielectric region between the plates, unexpected cross talk, significant alteration of the guide wavelength, and unexpected or unwanted coupling to neighboring lines.

These possible unpleasant consequences are generally not recognized or discussed in the literature, except for a single recent paper which provided no quantitative information. The present study has developed two different full-wave analyses for the class of conductor-backed lines, and has applied them to slot lines as an important example. A set of measurements was also taken on a particular conductor-backed slot line structure. The results obtained show that the numbers obtained from the two different theoretical approaches agree well with each other and with the measurements taken.

Several very interesting effects were found, including the fact that the power leakage rate is rather high. The results verify the concern expressed above regarding the potential dangers in the use of conductor-backed lines, and the study itself provides the first quantitative information regarding the seriousness of these effects.

3. OPTICAL MULTISTABILITY OF ANISTROPIC MICROPARTICLES

Professor K.M. Leung

It was shown in our previous work that a Rayleigh-sized spherical microparticle can exhibit optical bistable behavior and can also function as an optical transistor. In order to enhance the functionality and capabilities of microparticle photonics, it is important to investigate more complex microparticle components. For this purpose, we have recently extended our work from spherical to spheroidal microparticles.

In comparison with a spherical particle, a spheroidal particle has a few extra physical characteristics, such as the particle shape and the particle orientation with respect to the polarization of the incident field. As a result, it is capable of exhibiting a richer class of intrinsically nonlinear phenomena. We find that besides the usual bistable behavior, a total of five different types of tristable behaviors are possible, depending on the frequency of the incident light and the particle shape and orientation.

SECTION I:
ELECTROMAGNETICS

SECTION I: ELECTROMAGNETICS

A. NEW PHYSICAL EFFECTS INVOLVING OPEN DIELECTRIC STRUCTURES

Professors A.A. Oliner and M. Guglielmi

Unit EM7-1

1. OBJECTIVE(S)

This study is concerned with guiding, radiating and scattering effects involving open dielectric structures. The majority of electromagnetic waveguides are open and involve dielectric materials, and they therefore fall into this category. Certainly, most waveguides for millimeter-wave integrated circuits and all waveguides for integrated optics are in this category. Moreover, problems such as cross talk, leakage, and low Q, that arise in microwave integrated circuits, and coupling effects and blind spots that appear in many phased-array antennas, are due to the presence of dielectric material on those open structures. It should be clear, therefore, that these basic studies have important practical implications.

Before our investigation, almost all of the published literature on these topics involved a surface wave incident on a dielectric junction or grating at normal incidence, where the resulting boundary-value problem is two-dimensional, and TE and TM modes do not couple to each other. In many open dielectric waveguides and antennas for millimeter-wave integrated circuits and for integrated optics, however, the surface wave is obliquely incident. The boundary-value problems then change from the scalar, two-dimensional ones to vector three-dimensional ones, and the TE and TM modes no longer remain independent but are coupled together. The vector nature of these problems introduces new mathematical challenges, but, more interestingly, the mode coupling produces a rich variety of interesting and sometimes unexpected new physical effects. In our studies so far, we have found that a number of such effects arise in potentially important guiding and radiating structures, either leading to possible performance problems or providing new opportunities if those effects can be properly utilized.

We are continuing to explore these physical effects on old and new types of dielectric structure. It is, of course, necessary to first obtain the appropriate mathematical solutions; those solutions, or the approaches used to obtain them, are often of interest in themselves. We then examine the physical consequences of those solutions, and, where appropriate, assess their implications for device performance in millimeter-wave integrated circuits and antennas and in integrated optics.

2. SUMMARY OF RECENT PROGRESS

Major effort during the past year was placed on six topics, three of which are related to aspects of an important basic antenna type for millimeter waves. The three related aspects of the antenna investigation are described first, and they are grouped together under topic A in section 3. The antenna is the dielectric image guide leaky-wave antenna loaded by periodic metal strips, for which many measurements have been presented in the literature but for which no theory was previously available from which the antenna could be designed. The three related aspects under study, and discussed under section 3, are first, a detailed parametric analysis of the antenna behavior, second, a novel optimization procedure for tapering the antenna to control the sidelobes, and third, a new solution for scattering by a multimode grating that yields arbitrary accuracy. The other three topics are: a new type of two-dimensional scanning array for millimeter waves, a leaky-wave analysis of a high-gain printed antenna configuration that employs a superstrate, and a study of conductor-backed slot line for MMIC and microwave integrated circuits that provides full-wave analyses for the first time.

For the first topic, that of a detailed parametric analysis of the behavior of the dielectric image guide leaky-wave antenna, the phase and leakage constants of the leaky structure were determined as a function of frequency, dielectric constant, and geometric dimensions. From the trends in behavior, we are now able to design antennas to meet specified performance characteristics, something certainly not available previously. As an example, we present in section 3 the curve obtained when we wish to optimize the bandwidth over which the beam width remains constant.

The second topic involves a new method for optimizing the taper in the aperture distribution of the leaky-wave antenna studied above in order to control the sidelobe level in a specified way. As a challenging example, we chose a Taylor distribution corresponding to sidelobes which are all 35 dB below the main beam maximum. The problem is to specify the taper in the dimensions that satisfied the Taylor distribution requirement, but the difficulty is that only the width and location of the metal strips are accessible parameters. The novel design procedure we developed changes both the strip widths and the strip period *simultaneously* to accomplish this purpose. Since the strips can be deposited lithographically, or etched away, the new procedure allows one to design a mask that accomplishes the geometrical arrangement all at one time. The design procedure and the fabrication process are therefore practical for use at millimeter wavelengths.

The third topic is only indirectly related to the antenna itself, since it involves just a constituent of the antenna, namely, the metal grating placed on an air-dielectric interface. As a part of the analysis of the antenna, we had derived a solution for plane-wave scattering by such a grating. We are currently in the process of deriving an alternative solution, which involves a different series expansion technique and has the promise of yielding arbitrary accuracy. The earlier solution utilized a small-argument expansion.

The next topic actually makes use of the dual to the solution referred to above, that is, the solution previously obtained for plane-wave scattering by the metal-strip grating on an air-dielectric interface, but for the *opposite* incident polarization. This solution forms part of the overall solution for a new type of two-dimensional scanning antenna, with leaky-wave scan in elevation and phase-shift scan in the cross plane. The antenna possesses several key advantages: no grating lobes, no blind spots, and no cross polarization. The use of a periodic structure (grating) permits a wider scan range, as discussed in section 3.

The fifth topic relates to a superstrate-substrate structure that permits a simple printed-circuit antenna to radiate a narrow beam that scans with frequency. The new feature here is that we show that this performance can be elegantly described in terms of leaky waves. It is first shown that the leaky-wave approach reproduces all the asymptotic expressions and numerical values for the far field obtained by means of a straightforward field approach, but derived in a simpler way, using leaky waves. More important, however, is that the leaky-wave approach furnishes insight into the physical processes involved, and also provides new practical information, as explained in section 3.

The sixth and last topic applies to a set of potentially serious problems that arise in MMICs and microwave integrated circuits. Conductor backing has been introduced into such circuits when transmission lines such as slot line and coplanar waveguide are used, because of the many advantages that are provided. There are, on the other hand, possible unpleasant and unexpected consequences to their use that seem not to be fully recognized or understood. In addition, there are no full-wave analyses available that permit us to analyze quantitatively how serious these effects may be. Some of these potentially serious effects are described in section 3. We have developed two full-wave theoretical approaches, one purely numerical and the other in network form and analytical in nature, that agree well with each other and with measurements in a special case. These theoretical approaches are currently being employed to determine quantitatively the physical behavior corresponding to some of these potential surprises in specific cases in which either the slot line conductors or the backing conductor are of infinite or finite lateral extent.

3. STATE OF THE ART AND PROGRESS DETAILS

A. Dielectric Image Guide Leaky-Wave Antennas Loaded by Periodic Metal Strips.

In last year's Annual Report we presented a simple and accurate transverse equivalent network for the class of leaky-wave antennas shown in Fig. 1.

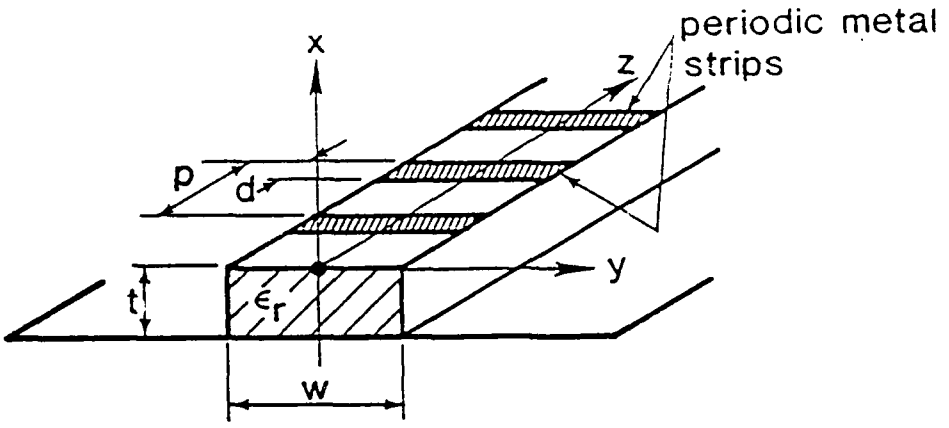

Fig. 1. Leaky-wave antenna consisting of a periodic array of metal strips placed on a dielectric image guide.

The theory developed allowed us to understand its basic behavior and to exert a great degree of control over its performance, showing for the first time how this class of antennas can be effectively designed to achieve desired characteristics.

The details of the theory developed and some of the results obtained were presented at a conference [1], at which the paper was awarded the Second Prize in the 1987 U.R.S.I. National Student Paper Prize Competition. Additional results and some applications of the theory developed were also presented at a later conference [2].

In the past year, our research efforts in connection with this class of antennas have been aimed in three main directions. First, we have performed a detailed parametric analysis of the antenna behavior when the grating discontinuity is uniform along the z direction of Fig. 1. Second, we have studied suitable non-uniform (tapered) grating geometries to achieve control over the sidelobe levels. Finally, we have begun the development of a new solution for the description of the grating discontinuity that will allow us to compute to an arbitrary degree of accuracy the elements involved in its network description.

(1) Description of the Parametric Analysis

The first step in the parametric analysis of this class of antennas is the derivation of a suitable set of constraints that can facilitate the initial choice of the structural parameters. Keeping in mind that we want to have only one main radiation lobe in the air region in Fig. 1, we have derived the approximate expressions shown in Table 1.

	Backward Quadrant	Forward Quadrant
Single Radiating Space Harmonic	$\epsilon_r > 1$	$\epsilon_r > q$
Single Mode in the Dielectric Layer	$\frac{t}{p} \leq \frac{\sqrt{\epsilon_r}}{2\sqrt{\epsilon_r - 1}}$	$\frac{t}{p} \leq \frac{\sqrt{\epsilon_r - 1}}{\sqrt{\epsilon_r - 1}}$

Table 1. The expressions shown can be used to choose a set of parameters so that the antenna in Fig. 1 has only one main radiation lobe.

Next, choosing a set of parameters appropriate for operation in the backward quadrant, we have obtained the antenna dispersion curve shown in Fig. 2. We then perturbed the structural parameters one at a time, observing that the real part of the complex propagation constant remains essentially unchanged while the imaginary part, the leakage rate α, can be strongly modified. The results obtained can be summarized as follows:

a. Increasing the obstacle size d/p generally increases the leakage rate but its frequency dependence remains essentially the same.

b. Decreasing the thickness d of the dielectric layer produces a twofold effect: the curve for α, the leakage rate, "flattens" and its average value increases.

c. Decreasing the value of the dielectric constant ϵ_r results in a generally "milder" leakage behavior.

As a result of the accurate parametric analysis performed, we are now able to design antennas that meet specified radiation characteristics. As an example, we show in Fig. 3 the results obtained when we optimize the antenna behavior for a constant half-power beamwidth over a maximized scan range.

(2) Optimized Aperture Distribution for Sidelobe Control

The antennas discussed in the previous section are uniform in the longitudinal direction (z direction in Fig. 1). As a result of this uniformity the antenna aperture distribution is exponentially decaying, and therefore not appropriate for sidelobe control. To achieve a specified sidelobe characteristic one requires a tapered aperture distribution. This means that the obstacle size d/p must be varied along the z direction in Fig. 1.

The theory that we have developed for this class of antennas allows us to design such tapered geometries using the assumption that the structure can be considered locally uniform. This assumption, however, can be introduced only

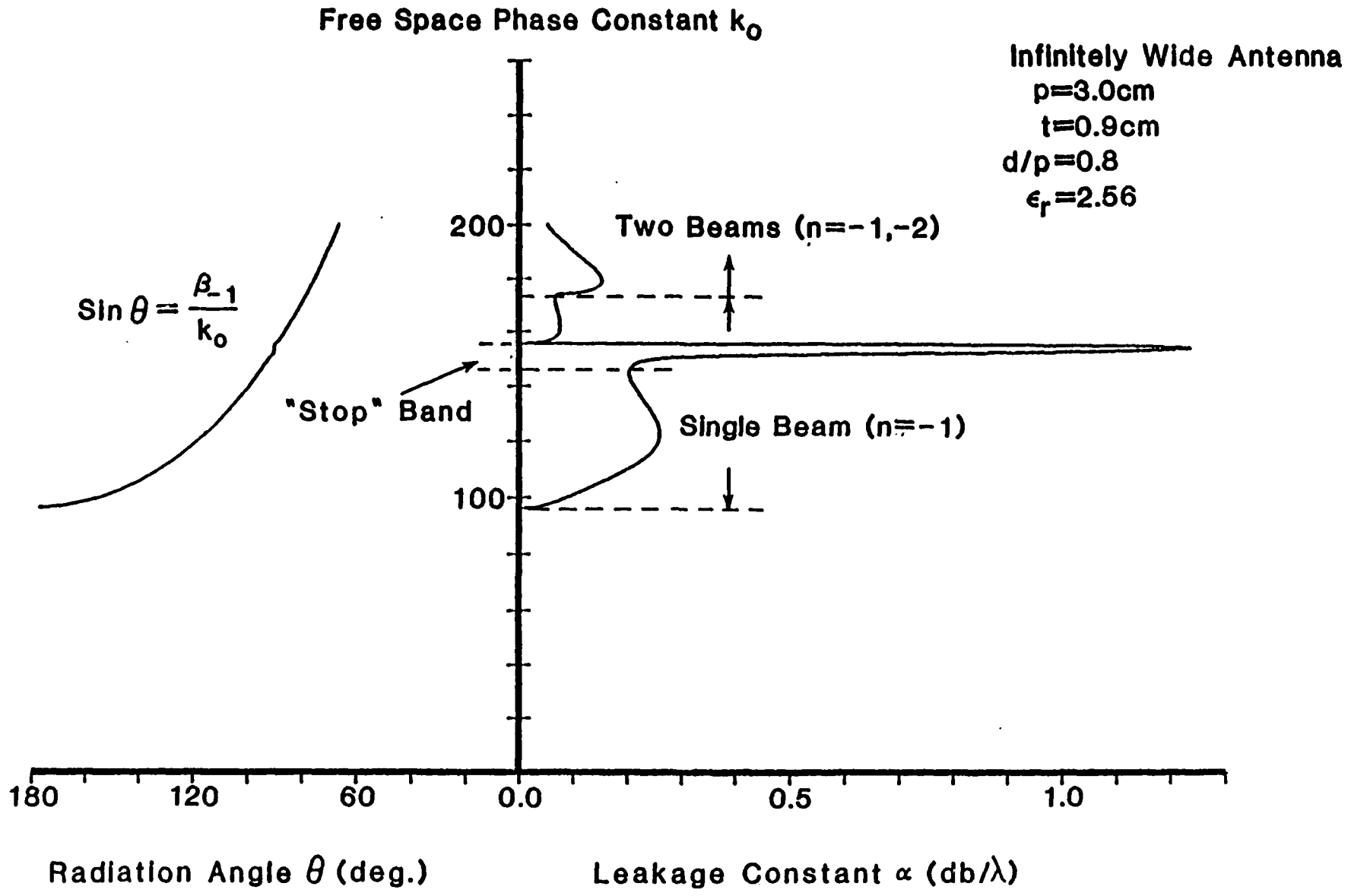

Fig. 2. Typical dispersion curve for the class of antennas shown in Fig. 1. The x axis to the left represents the real part of the complex propagation constant in terms of the angle of maximum radiation, while the x axis to the right represents the leakage constant α in dB per wavelength. The vertical axis represents the free space phase constant k_o.

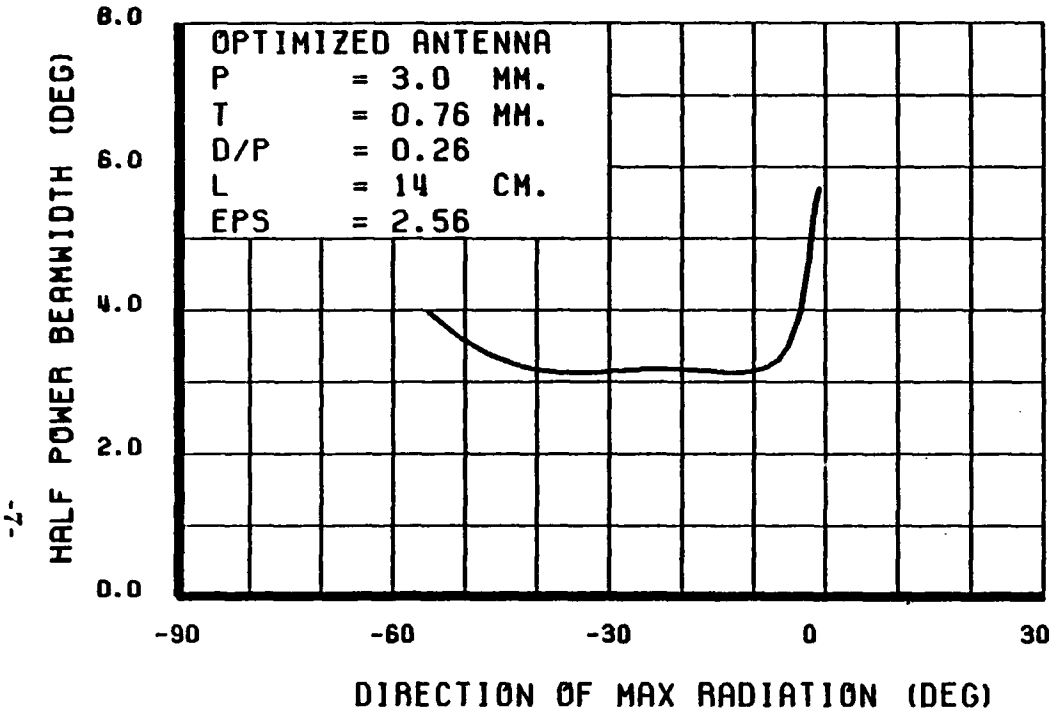

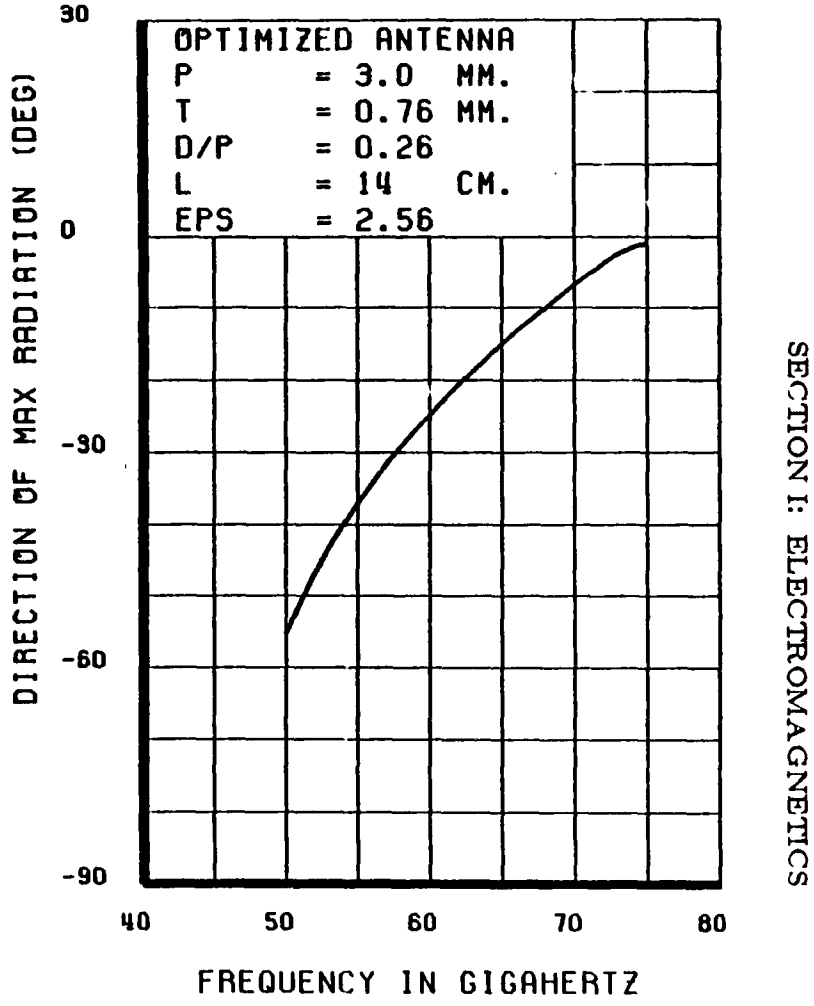

Fig. 3. The theory developed permits a great degree of control over the antenna performance. In this figure, we show the results obtained when we maximize the scan range over which the beamwidth is maintained constant.

if the rate of change of d/p along the z direction is small. In addition, changing the obstacle size d/p not only affects the leakage rate α but also the phase constant β_o of the structure. As a result, different sections of the antenna would have different phase constants and would radiate in slightly different directions, thereby degrading the overall antenna performance.

It is therefore evident that changing d/p alone is not sufficient for this type of optimization. A much better result is obtained if one varies at the same time both the obstacle size and the distance between adjacent metal strips, thereby obtaining the desired antenna in terms of a locally uniform and periodic structure.

As an example of this procedure, we have synthesized the required antenna geometry corresponding to the Taylor aperture distribution appropriate to a 35 dB sidelobe level. Figure 4 presents the radiation pattern thus obtained.

One feature that deserves more attention is the actual practical implementation of the required taper. Once a given aperture distribution is specified, the theory developed yields the width of each metal strip and the distance between adjacent strips for the whole structure. A mask can then be realized so that the whole system of radiating metal strips can be readily deposited on the top surface of the basic guiding structure. This feature is particularly attractive at millimeter wavelengths where, due to the reduced dimensions, mechanical simplicity is an important issue.

The work in connection with this optimization procedure has been done in collaboration with Professor J. Encinar, who visited Polytechnic University as a NATO Postdoctoral Fellow from Spain during 1987.

(3) Scattering by a Multimode Grating at a Dielectric Interface: A New Solution that Yields Arbitrary Accuracy

In a recent Ph.D. thesis [3], we developed a network description for a II2I! multimode metal-strip grating at a dielectric interface that is valid in the small-argument limit. This solution was obtained by solving a Cauchy singular integral equation of the type shown in (1).

$$f_n(\alpha\xi) = \frac{1}{\pi} \int_{-1}^{1} \frac{G_n(\alpha\xi')}{\xi - \xi'} d\xi' \qquad (1)$$

where $f_n(\alpha\xi)$ is known and $G_n(\alpha\xi')$ is the unknown. To obtain an explicit expression for $G_n(\alpha\xi')$ we expanded the known function $f_n(\alpha\xi)$ in a Taylor series with respect to a relevant "small" parameter α, obtaining

$$f_n(\alpha\xi) \cong a_o(n) + a_1(n)\alpha\xi + a_2(n)(\alpha\xi)^2 + \cdots \qquad (2)$$

Equation (2) was then used to obtain the analytical solution of (1). This procedure led in a few simple steps to an approximate closed form expression for the unknown $G_n(\alpha\xi)$ but had a limitation. When the number of terms

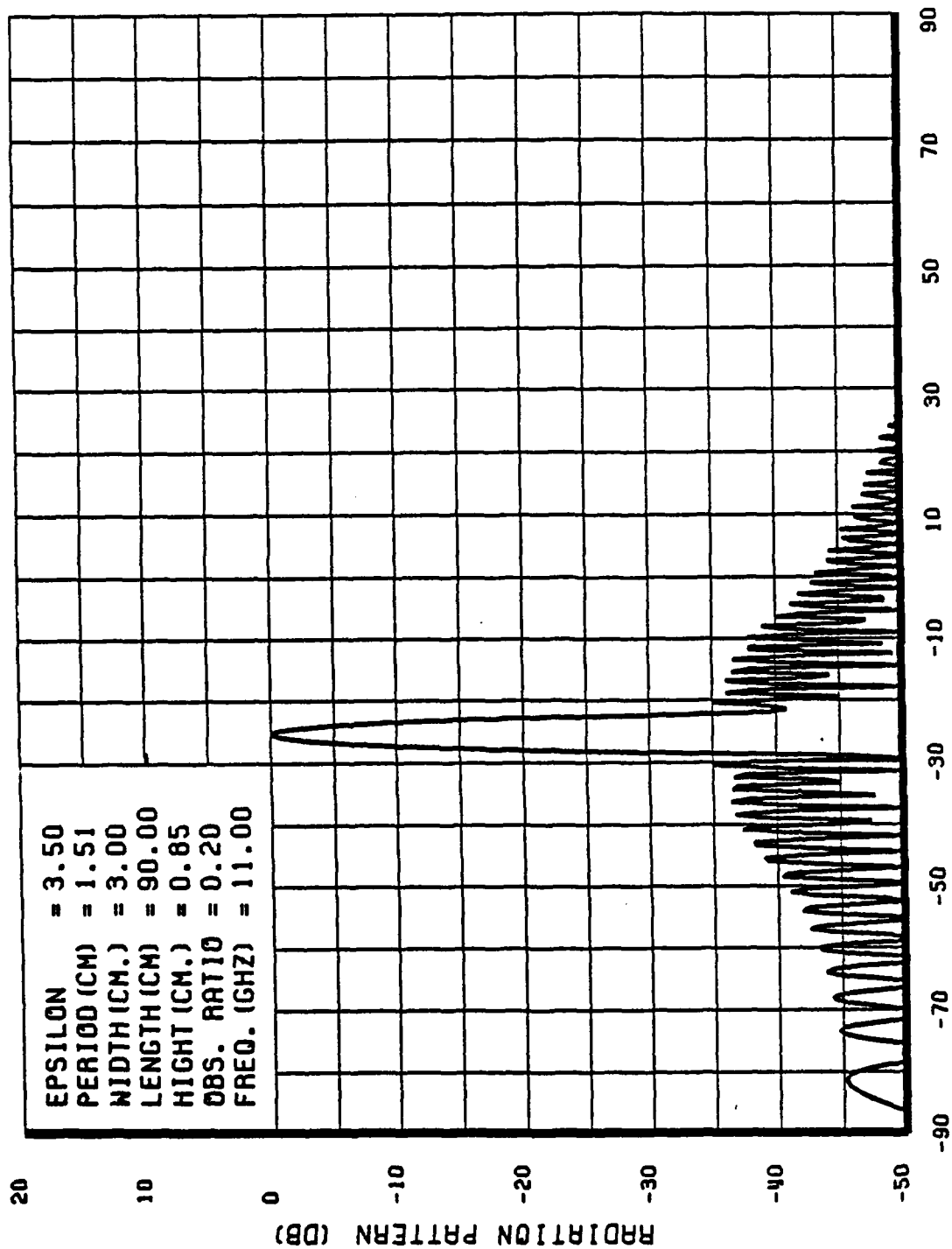

Fig. 4. Using the theory developed, we have designed a suitable tapered antenna geometry that yields the radiation pattern shown, with the first sidelobe 35 dB below the main radiation lobe.

included in (2) was increased, we ran into a serious problem in evaluating the proper expansion coefficients.

In order to solve this problem we have now adopted a different series expansion technique. Using Legendre Polynomials, we can write

$$f_n(\alpha\xi) = \sum_{k=0}^{\infty} b_k(n) P_k(\alpha\xi) \tag{3}$$

where the coefficients $b_k(n)$ are formally given by [4]

$$b_k(n) = (k+\frac{1}{2}) \int_{-1}^{1} f_n(\alpha\xi)\, P_k(\alpha\xi) d\,\alpha\xi \tag{4}$$

The integral in [4] can now be obtained in closed form for arbitrary values of k, thus permitting the evaluation of the function $G_n(\alpha\xi)$ to an arbitrary degree of accuracy.

At the present time we have completed all of the analytical work in connection with this new procedure, and we are in the process of developing a code to verify the accuracy of the results obtained. This work has been done in collaboration with Professor H. Hochstadt of the Mathematics Department of Polytechnic University.

B. A Novel Scanning Array for Millimeter Wavelengths

The scanning array that was devised and analyzed during the past year is a modification of the class of scanning arrays studied by us earlier [5,6]. Those arrays consisted of a linear array of leaky-wave line sources, where scanning in elevation is achieved by frequency scan or electronic scan of the leaky-wave line sources, and scanning in the cross plane is obtained by placing phase shifters at the feed ends of the successive line sources in the array. The angle in the cross plane then depends on the phase shift introduced between the successive line sources. The radiation in pencil beam form will scan in both elevation and azimuth in a conical scan manner. The leaky-wave line sources were made to be *uniform* along the length of the line sources in order to provide simplicity in their configuration. As a result, however, the scan in elevation is restricted to the forward quadrant only; the two-dimensional scan provided by the whole array then covers only half of space at best.

The leaky-wave line source in the array discussed here is *periodic* instead of uniform longitudinally, consisting of a periodic array of metal grids or slots, as shown in Fig. 5. The periodic grid is in fact still simple in configuration, and it can be fabricated at one time by lithographic means. The mask for such fabrication can incorporate the tapering of the aperture distribution for sidelobe control, following our improved procedure in Sec. A, (2).

The periodic nature of the leaky-wave line source permits greater flexibility

in scan coverage. If the period of the periodic strips were sufficiently large (somewhat greater than a half guide wavelength along the line source axis), the n = -1 space harmonic of the periodic array would become fast and would leak power away at some angle. The angular coverage in elevation would then comprise the whole background quadrant and some or all of the forward quadrant, depending on the parameter values.

It is easy to dream up a variety of array structures that should work well, but we are also restricted by the fact that we must be able to analyze the array accurately. In the antenna in Fig. 5, the solution for the array of metal strips placed on a dielectric layer comes from the same general integral equation solution as the one we used for the antenna described under A above, with the important difference that the polarization is opposite. The form of the equivalent network is similar, however, as are many of the basic features.

In the array in Fig. 5, the individual line sources each are fed by a dielectric-filled rectangular waveguide placed on its side, so as to create a horizontal electric field polarization. The electric field lines are then perpendicular to the metal baffles, so that the spacing between them can be whatever we wish; in particular, we can make them less than about $\lambda_0/2$ so that *grating lobes are automatically avoided*. We can also view the structure as a grounded dielectric layer with a metal grating on it. The periodic structure produces an infinity of space harmonics, all of which will be slow if the grating period is too small. For each of these space harmonics, including the $n = 0$ one, the field will then be above cutoff in the vertical direction in the dielectric regions but evanescent in the air regions. If the period is increased sufficiently, or alternatively if the frequency is increased sufficiently, one of these space harmonics (the $n = -1$ one) will become fast and will become propagating in the air regions in the vertical direction. As a result, a mode akin to a TEM mode in each parallel plate region will propagate at an angle toward the open top and will leak power away.

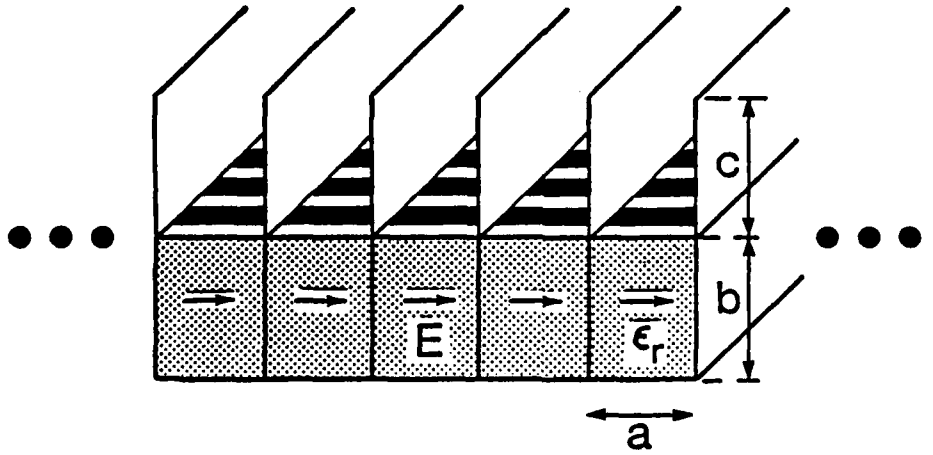

Fig. 5. Configuration of the novel two-dimensional scanning array composed of a linear array of leaky-wave line sources, for which there are no grating lobes, no blind spots, and no cross polarization.

The analysis of this array and numerical results for it show that when the ratio of strip width to period is varied the value of α changes greatly but the value of β is modified only very slightly. This behavior is just what we seek so that the beam width and the angle of the beam maximum can be specified essentially independently, and so that the antenna aperture can be tapered to control the sidelobe level.

For the dielectric constant value selected ($\epsilon_r = 4.0$), this array can scan in elevation essentially only in the backward quadrant, with only a small excursion into the forward quadrant. The angular coverage can be increased when ϵ_r is made larger, but we must take care that the second mode remains below cutoff. However, the angular coverage is already much greater than that obtained with the uniform apertures. Also, when the strips are singly periodic as indicated, the broadside angle corresponds to a stop band, and scanning in that narrow angular region must be omitted. By pairing the strips a quarter-guide-wavelength apart at the broadside angle, cancellation can occur and the array can be scanned through broadside as well, but we have not explored that option in this study.

An important advantage of this array is that the radiation into space has *pure* horizontal electric field polarization. Another important advantage is that, with the baffles present (of height c in Fig. 5), *no blind spots* are found in the scan angle behavior. Without any baffles, experience with other arrays indicates that blind spots are usually present when dielectric layers are part of the array configuration. The short baffles appear to prevent such an occurrence. In addition, they separate the discontinuities at the air-dielectric interface and at the open upper end, making the analytical result simpler.

The attributes of this novel array are, therefore, that there are no grating lobes, no cross polarization, and no blind spots. These significant advantages are combined with simplicity of structure, because the array is intended for application at millimeter wavelengths. The simplicity requires the use of leaky-wave line sources, which may not be suitable for certain scanning applications. The important new feature in this array, as compared with those having uniform apertures [5,6], is that the appropriate use of a periodic aperture permits a larger and more flexible scan angle coverage.

C. A Leaky-Wave Analysis of the High-Gain Antenna Configuration

A method for increasing the gain of a printed-circuit antenna was presented recently [7] which involves the use of a superstrate layer. The antenna element, which for simplicity was taken as a horizontal electric dipole, is embedded within a two-layer geometry consisting of a bottom (substrate) layer of dielectric constant ϵ_1 placed on a metal ground plane and a top (superstrate) layer of substantially higher dielectric constant, ϵ_2. For layer thicknesses for which the bottom layer is effectively a half "wavelength" thick in terms of the transverse (vertical) wavenumber in that medium, and effectively

a quarter "wavelength" thick in a similar fashion in the upper layer, a narrow radiated beam about any desired angle θ_p is produced. The above-mentioned condition was called a "resonance condition."

In [7] it was shown that as the frequency is lowered the beam scans from endfire to broadside. Asymptotic formulas were derived for the gain and the beamwidth as ϵ_2, the dielectric constant of the superstrate, is made large. In addition, radiation patterns were computed numerically.

The present study involves the recognition that this high-gain effect can be interpreted in terms of *leaky waves*. More precisely, the "resonance condition" found in [7] is actually a good approximation to the transverse resonance condition for the existence of a leaky mode on the structure. This leaky mode travels along the surface radially away from the exciting antenna, and it leaks power away as it travels. The wavenumber $\beta - j\alpha$ of the leaky wave along the surface defines the aperture distribution of the antenna, and determines the shape of the radiation pattern. The leaky-wave approach furnishes an alternative interpretation of the physical effect.

It is not necessary to employ the leaky-wave approach to obtain all the numbers for the far-field performance, but this approach furnishes *insight* into the physical processes involved, provides *new* practical information, and permits one to derive the same results as those reported in [7] in a much *simpler* way. The new practical information includes the knowledge of the field behavior along the surface in a simple convergent fashion. That information allows us to determine readily the size of the supporting structure necessary to produce the narrow-beam radiation patterns, a result that would be difficult to obtain otherwise.

An investigation of the leaky waves excited by the printed antenna shows that two leaky waves become dominant, a TE-mode leaky wave that determines the H-plane radiation pattern and a TM-mode leaky wave that determines the E-plane pattern. These patterns can be obtained from the leaky-wave properties in a simple and direct way. A comparison is presented in Fig. 6 of the H-plane patterns computed directly from the single TE-mode leaky wave and computed exactly numerically. For this case, the beam maximum is at 45°, and the dielectric constants of the substrate and the superstrate are 2.1 and 10.0, respectively. It is seen that the agreement between the two curves is very good, verifying that the field along the surface in that direction is indeed dominated by that *single* leaky wave. Contributions from the other leaky waves, if they were taken into account, would make up the difference between the two curves. We should also recognize that the leaky wave result is not only much simpler to obtain than the exact one, but it also readily exhibits the physics underlying the behavior.

This study has been conducted in collaboration with Professor D.R. Jackson of the University of Houston. The results obtained from the first phase have been presented at symposia and accepted for publication [8-10].

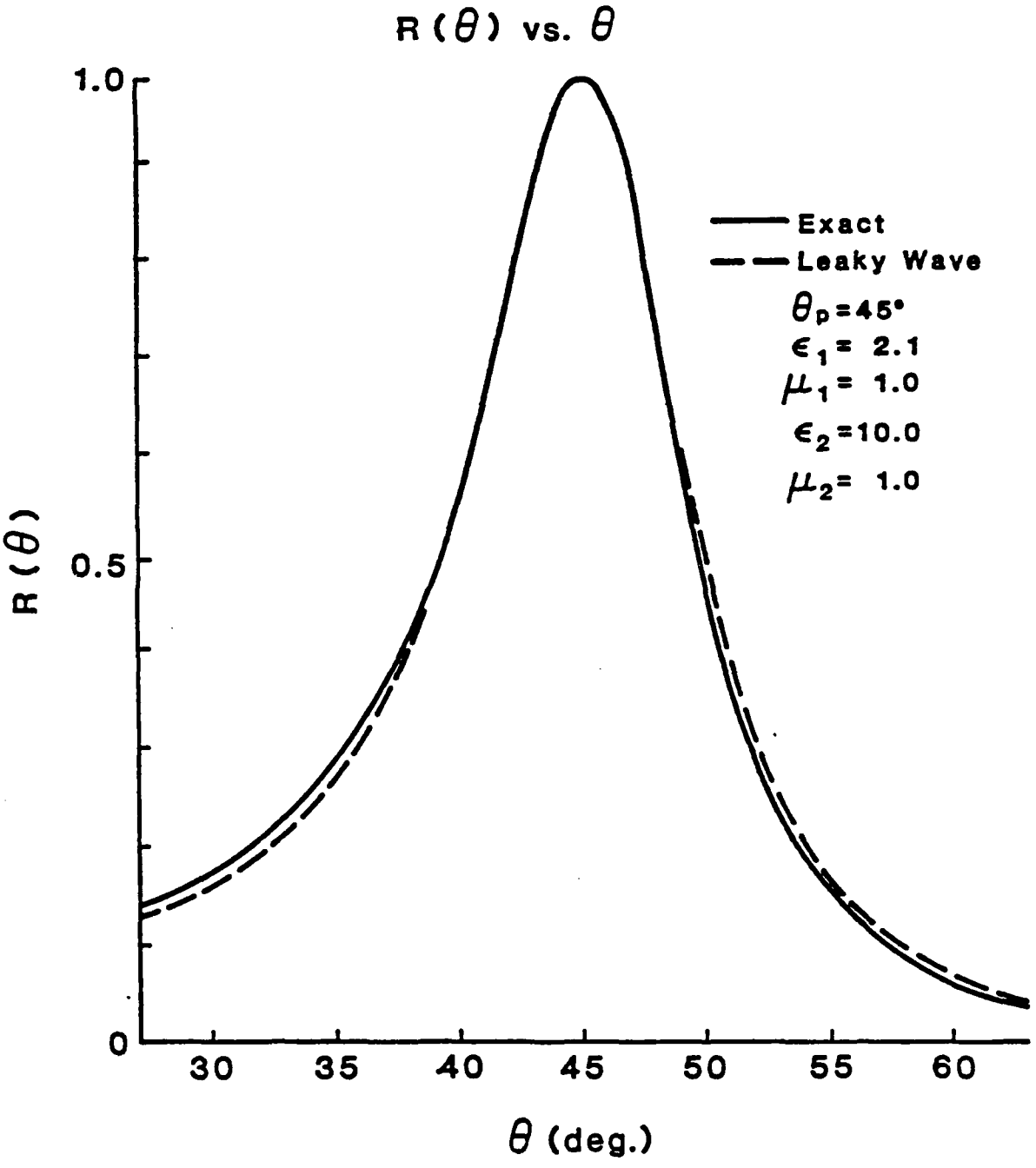

Fig. 6. Comparison of calculations for the H-plane radiation pattern of a high-gain printed-circuit dipole antenna, where the beam maximum is at 45°, and where the substrate and superstate dielectric constants are 2.1 and 10.0, respectively. The solid and dashed lines represent the exact numerical values and the result obtained from a single leaky wave only.

D. Conductor-Backed Slot Line: Dangers and Full-Wave Analyses

It is very tempting in microwave integrated circuits to introduce a conductor backing for slot line or coplanar waveguide because such conductor backing has many advantages. Among these advantages, as quoted in the literature [e.g., 11,12], are: lowers Z_o, lessens dispersion, improves mechanical strength, allows easier implementation of mixed coplanar-microstrip or slot line-microstrip circuits, helps in grounding floating regions, convenient for dc biasing, and provides a convenient heat sink. There are also certain important dangers, or serious potential problems, that are introduced by the use of conductor backing. These potential problems include leakage of power into surface waves or into the dielectric region between the plates, unexpected cross talk, significant alteration of the guide wavelength, and unexpected or unwanted coupling to neighboring lines. These possible unpleasant consequences seem *not* to have been discussed in the literature.

The type of potential problem outlined above depends on the *lateral extent*, or *width* , of either the conductor backing or the plates comprising the slot line or the coplanar waveguide. Several examples of conductor-backed slot line, with various conductors of infinite and finite lateral extent, are presented in Fig. 7; the upper shielding plate or cover, which is customarily there but plays a minor role, is omitted from Fig. 7 for simplicity (and clarity).

Structure (a), and its *equivalent in coplanar* waveguide, will always leak power into the dielectric-filled parallel plate regions, and the leakage rate is rather high, as we find quantitatively. Structure (b) represents the other extreme, a conductor-backed two-strip line; however, it is also a pair of coupled microstrip lines in its odd mode. That structure and those in (c), (d), (e) and (h) will not leak at lower frequencies but may leak into a surface wave in the outer regions at higher frequencies. All structures with finite metal lengths that are not short, such as (c), (e), (f) and (h), face the danger that when no leakage occurs the guide wavelength can be seriously altered from its expected value by the loading produced by the finite transverse line lengths. Structure (d), which involves only a short conductor back, and which is utilized in the de Ronde coupler [13], will not face this danger. Finally, in (g) and (h) coupling (desired or not) can occur between parallel slot lines not near each other on the same side or on opposite sides.

The only full-wave analyses that appear in the literature apply to the infinitely wide structure in (a) [11] and the other extreme in (b). The analysis that applies to (a) was actually performed for coplanar waveguide, but it could just as easily have been done for slot line. However, that calculation was made several years ago, before it was recognized that leakage could occur; that analysis is therefore incomplete since it misses the leakage effect altogether. Many full-wave analyses for the structure in (b) appear in the literature (see [14] for a very good summary), in the context of the odd mode of a pair of coupled microstrip lines. None of those treatments, however, inquired as to whether or not leakage into a surface wave could occur at the higher

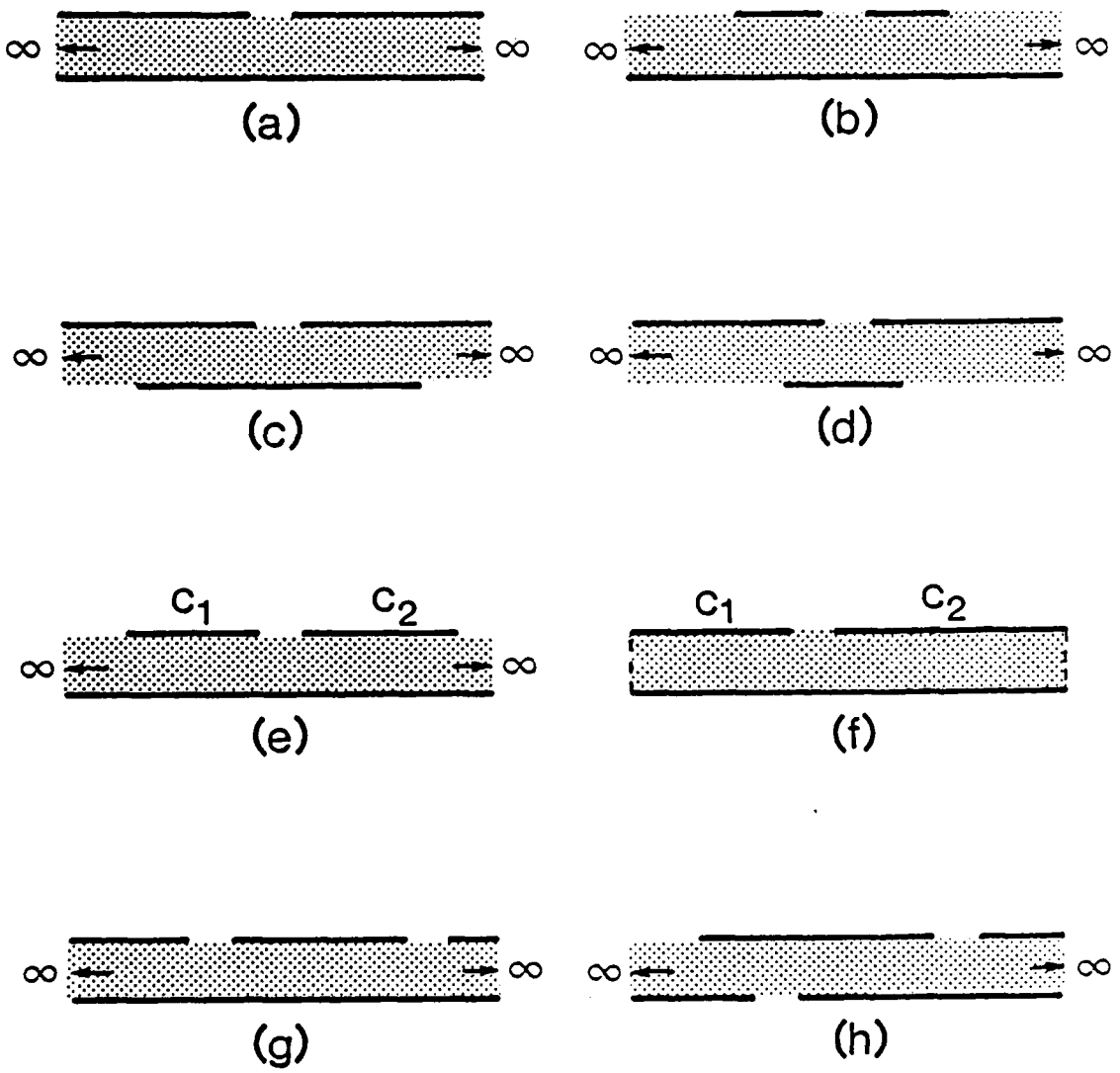

Fig. 7. Several examples of conductor-backed slot line, where either the slot line conductors or the backing conductor can be of infinite or finite lateral extent. The upper shielding plate or cover is omitted for clarity.

frequences. On the other hand, an approximate analysis [15] was performed for the two strips *without* conductor backing which does ask this question, and indeed answers it in the affirmative, with measurements to back up the conclusion. To our knowledge, there are no full-wave analyses for any of the other situations.

We have recently developed two methods of analysis that are applicable to all of the structures in Fig. 7, thereby providing for the first time a systematic full-wave analytical procedure for determining the effect of finite plate widths on the modal propagation characteristics. One method is based on mode matching and the other employs a new transverse equivalent network where the elements are expressed in simple closed form. Both methods were applied to the infinitely wide structure in Fig. 7(a), and the results from the two methods agreed rather well with each other. Measurements were also made for both the guidance and leakage properties. In addition to verifying that the conductor backing leads to a high leakage rate, the comparisons with measurement and those between the theories show that the theoretical methods are reliable. These studies are being conducted in collaboration with Professor H. Shigesawa and Dr. M. Tsuji of Doshisha University, Kyoto, Japan.

The several unexpected dangers that can arise when the plates are *finite* in lateral extent are continuing to be investigated quantitatively. Some of these effects may explain why designers of MMIC or microwave integrated circuits often find that components that work well separately fail when combined together.

4. REFERENCES

1. M. Guglielmi and A.A. Oliner, "Accurate Analysis of Metal-Strip-Loaded Image Guide Leaky-Wave Antennas," National Radio Science Meeting, Boulder, CO., January 12-15, 1987 (second prize winner of U.R.S.I. National Student Prize Paper Competition.
2. M. Guglielmi and A.A. Oliner, "A Practical Theory For Image Guide Leaky-Wave Antennas Loaded by Periodic Metal Strips," Proc. 17th European Microwave Conference, pp. 549-555, Rome, Italy, September 1987.
3. M. Guglielmi, "Radiation from a Metal-Strip Grating on a Dielectric Slab," Ph.D. Dissertation, Polytechnic University, June 1986.
4. N.N. Lebedev, *Special Functions and their Applications*, p. 53, Dover Publications Inc., New York, 1972.
5. A.A. Oliner and S.J. Xu, "A Novel Phased Array of Leaky-Wave NRD Guides," Digest National Radio Science Meeting, p. 139, Blacksburg, VA, June 15-19, 1987.
6. P. Lampariello and A.A. Oliner, "A Novel Phased Array of Printed-Circuit Leaky-Wave Line Sources," Proc. 17th European Microwave Conference, pp. 555-560, Rome, Italy, September 7-11, 1987.

7. D.R. Jackson and N.G. Alexopoulos, "Gain Enhancement Methods for Printed Circuit Antennas," IEEE Trans. Antennas Propagat. Vol. AP-33, pp. 976-987, September 1985.

8. D.R. Jackson and A.A. Oliner, "A Leaky Wave Analysis of the High-Gain Printed Antenna Configuration," Digest National Radio Science Meeting, p. 146, Blacksburg, VA, June 15-19, 1987.

9. D.R. Jackson, A.A. Oliner and N.G. Alexopoulos, "Fundamental Superstrate Effects on Printed-Circuit Antennas and the Role of Leaky Waves," Book of Abstracts, p. 267, XXIInd General Assembly of U.R.S.I, Tel Aviv, Israel, August 24-September 2, 1987.

10. D.R. Jackson and A.A. Oliner, "A Leaky-Wave Analysis of the High-Gain Printed Antenna Configuration," accepted for publication in the IEEE Trans. Antennas and Propagation.

11. Y.C. Shih and T. Itoh, "Analysis of Conductor-Backed Coplanar Waveguide," Electronics Letters, Vol. 18, No. 12, pp. 538-540, 10 June 1982.

12. G. Ghione and C.V. Naldi, "Coplanar Waveguides for MMIC Applications: Effect of Upper Shielding, Conductor Backing, Finite-Extent Ground Planes, and Line-to-Line Coupling," IEEE Trans. Microwave Theory Tech., Vol. MTT-35, pp. 260-267, March 1987.

13. F.C. de Ronde, "A New Class of Microstrip Directional Couplers," Digest IEEE International Microwave Symposium, pp. 184-189, 1970.

14. K.C. Gupta, R. Garg and I.J. Bahl, *Microstrip Lines and Slotlines,* Chap. 8, Artech House, Dedham, MA, 1979.

15. D.B. Rutledge, D.P. Neikirk and D.P. Kasilingam, "Integrated Circuit Antennas," in *Infrared and Millimeter Waves, Vol. 10,* pp. 1-90, 1983.

B. BEAM-WAVE PROPAGATION AND INTERACTIONS IN OPEN LAYERED MEDIA

Professor T. Tamir

Unit EM7-2

1. OBJECTIVE(S)

This investigation aims to provide a new and systematic approach to the propagation, scattering, guiding and coupling of beam waves in open layered structures, particularly those of the thin-film variety. In the past, problems involving wave progression through different media have been treated mostly in terms of plane waves of infinite extent, or in terms of strongly localized rays that connect a source to an observation point. However, an increasing number of application areas utilize fields that propagate by means of well-bounded beams, such as those provided by lasers. Because they occupy an intermediate position between unbounded plane waves and rays of infinitesimal cross-section, beams exhibit propagation characteristics that are different in many respects from either plane waves or rays. For example, they are subject to nongeometric lateral displacements, peculiar focal phase shifts, angular deviations, anomalous absorption effects, and other recently recognized phenomena that have not as yet been investigated except in a few special cases. It is thus desirable to study these phenomena and other related aspects in terms of beam fields, which are realistic and meaningful representations of many practical electromagnetic (and other) fields.

To achieve results that are relevant to a wide spectrum of applications areas, this study addresses basic aspects of beam propagation through, and guidance along, open layered configurations that are typical of a very broad variety of situations. For this purpose, we consider beams of the Gaussian form because they are more easily tractable from mathematical points of view and, fortunately, they are also of greatest practical application.

The configurations of interest are first expressed in terms of canonic models consisting of a single layer placed between two open media having different electromagnetic properties; structures with multiple layers can thereafter be treated as composite configurations made up of several individual canonic models. While the investigation has focused on lossless passive media, the projected work has also considered media with arbitrary absorption (or other) losses. Some of the specific aspects to be explored include beam-profile distortions, the interaction of beam waves with other (e.g., surface, leaky) waves, and the conversion of beam fields into other characteristic field types. Although phrased in electromagnetic terms, the results of this basic investigation are applicable also to other areas, such as acoustic waves along interfaces or layers, elastic waves along geophysical strata, plasmon waves in metal films, and other configurations involving waves and beams through or

along layered media.

2. SUMMARY OF RECENT PROGRESS

In the preceding yearly progress report, we mentioned that our studies had included three phases, namely (a) nonspecular phenomena in beams incident on multilayered media, which appear as peculiar beam-shifting and other effects; (b) new types of leaky waves supported by guiding structures; and (c) surface and leaky waves along general open configurations, such as thin-film structures for integrated optics, microwave acoustics and other areas of current interest. While all of these topics were pursued during the past year, most of the work during that period has focused on surface plasmon waves along thin metallic films.

In our previous yearly report, we have discussed that our work on leaky waves along canonic structures has determined all the possible types of such waves and has provided a detailed catalog of their properties. We found that a total of eight leaky-wave varieties are possible, of which half are forward-traveling and the other are backward-traveling. However, every type of layered configuration can support only some of these waves. Because the (rather novel) type of leaky waves having backward-traveling characteristics can occur only in the presence of metallic layers, we have examined such (plasmon-type) structures in detail.

In particular, we have explored thin metal film geometries of the type that permit the propagation of *long range surface plasmons* (LRSP) waves. In this context, a closer analysis of the various leaky waves that may be supported by such geometries has revealed novel plasmon waves having properties that are different from those reported so far. Specifically, by introducing a dielectric layer in parallel to the metal film, we have shown that plasmon waves can be generated having propagation lengths that are one or two orders of magnitude larger than those of the LRSP variety. We have therefore denoted this new variety by the name of *extended range surface plasmons* (ERSP) waves. In addition, we have determined the optimal conditions for exciting such ERSP waves by means of incident beams having Gaussian or rectangular profiles. The results obtained show that ERSP waves can provide fields with greatly enhanced intensities over very long distances. These properties are very useful for applications that require strong field interactions with nonlinear media.

Papers covering the above topics were written and presentations were made at several technical meetings.

3. STATE OF THE ART AND PROGRESS DETAILS

A. Background

The interest in beam fields was stimulated by applications in laser technology, fiber optics, ultrasonic diagnostics and other areas which have generated a number of fundamental studies of beam propagation through a variety of media. However, most of the studies have dealt with beams propagating over long distances through uniform or "slowly varying" media. Thus, comparatively few investigations have been carried out on beam fields interacting with abrupt transitions and/or multiple boundaries separated by distances of the order of a wave-length, such as occur in thin film configurations.

Because lasers generate beam fields, a considerable number of investigations on beams inside laser cavities were undertaken in the early sixties. These studies viewed the beams primarily in terms of ray optics and considered their interaction with mirror reflectors or thin lenses [1,2]. The fields of beams that are emitted by lasers into free space have also been studied, mostly in terms of their Hermite-Gaussian modes [1-3], and interest into the fine structure of those propagating fields is continuing to this day [4,5]. However, all of those studies are concerned primarily with a beam that propagates basically through a single uniform medium.

When the medium inside which the beam propagates is not uniform, the usual assumption has been that the medium properties change slowly over a distance of a wavelength, i.e., one deals with a slowly varying medium. The treatment has then involved a variety of techniques, which include complex rays [6,7], or the propagating-beam method [8], which relies heavily on numerical computations.

In contrast to the above, our study is concerned with beam fields that propagate through media that can change rapidly and are therefore characterized best by boundaries that separate media having different electromagnetic properties. In this context, most recent studies have dealt almost exclusively with the lateral Goos-Haenchen shift of beams incident under total reflection conditions at a single interface between different media [9-15]. Only a very few investigations have examined incidence of beams on layered configurations having two or more interfaces [16-19]. Of these, a considerable amount of basic work was carried out by us [17,19]; in this context, we have also shown that electromagnetic beam phenomena on layered configurations have analogous counterparts in acoustics [20,21], thus stimulating investigations in that area which are still continuing [22-34].

In addition to the (Goos-Haenchen) lateral displacement of the beam axis, recent studies have shown that the beam may also exhibit an angular deviation [11,26,27], and/or a focal shift [24,25]. However, those effects were examined only for beams incident from a denser medium onto a single interface to a rarer medium under total-reflection conditions. By extending an analytical pole-zero

approach recently developed by us [33], we have obtained qualitative and quantitative results for all of these effects for arbitrary incidence on multilayered structures [34]. This approach has revealed a hitherto unknown phenomenon, which manifests itself as a reduction or increase in the effective beam width. The unified analysis of the three (lateral, focal and angular) beam-shifting effects and the fourth (beam-waist modification) phenomenon were described by us in previous progress reports and subsequently published [34-38].

B. Beam Excitation of Plasmon Waves Along Metal Films

As shown by us in the past [31-38], the nonspecular effects described above are intimately related to the excitation of leaky waves which can be supported by the pertinent layered structures. As part of the effort during the preceding year, we have therefore devoted a large portion of our studies to explore and classify the various varieties of leaky waves that can be guided by general layered media of the type described in Fig. 1. The results of that study were reported in the previous annual report, and most of the relevant material has also been published [39,40,41,43]. While we have continued these general studies of leaky-wave fields, we have concentrated during the past year on the canonical configurations described in Fig. 1 for the specific case where the layer shown therein by $\epsilon(z)$ contains multiple lossy or lossless dielectric and/or metal layers.

Because strong interest has recently been shown [42,43] in plasmon waves guided by thin metal films, we have specifically focused on the particular leaky waves that are responsible for the plasmon modes. The general situation we examined is then shown in Fig. 2, wherein a beam is assumed incident in a prism placed upon a multilayered geometry which includes a metal film. The (leaky-wave) plasmon modes excited by the incident beam are then characteristic solutions of the pertinent boundary-value problem, with fields in the form

$$F = F_j \exp\left[ik(\kappa x + \tau_j z) - i\omega t \right] , \tag{1}$$

where j denotes the specific layer under consideration and $k=2\pi/\lambda$. Here κ and τ_j are normalized wavenumbers which satisfy

$$\kappa^2 + \tau^2 = \epsilon_j , \tag{2}$$

and ϵ_j refers to the dielectric constant of the j^{th} layer. The wavenumbers κ and τ_j are found from Eq. (2) in conjunction with a dispersion (secular) relation in the form

$$D(\kappa) = f(\kappa;\tau_j) = 0 . \tag{3}$$

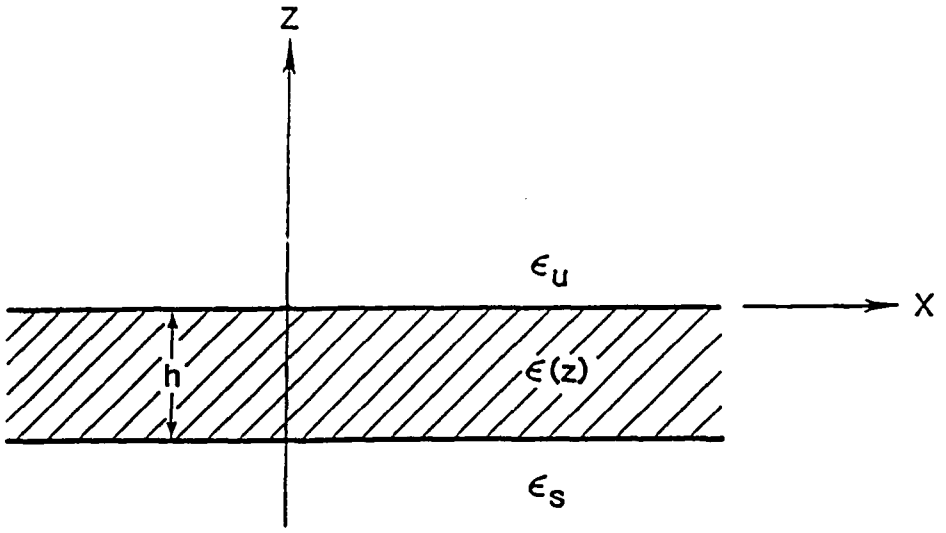

CANONIC CONFIGURATIONS FOR $\epsilon(z) = \epsilon_h = \text{const.}$

Duct:	$\epsilon_s > \epsilon_h > \epsilon_u > 0$
Transition:	$\epsilon_s > \epsilon_h > \epsilon_u > 0$
Gap:	$\epsilon_s > \epsilon_u > \epsilon_h > 0$
Plasma:	$\epsilon_s > \epsilon_u > 0 > \epsilon_h$

Fig. 1 Open layered structure supporting leaky waves and the canonic configurations that characterize typical situations.

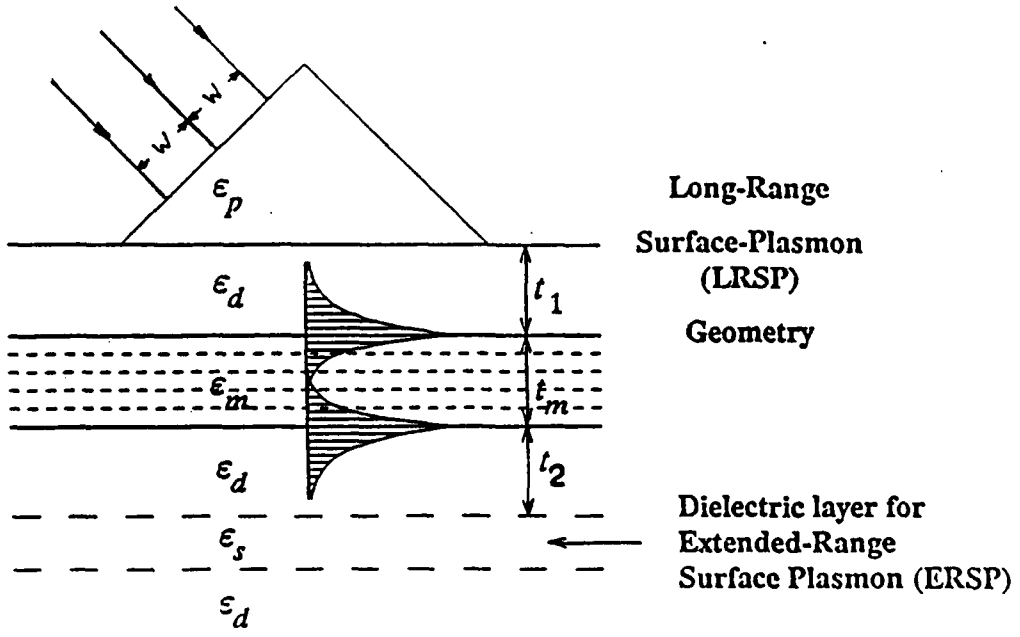

Fig. 2 Geometry for exciting plasmon waves by means of an incident beam of width 2w. In the absence of the dielectric layer shown by dashed lines, the configuration corresponds to Sarid's structure [42] for LRSP waves. The presence of the dielectric layer indicated by dashed lines permits the excitation of ERSP waves having much longer propagation ranges.

By solving Eq. (3) under certain restricted conditions, Sarid has shown [42] the possibility of exciting plasmon waves having long propagation lengths, which were subsequently labelled *long range surface plasmons* (LRSP) waves. We have verified the presence of such LRSP waves and have shown [44] that they can be more strongly excited if the angle of the incident beam is offset from the angle that satisfied a reflection dip. (This reflection-dip condition had in the past been assumed to provide the best excitation parameters.) More interestingly, however, we have solved the dispersion equation (3) under more general conditions and have found that plasmon waves can be generated with propagation lengths that are considerably longer than those of the previously known LRSP waves.

To clarify these novel plasmon wave types, consider Fig. 2 in which the conventional LRSP is indicated by solid lines. This consists of the prism, a gap of thickness t_1, a metal film of thickness t_m and a substrate having a dielectric constant ϵ_d. To obtain the larger propagation ranges, an additional dielectric layer having a dielectric constant $\epsilon_s > \epsilon_d$ is introduced, as shown by the dashed lines in Fig. 2. The function of the additional layer is to serve as a planar waveguide whose field can couple to the surface plasmon guided by the metal film.

We have thus shown [45] that this coupling effect provides a mechanism whereby the additional layer acts as an energy reservoir which increases the power storage of the system. As a result, the net propagating plasmon wave can progress over a distance L_e which is more than one order of magnitude larger than the propagation range L_o of the (ordinary) LRSP waves known so far [42,43]. To distinguish between the two plasmon waves, we label the plasmon having the larger (extended) range as an *extended range surface plasmon* (ERSP) wave.

The importance of the ERSP wave is illustrated in Fig. 3(a), where the ratio L_e/L_o between the propagation ranges mentioned above is shown by the solid line. As a function of the separation t_2 between the metal film and the auxiliary dielectric layer, it is clearly possible to obtain ratios $L_e/L_o = 100$ and larger. In Fig. 3(b), the power density ratio P_{xe}/P_{xo} between the ERSP and LRSP is shown by the solid line. This ratio is important for field interactions with non-linear media because the power density P_{xo} of the LRSP wave is very large in the metal film compared to the power flux of the incident beam that excites the plasmon field. As can be seen from Fig. 3(b), the ratio P_{xe}/P_{xo} is unity or larger, so that the excitation of the ERSP wave can provide a considerably longer propagation range at no reduction in field enhancement.

To complete the picture, we have investigated the presence of small losses in the dielectric media. The results are shown by the dotted lines in Fig. 3, which show that the propagation range L_e can be about 100 times larger than L_o at $t_2 \simeq 1.5\,\mu m$. Under those conditions, $P_{xe}/P_{xo} \simeq 0.85$, which implies that the field intensity enhancement achieved by the ERSP wave is only 15% lower than that of the LRSP.

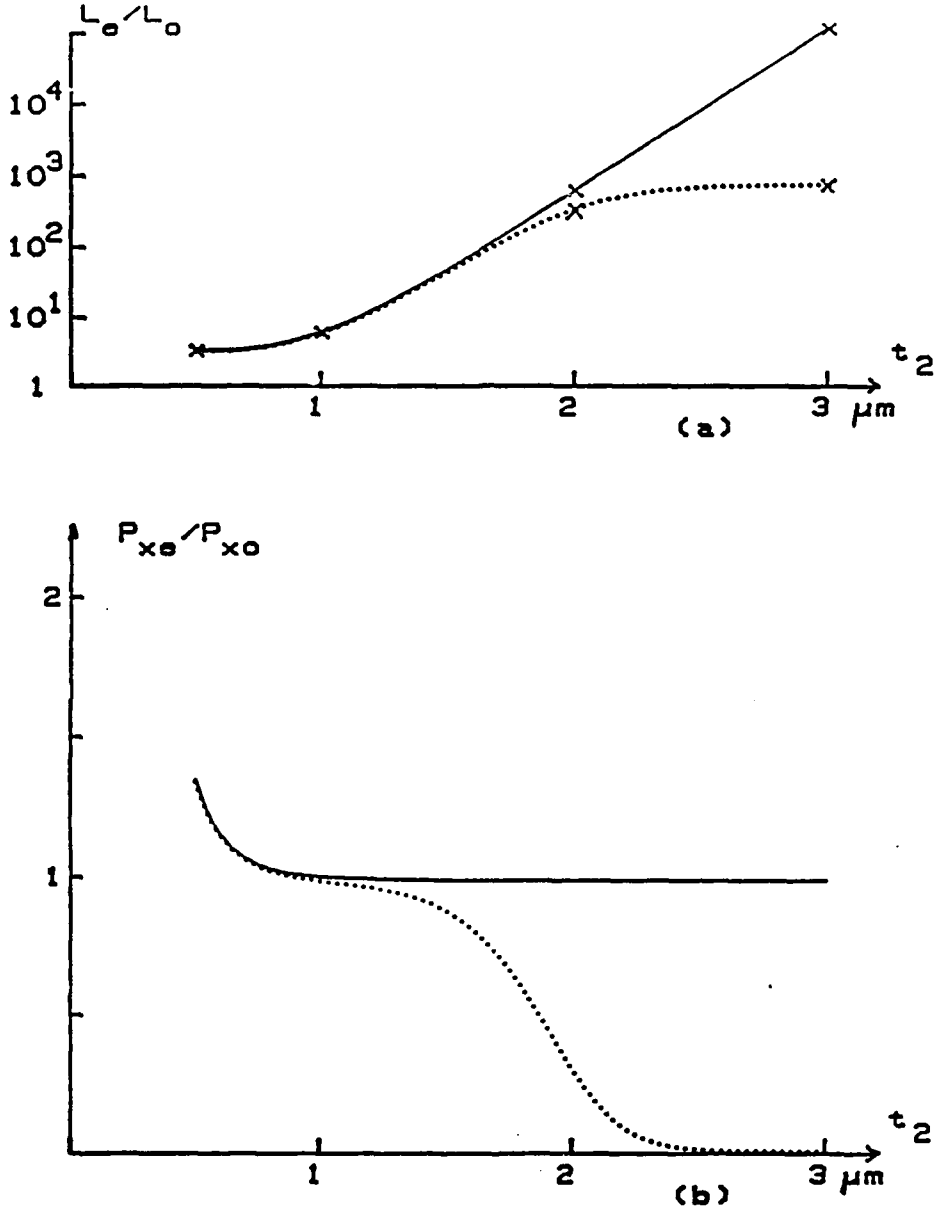

Fig. 3 Variation of ERSP properties compared to those of LRSP waves, as functions of the separation t_2 between the metal film and the auxiliary dielectric layer (shown by dashed lines in Fig. 2).

(a) Ratio L_e/L_o between the propagation length of the ERSP wave and that of the LRSP wave.

(b) Ratio P_{xe}/P_{xo} between the power densities in the metal in the ERSP wave and that of the LRSP wave.

In all cases, the solid lines refer to lossless dielectric materials. In the presence of materials having realistic losses, the results are shown by the dotted lines.

As a result, we find that the plasmon waves of the ERSP variety in realistic geometries can have propagation ranges of the order of 1 cm or larger with an attendant field enhancement that is only slightly smaller than that of the much shorter-propagating LRSP waves. The excitation of ERSP waves therefore produces remarkably improved conditions over long distances in non-linear regimes.

Publications concerning the above effects have been already made [44-46] and a Doctoral thesis dealing with the detailed work is presently being written [47].

4. REFERENCES

1. J.A. Arnaud, *Beam and Fiber Optics,* Chapters 1 and 2, Academic Press, 1976.

2. H. Kogelnik, "Propagation of laser beams," Chapter 6 in *Applied Optics and Optical Engineering,* vol. VII, Academic Press, 1979.

3. L.S. Dickson, "Characteristics of a propagating Gaussian beam," Appl. Optics, vol. 9, pp. 1854-1861, August 1970.

4. L. Lewis, "The propagation of Gaussian beams very near the sources," Radio Science, vol. 10, pp. 555-563, May 1975.

5. W.H. Carter, "Focal shift and concept of effective Fresnel number for a Gaussian laser beam," Appl. Optics, vol. 21, pp. 1989-1994, June 1982.

6. G.A. Deschamps and P.E. Mast, "Beam tracing and applications," Proc. Symp. Quasi-Optics, pp. 379-395, Polytechnic Press, 1964.

7. S. Choudhary and L.B. Felsen, "Analysis of Gaussian beam propagation and diffraction by inhomogeneous wave tracking," Proc. IEEE, vol. 62, pp. 1530-1541, November 1974.

8. M.D. Feit and J.A. Fleck, Jr., "Mode properties and dispersion of two optical fiber-index profiles by the propagating beam method," J. Opt. Soc. Amer., vol. 19, pp. 3140-3150, September 1980. Refer also to the bibliography therein.

9. S. Nemoto and T. Makimoto, "Reflection and transmission of two-dimensional Gaussian beam at the plane interface of dielectrics," Electron. Commun. Japan, vol. 54-B, pp. 30-35, December 1971.

10. B.R. Horowitz and T. Tamir, "Lateral displacement of a light beam at a dielectric interface," J. Opt. Soc. Amer, vol. 61, pp. 586-594, May 1971.

11. J.W. Ra, H.L. Bertoni and L.B. Felsen, "Reflection and transmission of beams at a dielectric interface," SIAM J. Appl. Math., vol. 24, pp. 396-413, May 1973.

12 S. Kozaki and Y. Mushiake, "Total reflection of a Gaussian beam from an inhomogeneous medium," J. Appl. Phys., vol. 46, pp. 4098-4100, September 1975.

13. S.Y. Shin and L.B. Felsen, "Lateral shifts of total reflected Gaussian beams," Radio Science, vol. 12, pp. 551-564, July-August 1977.

14. J.P. Hugonin and R. Petit, "Etude generale des deplacements a la reflexion totale," J. Optics (Paris), vol. 8, pp. 73-87, February 1977.

15. K. Yasumoto and Y. Oishi, "A new evaluation of the Goos-Haenchen shift and associated time delay," J. Appl. Phys., vol. 54, pp. 2170-2176, May 1983.

16. J.E. Midwinter and F. Zernike, "Experimental studies of evanescent wave coupling into a thin-film waveguide," Appl. Phys. Lett, vol. 16, pp. 198-220, March 1970.

17. T. Tamir and H.L. Bertoni, "Lateral displacement of optical beams at multilayered and periodic structures," J. Opt. Soc. Amer., vol. 61, pp. 1397-1413, October 1971.

18. O. Costa de Beauregard, C. Imbert and Y. Levy, "Observation of shifts in total reflection of a light beam by a multilayered structure," Phys. Rev., vol. D15, pp. 3553-3562, 1977.

19. V. Shah and T. Tamir, "Absorption and lateral shift of beams incident upon lossy multilayered media," J. Opt. Soc. Amer., vol. 73, pp. 37-44, January 1983.

20. H.L. Bertoni and T. Tamir, "Unified theory of Rayleigh angle phenomena for acoustic beams at liquid-solid interfaces," Appl. Physics, vol. 2, pp. 157-172, October 1975.

21. H.L. Bertoni and T. Tamir, "Reflection phenomena for acoustic beams incident on a solid at the Rayleigh angle," Proc. 1973 IEEE Ultrasonics Symp., pp. 226-229, IEEE Press (New York), 1974.

22. J.M. Claeys and O. Leroy, "Reflection and transmission of bounded sound beams on half-spaces and through plates," J. Acoust. Soc. Amer., vol. 72(2), pp. 585-590, August 1982.

23. A.N. Norris, "Back reflection of ultrasonic waves from a liquid-solid interface," J. Acoust. Soc. Amer., vol. 73(2), pp. 427-434, February 1983.

24. M. McGuirk and C.K. Carniglia, "Angular spectrum representation approach to the Goos-Haenchen shift," J. Opt. Soc. Amer., vol. 67, pp. 103-107, January 1977.

25. C.K. Carniglia and K.R. Brownstein, "Focal shift and ray model for total internal reflection," J. Opt. Soc. Amer., vol. 67, pp. 121-122, January 1977.

26. Y.M. Antar and W.M. Boerner, "Gaussian beam interaction with a plane dielectric interface," Can. J. Phys., vol. 52, pp. 962-972, 1974.

27. I.A. White, A.W. Snyder and C. Pask, "Directional change of beams undergoing partial reflection," J. Opt. Soc. Amer., vol. 67, pp. 703-705, May 1977.

28. V. Shah and T. Tamir, "Brewster phenomena in lossy structures," Optics Commun., vol. 23, pp. 113-117, October 1977.

29. V. Shah and T. Tamir, "Anomalous absorption in thin-layered media," Optics Commun., vol. 37, pp. 383-387, June 1977.

30. A. Amittay, P.D. Einziger and T. Tamir, "Experimental observation of anomalous electromagnetic absorption in thin-layered media," Appl. Phys. Letters, vol. 38, pp. 754-756, May 1977.

31. C.W. Hsue and T. Tamir, "Lateral beam displacements in transmitting layered structures," Optics Commun., vol. 49, pp. 383-387, April 1984.

32. C.W. Hsue and T. Tamir, "Lateral displacement of beams refracted by layered media," J. Opt. Soc. Amer., vol. 83, p. 1913, December 1983.

33. C.W. Hsue and T. Tamir, "Lateral displacement and distortion of beams incident upon a transmitting-layer configuration," J. Opt. Soc. Amer. A, vol. 2, pp. 978-988, June 1985.

34. T. Tamir, "Nonspecular phenomena in beam fields reflected by multilayered structures," Opt. Soc. Amer. A, vol. 3, pp. 558-565, April 1986.

35. H.L. Bertoni, C.W. Hsue and T. Tamir, "Nonspecular reflection of convergent beams from a liquid-solid interface", Traitement du Signal, vol. 2, pp. 201-205, July-August 1985.

36. C.C. Chan and T. Tamir, "Focal and angular shifts of Gaussian beams reflected near the critical angle," J. Opt. Soc. Amer. A, vol. 2, p. 45, December 1985.

37. T. Tamir, "Nonspecular phenomena in beam fields reflected by stratified media", Proc. Intern. Symp. Electromagnetic Theory, pp. 622-624, Budapest, Hungary, August 1986.

38. W. Nasalski and T. Tamir, "Composite beam-shifting effects under critical incidence conditions," 1986 Annual Opt. Soc. Amer. Meeting, Seattle, WA, October 1986.

39. F.Y. Kou and T. Tamir, "Evolution of TM surface and leaky waves guided by asymmetric layer configurations," J. Opt. Soc. Amer. A, vol. 3, pp. 417-425, April 1986.

40. T. Tamir and F.Y. Kou, "Varieties of leaky waves and their excitation along multilayered structures," IEEE J. Quantum Electronics, vol. 2E-22, pp. 544-551, April 1986.

41. T. Tamir and F.Y. Kou, "Classification of leaky waves supported by multilayered structures," Proc. URSI Intern. Symp. Electromagnetics Theory, pp. 141-143, Budapest, Hungary, August 1986.

42. D. Sarid, "Long-range surface-plasma waves on very thin metal films," Phys. Rev. Lett. vol. 67, pp. 1927-1930, December 1981.

43. J.J. Burke, G.I Stegeman and T. Tamir, "Surface polariton-like waves guided by thin, lossy metal films," Phys. Rev. B, vol. 33, pp. 5186-5201, April 1986.

44. F.Y. Kou and T. Tamir, "Enhanced excitation of long-range surface plasmon modes", 1986 Annual Opt. Soc. Amer. Meeting, Seattle, WA, October 1986.

45. F.Y. Kou and T. Tamir, "Range extension of surface plasmons by dielectric layers," Optics Lett., vol. 12, pp. 367-369, May 1987.

46. F.Y. Kou and T. Tamir, "Optimized excitation of surface plasmons in metal films," 1987 Annual Opt. Soc. Amer. Meeting, Rochester, NY, October 1987.

47. F.Y. Kou, "Excitation of leaky waves and surface plasmons along dielectric and metallic layers," Ph.D. Dissertation, Polytechnic University, expected January 1988.

C. MIXED SPECTRAL TECHNIQUES FOR WAVE PROPAGATION AND DIFFRACTION

Professor L.B. Felsen

Unit EM7-3

1. OBJECTIVE(S)

High frequency or transient propagation in, or transmission through, layered media, and high frequency or transient scattering by impenetrable and penetrable targets usually requires synthesis in terms of a large number of basic wave processes. For the guiding or ducting problem, these wave processes are either normal (discrete and continuous) modes or ray-optical fields. For the transmission problem, the basic wave processes are traveling waves which undergo multiple internal reflection at the layer boundaries. For the transient scattering problem, the wave processes involve multiple wavefront and resonance fields. Because descriptions by multiple propagation events are often poorly convergent and do not provide physical interpretation in compact form, it is desirable to seek collective descriptions of multiple phenomena.

Thus, the objective of this fundamental study is the construction of a new theory of propagation, transmission and scattering that has broad implications for a general class of electromagnetic and other wave problems. The approach is to seek suitable spectral representations in the spatial and temporal domains and to adapt these by arguments of asymptotic localization to successively more complicated environments. The basic spectral building blocks are time-harmonic and transient local plane waves, and the spectra may be real or complex. Localized spectra can represent ray fields, true and local mode fields, hybrid ray-mode forms, wavefront-resonance phenomena, and, in more fleshed-out form, also transitional effects where these simple compact spectral formulations may fail. The tools involve the theory of spectral representations and asymptotic treatment of integrals and partial differential equations.

2. SUMMARY OF RECENT PROGRESS

This section presents a brief summary of recent progress; more detailed descriptions of selected portions are contained in the next section.

SECTION I: ELECTROMAGNETICS

A. Time-Harmonic Fields

(1) *Wave Coupling into Large Enclosures*

One phase of our investigations aimed at understanding propagation in rather general environments, especially at high frequencies, has been concerned with wave coupling into enclosed guiding regions via openings in the enclosure. Our goal here, as in all of our model studies, is to arrive at a "good" parameterization of complicated propagation and diffraction phenomena. Good parameterizations are stable under perturbation and can therefore be extended from an idealized prototype to more general configurations belonging to the same phenomenological class. From this perspective, we have examined in detail the coupling of a plane wave into a large open-ended parallel plane waveguide. Although this problem is classical, we have asked new questions, especially within the framework of our self-consistent hybrid ray-mode format, which is a crucial constituent in the good parameterization scheme. Selected results are summarized in Section 3. A similar study of plane wave coupling into an open-ended circular waveguide is nearing completion.

(2) *Complex Rays and Beams*

The virtues and limitations of complex ray and paraxial Gaussian beam (GB) theory continue to be explored for pertinent model problems, with emphasis on questions relating to algorithm implementation, and also with respect to a *novel* usage of GB's as basis elements in rigorous field representations spanning a *discretized* (configuration)-(wavenumber) phase space [1,2]. A detailed prototype study of the complex ray method for beam reflection near critical incidence has been completed and published [3].

B. Transient Fields

Our general spectral theory of transients (STT) [4], which represents transient wave phenomena as superpositions, over *spatial* wavenumber spectra, of *transient plane waves* instead of the usual decomposition into, and reconstruction via, time-harmonic wave fields, has been applied to pulsed input signals, especially those generating pulsed focused beams. The analysis for one such input, the complex source pulsed beam, is described in more detail in Section 3. The analysis for another, the focus wave-mode, is nearing completion.

C. Effects of Random Media

This new phase, which was introduced in the previous progress report and which has been supported by the Rome Air Development Center under a special fund (but administered through JSEP), addresses the modification of high frequency propagation and diffraction phenomena when the ambient propagation medium undergoes weak large-scale random fluctuations. Such effects are important for millimeter and optical wave propagation in the atmosphere, and in other environments with properties so complicated as to require statistical treatment. Our aim has been to construct a new stochastic geometrical theory of diffraction (SGTD) which attempts to merge the constructs of deterministic GTD with the stochastic modifications introduced by the fluctuating medium.

Formulation of the theory has been completed, and we have shown how it would be applied to reflection from, and refraction through, curved interfaces, to edge diffraction, and to diffraction by small scatterers embedded within the fluctuating environment [5-7]. A comprehensive manuscript is in preparation. The theory, which embodies approximations, must now be tested by numerical experiments and comparisons with other solutions (if they exist) or with experimental data. This work is presently in a (hopefully temporary) state of suspension because Dr. R. Mazar, a visiting post-doctral scientist who provided the expertise in random propagation theory, has now returned to his home country (Israel).

3. STATE OF THE ART AND PROGRESS DETAILS

A. Background

Many electromagnetic propagation environments, whether natural or man-made, are so complicated that direct solution of the field equations to determine signal characteristics is beyond the scope of present analytical and computational capabilities. At high frequencies, propagation can be localized and approximated as ray fields which undergo reflection, refraction and/or diffraction on their path from a source at S to an observer at P. While ray theory provides a fundamental view of the propagation process by tracking local plane wave fields emanating at the source, such tracking becomes cumbersome when many ray paths exist between S and P. It would therefore be desirable to deal with multipath effects *collectively*. In guided propagation *along* a refracting channel, rays may form caustics (convergence or focusing zones of enhanced field strength) where simple ray theory fails. When these caustics are sufficiently distinct, one may correct ray theory by uniform asymptotic transition functions, but situations arise for rays with many reflections where an accumulation of caustics makes such corrections impractical and even impossible. Here, again, a collective alternative to multiple ray reflections, for example, by employing guided modes, is desirable or actually necessary. However, the modal approach to ducted propagation is beset with similar difficulties when

the required number of modes is large. It would then be useful to express the interference properties of clusters of modes collectively in terms of simpler events.

The preceding discussion makes evident the importance of collective treatment of mode or ray fields when many of these are required to synthesize the signal in a particular transmission or guided propagation channel, or when failures in approximate mode or ray theory make these descriptions inapplicable. Substantial progress in this direction has been made through the new *hybrid ray-mode* theory developed by us. It has been shown how clusters of ray fields excited by a localized source can *rigorously* be converted into clusters of guided mode fields plus a (usually small) remainder, and vice versa. The theory has been applied to a series of "canonical" problems involving guided electromagnetic propagation along concave surfaces (here, the guiding mechanism is provided by "whispering gallery" effects), in tropospheric ducts, in plane parallel homogeneously filled waveguides, and in graded index waveguides. The theory has also had impact on other fields such as underwater acoustic propagation and, with generalization to time-dependent signals, the modeling of seismic events. Concern in these applications has been with the greater computational efficiency of the hybrid formulation, with the avoidance of singular regions in ray fields or mode fields by filling these regions with mode fields or ray fields, respectively, and also with the penetrating physical insight of the propagation mechanism provided by the hybrid method. The collective approach linking ray fields and mode fields has been applied also to the complex spectra emitted by a source at a complex location. Such a source generates in physical space a Gaussian beam, and therefore makes the important class of beam propagation and diffraction problems amenable to the hybrid format. When a guiding environment exhibits weak variations *along* the guiding direction, the constructs above are generalized, by localization, to accommodate adiabatically adaptive wave phenomena. This has been formalized in our intrinsic mode and scaled spectrum theory. All of these accomplishments have been documented in a comprehensive series of publications, cited in previous reports.

B. Selected Results

(1) *Rays, Modes and Beams for Plane Wave Coupling into a Wide Open-Ended Parallel-Plane Waveguide*

A plane wave incident obliquely onto the open end of a wide parallel-plane waveguide generates an interior field that resembles a geometric optical sheet beam whose initially well-defined shape gets diffused after undergoing multiple reflection. This behavior can be confirmed, but not physically well explained, from numerical results obtained by summing over the aperture-excited guided modes. A phenomenologically incisive representation (a good parameterization) is obtained by subjecting the guided mode sum to partial Poisson summation that yields an exact hybrid field comprising the multiple reflected geometric optical beam, some multiple reflected edge-diffracted rays, some guided modes,

plus remainder terms. Asymptotic approximations reduce these exact forms to the wave constituents of the nonuniform and, when required, uniformized geometrical theory of diffraction. These basic features are illustrated by numerical results presented for various parameter regimes. They delineate the ranges of applicability of the asymptotic forms and also the relative importance of the individual wave contributions. In the parameter range where geometrical features of the field can still be resolved, the hybrid form is not only physically appealing but also numerically more efficient than alternatives involving only rays or only modes.

The physical configuration is shown in Fig. 1, which also schematizes the relevant ray phenomena (Fig. 1a), the physical optics (PO) method employed for calculation of the reference solution by modal summation, and the decomposition of a typical guided mode into four modal ray congruences. The edge diffracted ray fields are decomposed into four ray species in a similar manner. The hybrid ray-mode decomposition is schematized in Fig. 2. It shows the multiply reflected geometric optical (GO) beam and also the multiple reflected edge diffracted ray fields, which can be taken to arrive from an array of image sources (Fig. 2a); the total field calculated in this manner can be converted into the complete set of guided modes. For the hybrid form, only the *relevant* ray fields are converted (Fig. 2b); their departure angles lie in the shaded sections. Figures 3 and 4 show typical results obtained by the strategies. Details may be found in reference 8.

(2) *Complex-Source Pulsed Beams*

By assigning complex values to the source coordinates and pulse-initiation time of the time-dependent Green's function in free space, one may generate a new exact field solution that behaves like a propagating pulsed beam. Although the conventional pulsed line source response is known in closed form, the complex extension cannot be performed directly thereon because of the nonanalytic behavior of the causal field. The analytic continuation has been carried out by spectral analysis and synthesis, utilizing the recently formulated spectral theory of transients (STT) [4]. This approach not only guarantees uniqueness but also elucidates the spectral content of the resulting waveform, which is composed of contributions from singularities in the complex spectral wave-number plane. The new pulse solution is of interest not only in free space but also, by similar analytic extension of time-dependent Green's functions in more complicated environments, for the direct construction of the transient field produced in these environments by the incident pulsed beam.

We exemplify construction of the solution for the two-dimensional case in a $\varrho = (x,z)$ coordinate system. The conventional time-dependent Green's function for real (ϱ',t'), where $\varrho'=(x',z')$ is the source location and t' is the source initiation time, is known to be given in closed form by

$$G(\varrho,\varrho',t,t') = \frac{1}{2\pi\Delta} H\left[t - t') - s/v\right], \quad \Delta = \left[(t - t')^2 - (s/v)^2\right]^{1/2}. \quad (1)$$

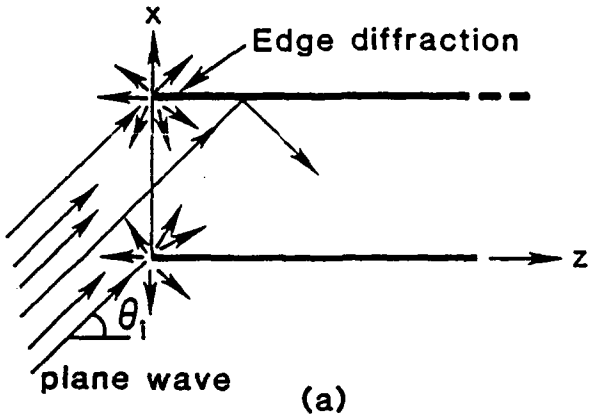

(a)

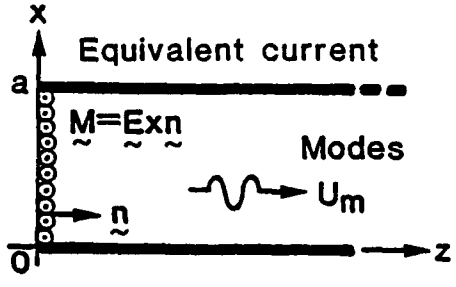

(b)

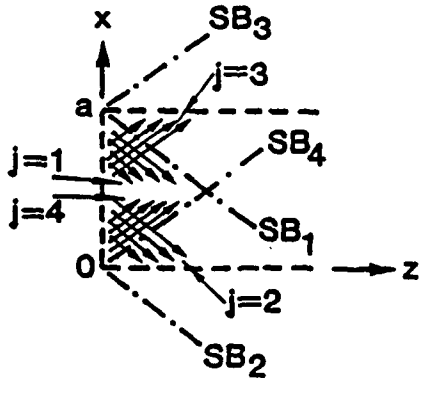

(c)

Fig. 1 Plane wave excitation of open-ended parallel-plate waveguide.
(a) Physical configuration and GTD schematization of waveguide mode excitation.
(b) PO formulation in terms of equivalent magnetic currents M_y on a perfect conductor closing the waveguide aperture at $0 \leq x \leq a$, $z=0$.
(c) Modal congruences $j=1,\ldots,4$ and their shadow boundaries SB_j.

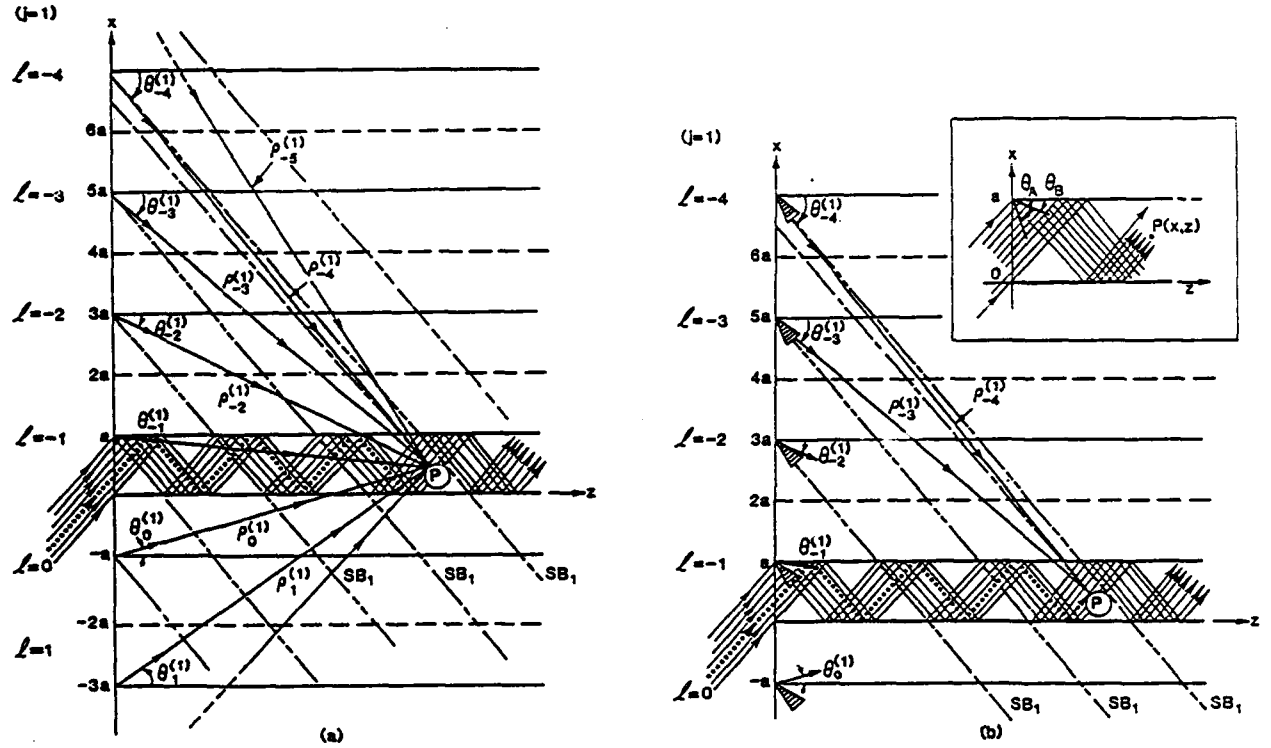

Fig. 2 GO beam due to all species, and image construction of multiple reflected edge-diffracted rays for ray species j= 1. SB_1 denotes the shadow edge of the multiple reflected truncated plane wave; the GO ray contribution at P due to this wave is shown as ——·——.
(a) Full conversion of modes to rays through Poisson sum formula; all multiple reflected rays are required.
(b) Partial conversion of modes u_m, $M_1 \leq m \leq M_2$, to rays; only those rays whose departure angles $\theta_1^{(1)}$ lie in the shaded interval $\theta_A \leq \theta \leq \theta_B$ are necessary.

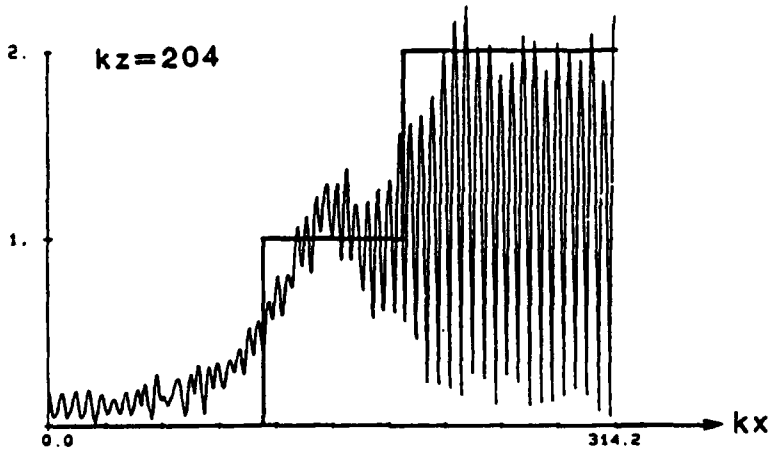

Fig. 3 Field magnitude along cross section kx=204 in a waveguide with normalized width ka=100π, where k is the wavenumber. 100 modes can propagate here. Plane wave incidence angle θ_i=30°. The reference solution (solid curve) is generated by mode summation. The rectangular trace outlines the GO beam.

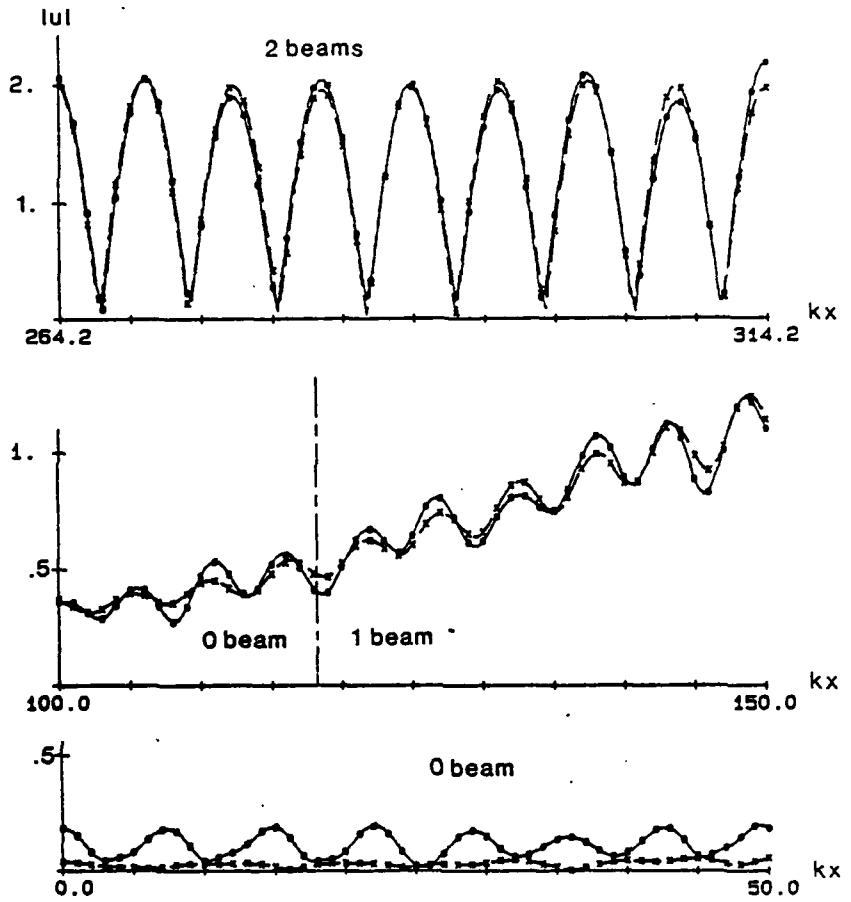

Fig. 4 Detailed fields over portions of the cross section in Fig. 3. GO beam regions are indicated. *Solid curve: 100 modes. Dashed curve* (hybrid): 4 rays + 40 modes.

Here $H(\alpha)=1$ or $H(\alpha)=0$ for $\alpha>0$ or $\alpha<0$, respectively, v is the wave propagation speed in the (nondispersive) medium, and

$$s = \left[(x-x')^2 + (z-z')^2\right]^{1/2} \tag{2}$$

is the distance from $\underline{\rho}'$ to the observer at $\underline{\rho}$.

When the source location $\underline{\rho}'$ is made complex, direct substitution into the closed-form expression for the time-harmonic free-space Green's function $\hat{G}(\underline{\rho},\underline{\rho}',\omega)$ is known to generate at real observation points $\underline{\rho}$ a closed-form field that behaves like a Gaussian beam. The proper analytic continuation of the complex distance s in Eq. (2) from real to complex values is easily established in this case. However, for the causal transient field in Eq. (1), the interpretation of complex $\underline{\rho}'$ and (or) t' substitution is less obvious. The problem can be resolved by the spectral analysis and synthesis route of STT. We choose

$$x' = 0, \quad z' = ib, \quad b > 0, \tag{3}$$

which, under time-harmonic conditions, is known to generate a beam field with maximum along the z axis, waist at $z=0$, and beam width determined by b (Fig. 5). For the time-dependent case, we also assign the complex value

$$t' = ib/v \tag{4}$$

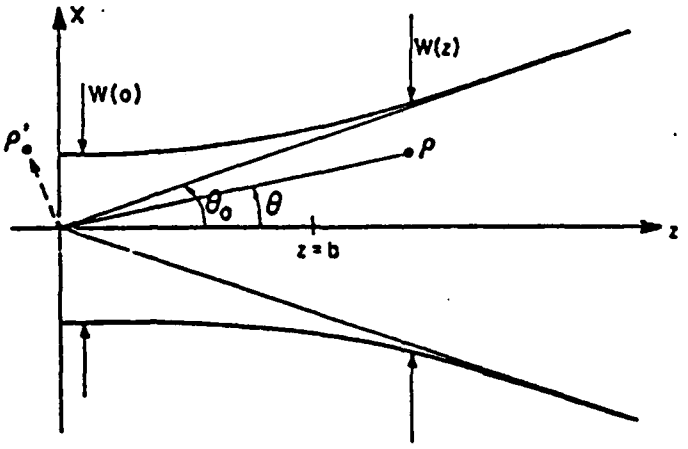

Fig. 5 The z-directed beam generated by a time-harmonic line source at the complex location $\underline{\rho}'=(x',z')=(0,ib)$. The complex source location is schematized by a dashed line. The parameter b is related to the beam width at the waist by $W(0)=(b/k)^{1/2}$. At any location z, the beam width is $W(z)=W(0)[1+(z/b)^2]^{1/2}$.

to the source-initiation time.

By STT, the source-excited transient field is synthesized as a spectrum of source-excited transient plane-waves $A(\xi)/[t-t'-\tau(\xi)]$, where ξ is the spatial wavenumber corresponding to the x-coordinate. Explicitly [9]

$$G = \mathrm{Re}\, G_+^+ \tag{5}$$

where

$$G_+^+(t) = \sum_{\hat{\xi}(t)} - \frac{1}{\pi} \frac{A(\hat{\xi})}{\tau'(\hat{\xi})}$$

$$+ \frac{1}{2\pi^2} \int_1^\infty \left[\frac{A(\xi)}{t-t'-\tau(\xi)} - \frac{A(\xi^*)}{t-t'-\tau(\xi^*)} \right] d\xi \,, \tag{6}$$

and

$$\tau(\varrho,\varrho';\xi) = \frac{1}{v} \left[(x-x')\xi \pm (z-z')\sqrt{1-\xi^2} \right] \,, \quad z \gtrless z' \,, \tag{7a}$$

$$A(\varrho,\varrho';\xi) = \frac{1}{2\sqrt{1-\xi^2}} \,. \tag{7b}$$

The integral in (6) may be evaluated in terms of the singularities of the integrand in the complex ξ plane. These involve the singularities of A and τ, and the time-dependent poles $\hat{\xi}(t)$

$$\tau[\hat{\xi}(t)] = t-t' \tag{8}$$

that describe the transient local plane waves arriving at the observer at time t. The two roots of Eq. (8) are

$$\xi^\pm = \left[(x-x')(t-t') \pm i(z-z')\Delta \right] v/s^2 \,. \tag{9}$$

where

$$\Delta = \left[t^2 - \left(\frac{\rho}{v}\right)^2 - 2i\frac{b}{v}\left(t - \frac{\rho}{v}\cos\theta\right) \right]^{1/2} \,,$$

$$-\pi < \arg\Delta \leq 0 \tag{10}$$

and

$$s = (\rho^2 - b^2 - 2ib\rho\cos\theta)^{1/2} \,, \tag{11}$$

with

$$\mathrm{Re}\, s \geq 0 \tag{12}$$

Here, $\rho \equiv (x^2+z^2)^{1/2}$ and $\theta \equiv \sin^{-1}(x/\rho)$. The integral can now be reduced to

the closed form

$$G(\rho,\rho';t,t') = \mathrm{Re}\left[\frac{1}{2\pi\Delta}\left(1+\frac{1}{\pi i}\log\frac{t-t'+\Delta}{s/v}\right)\right], \qquad (13)$$

with

$$-3\pi/2 < \mathrm{Im}\log \leq \pi/2 \ . \qquad (13a)$$

This result constitutes the *unique* analytic continuation of (1) from real to complex source coordinates.

The waveform generated in this manner has the characteristics of a pulsed beam in the $z>0$ region, which is of concern here (see Fig. 6). The field peaks at approximately $t=\rho/v$, preceded by a weak precursor. The strongest peaks occur near the z-axis and reach a maximum on axis. Additional details pertaining to the physical behavior of this pulse, as well as pulse shapes generated by other choices of parameters and alternative analytic continuation of the complex distances, may be found in reference 9. The three-dimensional version of the complex space-time source coordinate substitution has been explored as well.

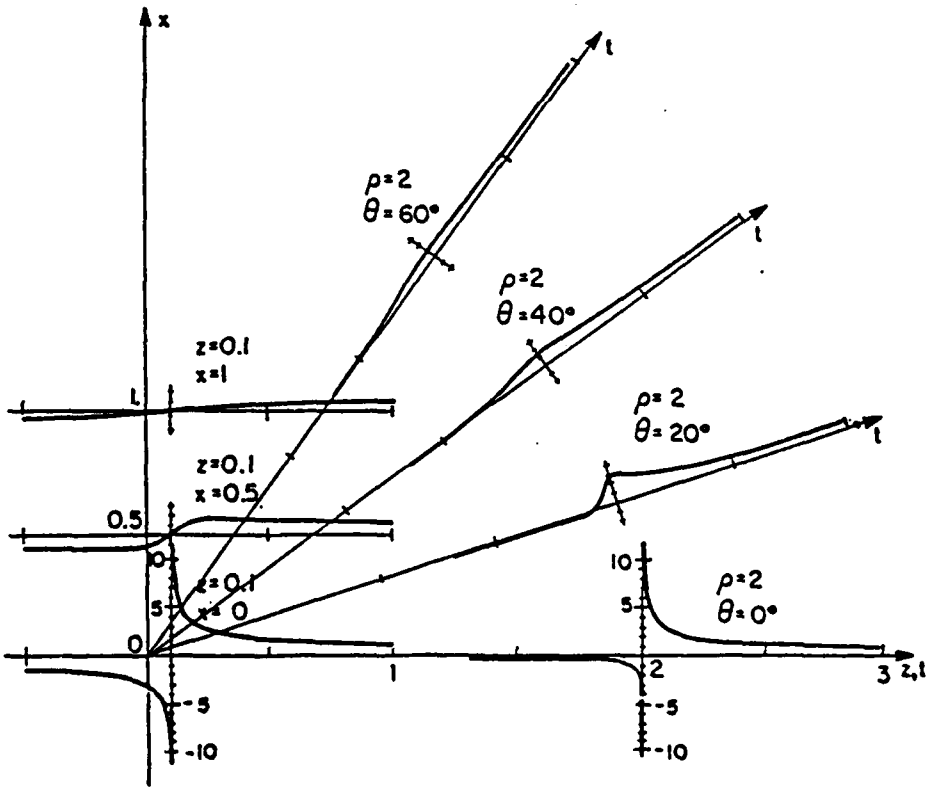

Fig. 6 Pulsed-beam waveform at various observation points z/b=0.1, near the initial plane, and in the far zone $\rho/b=2$. The waveform is normalized to (b/v)G. The normalized time (v/b)t and space coordinates (x/b, z/b) are drawn to the same scale.

The pulsed beams described above are unique in that they represent analytic continuations of Green's functions. It is therefore suggestive that they may be useful for synthesis of more general source distributions designed to create well-focused fields. This is presently under investigation. As already mentioned, another important attribute is the ability to generate *directly*, again by extension to complex (ϱ', t') coordinates, the response to the pulsed beam in any environment from the impulse response in that environment.

4. REFERENCES

1. P.D. Einziger, S. Raz and M. Shapira, "Gabor Representation and Aperture Theory," J. Opt. Soc. Am. A3, p. 508-522 (1986).

2. J.J. Maciel and L.B. Felsen, "On Gaussian Discretization of Radiation from Distributed Aperture Fields," paper presented at AP-S/URSI Symposium, Virginia Polytechnic (1987).

3. I.T. Lu, L.B. Felsen, Y.Z. Ruan and Z.L. Zhang, "Evaluation of Beam Fields Reflected at a Plane Interface," IEEE Trans. Ant. Propagat., AP-35, p. 809-817 (1987).

4. E. Heyman and L.B. Felsen, "Weakly Dispersive Spectral Theory of Transients: I-Formulation and Interpretation; II-Evaluation of the Spectral Integral," IEEE Trans. Ant. Propagat., AP-35, p. 80-86 and p. 574-580 (1986).

5. R. Mazar and L.B. Felsen, "Edge Diffraction of High Frequency Coherence Functions in a Random Medium," Opt. Letts., 12, p. 46-48 (1987).

6. R. Mazar and L.B. Felsen, "Geometrical Theory of Diffraction for High Frequency Coherence Functions in a Weakly Random Medium," Opt. Letts., 12, p. 146-148 (1987).

7. R. Mazar and L.B. Felsen, "Stochastic Geometrical Theory of Diffraction in a Random Medium with Inhomogeneous Background," Opt. Letts., 12, p. 301-303 (1987).

8. H. Shirai and L.B. Felsen, "Rays, Modes and Beams for Plane Wave Coupling into a Wide Open-Ended Parallel-Plane Waveguide," Wave Motion. 9, p. 301-317 (1987).

9. E. Heyman and B.Z. Steinberg, "Spectral Analysis of Complex Source Pulsed Beams," J. Opt. Soc. Am., A4, p. 473-480 (1987).

SECTION II:
SOLID STATE

A. X-RAY COUPLED WAVE INTERACTIONS AT CRYSTAL SURFACES

Professors H.J. Juretschke and B. Post

Unit SS7-1

1. OBJECTIVE(S)

To use the multiple interaction of x-rays in a Bragg geometry in order to develop simple and compact methods for obtaining direct phase information about the crystal scattering factors, and for characterizing the mode structure; to extend the interactions to include coupling to other waves that can modify the mode structure, and that can be used to explore nonlinear interactions of x-rays; and to understand the local x-ray fields in the immediate surface region of the solid, as well as the effect of stringent boundary conditions on all modified x-ray waves, especially those originating in the interior. High resolution x-ray diffraction experiments will be supported by theoretical studies of the predictions of n-beam dynamical theory, and by rigorous extensions of the theory to include the coupling with other waves.

2. SUMMARY OF RECENT PROGRESS

The progress made by the two investigators in this unit is summarized separately below.

The main research on the dynamical theory of coupled wave phenomena for x-rays (H.J. Juretschke) has concentrated on probing the validity of the approximate n-beam formulation developed earlier [1] in the presence of deviations from the perfect periodicity which forms the usual underlying starting condition for most dynamical effects. This work establishes the framework for applying the theory to real crystals, and at finite temperatures. In addition, that theory has been expressed explicitly for applying corrections to high precision structure factor determinations due to the neighboring n-beam interaction regions. High precision experimentation has now reached the point where such corrections cannot be ignored. As to earlier work, the two papers discussed in last year's report have not been published [2,3].

Two papers dealing with the experimental determination of x-ray reflection phases have been published in 1987. These dealt with the determination of the phases of ultra weak reflections [4] and with the optimization of experimental conditions for enhancing the visibility of phase indications [5]. Two additional papers dealing with the determination of the phases of reflections from acentric organic crystal (benzil), are being prepared for publication.

3. STATE OF THE ART AND PROGRESS DETAILS

A. Theory (H.J. Juretschke)

(1) *The Effect of Thermal Phonons on Diffraction Near an n-Beam Point*

Two of the lines of investigation we have been developing previously have been combined in this study. These are: the theory of diffraction near an n-beam point; and the effect of phonons on the dynamical diffraction of x-rays. The main result of the first line of research has been that the first order corrections due to the presence of the n-beam point can be taken into account fully within the traditional two-beam formulation merely by modifying both the structure factors and the origin of the dispersion surface (Lorentz point) of the pure two-beam case. The major result of the second line of research is the incorporation of phonons within a self-consistent dynamical approach, such that phonon-excited x-ray fields are also fully dynamical.

The influence of phonons on diffraction near an n-beam point is of interest for a number of reasons. Since phonons destroy the translational periodicity of a perfect crystal, such a study is a test of how many of the dynamical features predicted by theory for a perfect crystal survive when the perfection is reduced, either by phonons or by the practically equivalent deviations from periodicity caused by weak mosaic structure. In addition, such a study can make quantitative predictions about the influence of temperature on diffraction when more than one structure factor is involved. It is common practice in that case to assign a Debye-Waller factor correction separately to each structure factor, although the validity of this practice has apparently never been investigated in detail. It is most likely based on the argument that for incoherent thermal phonons all multiple scattering effects between different diffracting planes average out to zero. Finally, such a study also sheds light on how the modified two-beam formulation of diffraction near an n-beam point is affected by temperature, and in what manner it may need to be renormalized at each temperature.

It has now been shown in our study that phonons can be incorporated in the modified two-beam formulation without any complications, and that the main results of their presence are:

a) The intrinsic modified two-beam parameters of diffraction (structure factors, absorption, etc.) remain completely the same as in the absence of phonons, just as in a pure two-beam case. The only change is that, just as in that case, there appear Debye-Waller factors and thermal diffuse scattering.

b) The Debye-Waller factor is entirely that of the primary two-beam interaction, and is a prefactor of the modified structure factor. The other two-beam structure factors contributing to this modified structure factor show no additional temperature softening. Hence none of the fine structure in diffraction associated with the modified structure factor disappears in the presence of phonons, but is merely broadened in the manner characteristic

of all temperature effects in two-beam diffraction.

c) Since the above is true for deviations from periodicity caused by weak mosaic structure (thermal phonons are practically static on the time scale of x-rays). Hence, certainly mildly imperfect crystals are expected also to show all the diffraction fine structure of perfect crystals, suitably broadened by characteristic averaging. Of course, since this averaging may involve a distribution of asymmetric line features, some of this asymmetry may become obscured.

The underlying reason for the above results is that phonon-excited x-rays near an n-beam situation are also subject to n-beam interactions, and that the many more coherent coupling channels existing here undergo cancellations leading to a net effect due to the primary interaction alone.

It is concluded from this study that both thermal and mosaic effects can be handled in the neighborhood of an n-beam point entirely in the traditional two-beam fashion, but now with respect to the modified two-beam parameters. Therefore, the dynamical theory of these effects is not confined to perfect crystals, as already established experimentally (e.g. see Ref. 6). This work has been accepted for publication in Acta Crystallographica. A preliminary report of it was presented at the 14th International Congress of Crystallography in Perth, Australia, in August 1987.

(2) *Corrections Due to Multple Beam Interactions in High Accuracy Two-Beam Structure Factor Determinations*

Recently there has been increased activity in the determination of two-beam structure factors to high accuracy, as a means of studying electron distributions in chemical bonds of valence crystals such as Si. At the 0.1% level of accuracy, it becomes necessary to take into account a number of corrections, among which is the contribution from neighboring multiple interaction points.

Our previously developed theory for the asymptotic effects of such interactions gives a full prescription for the needed corrections, which is quantitative, and which can be easily carried out once the relative location and identification of the neighboring interaction points are known. Hence it was considered worthwhile to formulate such a correction procedure as an explicit application of the theory. As applied to recent measurements of Si(12 12 0) with AgK_α radiation [6], it predicts, under the most favorable circumstances, corrections at least of the order of 0.1%. However, since in the tradition of most such measurements, no information is supplied about the exact orientation of any two-beam experiment in reciprocal space, it is difficult to apply the method to a specific situation, in which it is likely that the corrections would in fact be larger. But the sample computation makes clear that such corrections cannot be ignored at the 0.1% level; in order to be applied, of course, the experimental information must include a full indexing of all neighboring multiple interaction points. It is hoped that as a result of this study, such information will be provided routinely in future experimental work.

This work was presented at the "Accuracy in Structure Factor Determination" Symposium in Warburton, Victoria, Australia, in August 1987. It will be published in the Australian Journal of Physics.

B. Experimental (B. Post)

During the past year we have continued our investigation of relevant variables involved in the experimental determination of x-ray reflections phases. The sensitivity of our procedures has been demonstrated by determining the phases of the very weak "forbidden" reflections of germanium, using CuKa1 radiation. Invariant triplets of germanium reflections were generated in n-beam patterns. Each triplet included two strong reflections whose phases were known, in addition to the one "forbidden" reflection. Triplet phases were clearly displayed in the asymmetric line profiles of the n-beam interactions; subtraction of the pairs of known phases yielded the phases of the corresponding forbidden terms [4].

Experimental conditions for optimizing the phase indications shown in n-beam patterns have also been studied.

Large numbers of phases of acentric organic crystal (benzil) have been determined using CuKa1 and CrKa1 radiations. The experimental findings correspond satisfactorily with phases calculated from published data. They indicate that experimental values of phase angles of individual reflections can be determined to $\pm 45°$, or and possibly to $\pm 30°$. Providing that information to crystallographers should make possible the determination of many crystal structures which have resisted solution up to the present.

4. REFERENCES

1. H.J. Juretschke, Acta Cryst. A40, 449 (1984).
2. H.J. Juretschke and F. Wasserstein-Robbins, Phys. Rev. B35, 4010 (1987).
3. H.J. Juretschke, Phys. Rev. B35, 4018 (1987).
4. B. Post and J. Ladell, Acta. Cryst. A43, 173-179 (1987).
5. B. Post and W. Kiszenick, Acta. Cryst. A43, 568-572 (1987).
6. S.A. Kshevtskii, I.P. Mikhailyuk and M.I. Polyak, Sov. Phys. Cryst. 30, 145 (1985).
7. M. Deutsch and M. Hart, Phys. Rev. B31, 3846 (1985).

B. MICROSTRUCTURE PHOTOPHYSICS

Professor S. Arnold and K.M. Leung

Unit SS7-2

1. OBJECTIVE(S)

Our objective is to develop a quantitative understanding of the detailed interaction of electromagnetic radiation with microstructures of dimensions (a) comparable to and much less than the wavelength (λ) of the incident radiation. In some cases the broad features of this interaction, and especially the enormous resonant enhancements, may be understood qualitatively by using a classical model for the local electromagnetic field (e.g., surface enhanced Raman scattering) [1]. In others this approach has not proven to be fruitful (e.g., enhanced photoemission from small Ag particles) [2]. The lack of a cohesive framework must in part be due to the limitations of the current classical model in the face of the properties of real materials and structures. Unfortunately careful attention has not been paid to these limitations. This neglect has usually been dictated by experimental bounds or by theoretical limitations. But, at this time, a fuller understanding of the limitations, and, by implication, a more systematic exploitation of their remarkable consequences, rests precisely on more attention to detail and on quantitative comparison of experiment and theory.

Here we propose such a study, relying on tight interplay between theory and experiment, that emphasizes both far field and near field features such as elastic scattering and fluorescence, on single structures of fully characterized geometry, and extending into a limit $a/\lambda << 1$ where particle properties are expected to deviate from their macroscopic behavior.

In the coming period *special emphasis* will be placed on *nonlinear processes.* This is an especially challenging area since nonlinear theory for the interaction of radiation with a particle of a generalized size is virtually nonexistent. However, in the particular case of spherical particles, and most probably for particles of other regular morphologies, resonances having unprecedentedly high Q's have been detected. Thus the field strength within a particle even in the presence of a laser of modest power easily produces a sizable nonlinear effect. For example, just this last period we have demonstrated Optical Bistability with a threshold intensity in the W/cm^2 range [3]. More will be said about this effect in the summary. All of our work thus far implies that this area is fertile for both basic and practical results. On the practical side we see a new technology evolving, *Microparticle Photonics.*

2. SUMMARY OF RECENT PROGRESS

This section presents a brief summary of recent progress; more detailed descriptions are contained in the next section in conjunction with the state of the art so that the nature of the contributions can be understood more clearly.

The program in Microstructure Photophysics is composed of two interactive parts. Experiments are carried out at the Microparticle Photophysics Laboratory (MP^3L) under the direction of S. Arnold, while theoretical work on associated phenomena is carried out by K.M. Leung. We have been fortunate during the past year in as much as the group has grown by one member (L.M. Folan) and the laboratory has been enlarged to include a dynamics component with measurement capabilities down to a few picoseconds. This past year has been particularly productive in two major areas which will be discussed below (Secs. 2A and 2B). In addition the past year has brought further independent funding for the experimental and theoretical studies from NSF (to S. Arnold and L.M. Folan) and ONR (to K.M. Leung), respectively. .

A. Rayleigh Particle Optical Bistability (OB)[4]

The primary report predicting Rayleigh particle OB in semiconductors is now published. Over this last year these calculations have been extended to a nonspherical particle where Optical Tristability is found. Although our work is seminal in this area, a number of workers are currently jumping into the fray. A review of the past year's theoretical progress in different labs will be discussed in Section 3.

B. Mie Particle Optical Bistability [3]

In A. the work is theoretical. The insights gained from these models have been used in the MP^3L to provide the first demonstration of microparticle OB. This work has recently been published, and a patent disclosure is in progress. Work over the last year has taken our initial single resonance model for the optical bistability of a cloud droplet and extended it to multiple resonances through a model which can be considered nearly comprehensive.

A number of other research projects which are relevant to the above have been investigated during the year and have led to additional publications. In all the publications already credited to JSEP for the current contract are:

1. K.M. Leung, "Propagation of Nonlinear Surface Polaritons," Phys. Rev.A, 31, 1189 (1985).

2. S. Arnold, E.K. Murphy, and G. Sageev, "Aerosol Particle Molecular Spectroscopy," Appl. Opt., 24, 1048 (1985).

3. K.M. Leung, "Aerosols of Anisotropic Metallic Microparticles as Artificial Kerr Media," Opt. Lett., 10, 347 (1985).

4. A.B. Pluchino and S. Arnold, "A Comprehensive Model of the Photophoretic Force on a Spherical Microparticle," Opt. Lett., 10, 261 (1985).

5. L.M. Folan, S. Arnold and S.D. Druger, "Enhanced Energy Transfer within a Microparticle," Chem. Phys. Lett., 118, 322 (1985).

6. S. Arnold and N. Hessel, "Photoemission from Single Electrodynamically Levitated Microparticles," Rev. Sci. Inst. 56, 1066 (1985).

7. K.M. Leung, "P-Polarized Nonlinear Surface Polaritons in Materials with Intensity Dependent Dielectric Functions," Phys. Rev. B, 32, 5093 (1985).

8. K.M. Leung, "Optical Bistability in the Scattering and Absorption of Light from Nonlinear Microparticles," Phys. Rev. A 33, 2461 (1986).

9. S.Arnold and L.M. Folan, " A Fluorescence Spectrometer for a Single Electrodynamically Levitated Microparticle," Rev. Sci. Inst., 57, 2250 (1986).

10. S. Arnold, K.M. Leung and A.B. Pluchino, "The Optical Bistability of an Aerosol Particle," Opt. Lett. 11, 800 (1986).

11. K.M. Leung and He Ming-Guo, "Tristable Optical Behavior of Anisotropic Rayleigh-sized Microparticles," Submitted to J. Wave-Material Interaction.

12. S.D. Druger, S. Arnold, and L.M. Folan, "Theory of Enhanced Energy Transfer between Molecules Embedded in Spherical Dielectric Microparticles," J. Chem. Phys. 87, 2649 (1987).

13. S. Arnold, and L.M. Folan, "A Spherical Void Electrodynamic Levitator," Rev. Sci. Inst. 58, 1732 (1987).

14. L.M. Folan and S. Arnold, "Determination of Molecular Orientation at the Surface of an Aerosol Particle by Morphology Dependent Photoselection," Opt. Lett. (Jan.-88).

15. S. Arnold, "Spectroscopy of Single Levitated Micron Sized Particles," in Optical Effects Associated with Small Particles Eds. P.W. Barber and R.K. Chang (World Scientific Publishing, 1988).

3. STATE OF THE ART AND PROGRESS DETAILS

The area of nonlinear physics is concerned with physical phenomena that are based on a nonlinear response of a medium to incident electromagnetic radiation. The nonlinearities responsible for most of these phenomena in the past are often quite weak and therefore the processes involved are actually quasi-linear. Consequently, theoretical threatments have been almost exclusively perturbative in nature, and experimentally, no minimum threshold powers are needed to see these effects.

Recently there are growing interests in *intrinsically* (or fully) nonlinear interactions of electromagnetic radiation with matter. The nonlinearities appearing in the dielectric function are rather strong and Maxwell's equations become a set of coupled nonlinear partial differential equations. Calculations of these effects must be carried out in a fully *non-perturbative* fashion. The arsenal of mathematical techniques such as Green's functions, Fourier transforms and integral equation methods, which are so successful in dealing with linear problems, are totally incapable of treating these intrinsically nonlinear physical phenomena. The associated effects are not merely small extensions of the linear or quasi-linear ones, but must be regarded as separate entities with characteristic behavior such as hysteresis and switching, having no counterpart what-soever in the linear limit. With the incident field as an extra physically controllable parameter, which actively and quite spontaneously changes the effective value of the dielectric function of the medium, a host of entirely new phenomena are possible.

The distinct nature of nonlinear effects is especially true in the case of interactions of intense electromagnetic radiation with microstructures where such effects are expected to be enhanced owing to two separate mechanisms. The first is the so-called dielectric confinement or local field effect which increases the local field intensity in the neighborhood of microstructures when the frequency is close to the surface plasmon or morphological resonances. This mechanism is responsible for the sizable enhancement of a variety of linear processes, such as surface enhanced Raman scattering [1], as well as nonlinear processes, such as the lowering of thresholds for lasing [5] and optical switching [4]. It is advantageous to have high local intensity especially for nonlinear processes since the magnitudes of the effects go up faster than linearly with intensity. The second mechanism has to do with the fact that nonlinearities in microcrystals and microparticles can actually be much larger than those found in bulk materials. This is due to electronic localization or quantum size effects, which are responsible for a host of unusual phenomena, including enhanced nonlinearities, even at room temperature, in semiconductor heterojunctions and superlattice structures [6]. The electrons and holes are squeezed into a two dimensional space. In the case of microparticles electrons are confined on all sides by the boundaries and therefore they are expected to behave more like zero-dimensional objects or quantum dots, with enhanced exciton lifetime.

Our research in this exciting new area has resulted in some very encouraging results which will be discussed below. Our work has been followed up by

others, especially the group at Bell Laboratories [7].

A. Rayleigh Particle Optical Bistability (OB) and Optical Tristability (OT)

For a given optically nonlinear material the OB behavior of a spherical Rayleigh particle can only be controlled with the intensity and the frequency of the incident light. In order to increase the capability of *microparticle photonics,* we want to investigate more complex microparticle devices. For this purpose we have recently extended our work on the OB of spherical Rayleigh particles to nonspherical (spheroidal) particles [8].

We find that because of their additional physical characteristics, such as the particle shape and the orientation of the particle with respect to the incident light, spheroidal particles are capable of exhibiting a much richer class of intrinsically nonlinear behavior. Depending on the frequency of the incident light and the particle shape and orientation, we find that, besides OB behavior, a total of five different types of optical tristability (OT) behaviors are possible. The regions in parameter space where these five (iv) types of OT behaviors occur are shown in Fig. 1 for fixed particle shape. Region (vi) where only OB can exist, and region (vii) where the internal intensity is a single-valued function of the incident intensity are also shown.

We should also point out that nonspherical particles do exist, and can be found in the earth's atmospheres, interplanetary space, and in interstellar media. In addition such particles can be fabricated in the laboratory. In fact a two dimensional array of silver particles each shaped as an ellipsoid of revolution has been made a number of years ago for the study of surface enhanced Raman scattering [9]. In addition Ashkin has demonstrated that such particles can be constructed through optical levitation [10].

B. Mie Particle Optical Bistability [3]

Unlike the Rayleigh particle we require no frequency dependence in the dielectric function to insure field enhancement in the Mie case. Resonances are assured by the phase matching of waves which circumnavigate the perimeter of the particle. Indeed these resonances may have Q's greater than 10^6 [11]. Consequently, the field enhancements within the particles are projected to be enormous. One recent article calculates the field at the surface of a particle several microns in size to be 9 orders of magnitude larger than the field of the wave incident on the particle(under resonant conditions) [12]. Thus a slight change in the dielectric function, size or shape of the particle with intensity can lead to catastrophic effects. This is best demonstrated by our work on a simulated cloud droplet.

A cloud droplet's size is controlled by transport through its phase boundary. If the droplet is placed in an atmosphere at the same vapor pressure as its surface, it does not evaporate. Optical absorption by the droplet causes its

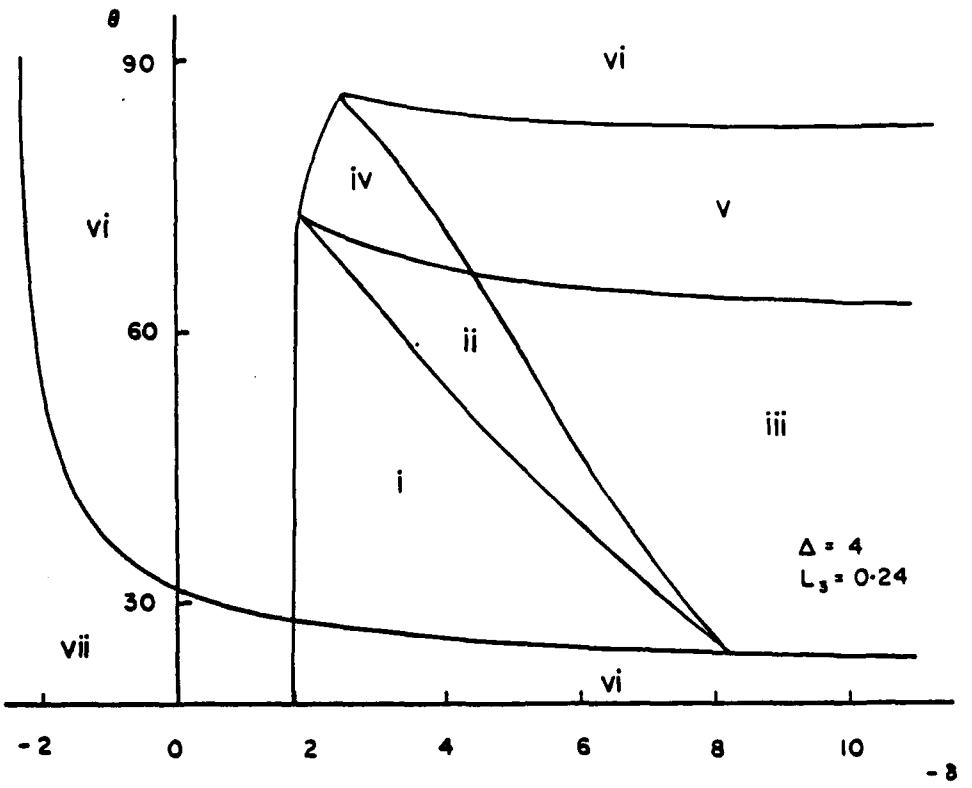

Fig. 1 Diagram showing the parameter regions which exhibit different types of nonlinear optical response of a spheroidal particle with a self-focusing Kerr nonlinearity. Here q is the angle between the polarization of the incident light and the long symmetry axis of the particle, and d is the frequency detuning.

surface vapor pressure to increase, and its size to decrease. If the absorbed energy is from a narrow band laser, one observes bistable behavior in light scattering from the droplet by scanning wavelength [3] or intensity [13]. In Ref. [3] we developed a heurestic model for this behavior based on an optical response having a simple Lorentzian shape. Over this last period, we have taken a different approach in order to provide a more comprehensive model. Our approach is a graphical one which tries to predict "equilibrium" states through the graphical solution of two equations. The first is an equation which expresses the fact that the optical size X (circumference/wavelength) decreases in the presence of light of intensity I [14,15],

$$X = X_0 - \tau Q_a(X) I \ . \qquad (1)$$

The second is an expression for the absorption efficiency Qa(X) as obtained from Mie theory,

$$Q_a(x) = \frac{2}{X^2} \sum_{q=1}^{\infty} (2q+1) \left\{ f_q(X,mX) + g_q(X,mX) \right\} \ , \qquad (2)$$

where m is the refractive index and, f_q and g_q are the absorption contributions associated with internal fields with angular mode number q and are of TE and TM type respectively. Since the cloud droplet interaction occurs at an intensity less than 100W/cm^2 [3], refractive index variations are not anticipated and the right hand side of Eq. (2) is simply a function of X. Unfortunately, even with this simplification an analytical solution of Eqs. (1) and (2) is not possible, however a graphical approach provides an accurate means for obtaining results from which physical implications can be drawn. Figure 2 shows the basic scheme. The straight line is a plot of Eq. (1) while the curved line represents a calculation based on Eq. (2) over a small region in optical size. The meaning of X_{10} is that the calculation is carried out at a particular wavelength λ_1 for which the optical size at an infinitesimally small intensity is X_{10} (and the corresponding radius is a_0). Since intensity controls the slope of the straight line, absorption by the particle is particularly sensitive to intensity. By the same token an increase in wavelength for the same intensity is represented by shifting the straight line to the right without changing its slope. Such a wavelength scan also produces a significant effect on the particle absorption efficiency. Both of these effects are most pronounced in the region of a morphological resonance. In such a region either f_q or g_q is resonantly enhanced and *bistable effects are anticipated.*

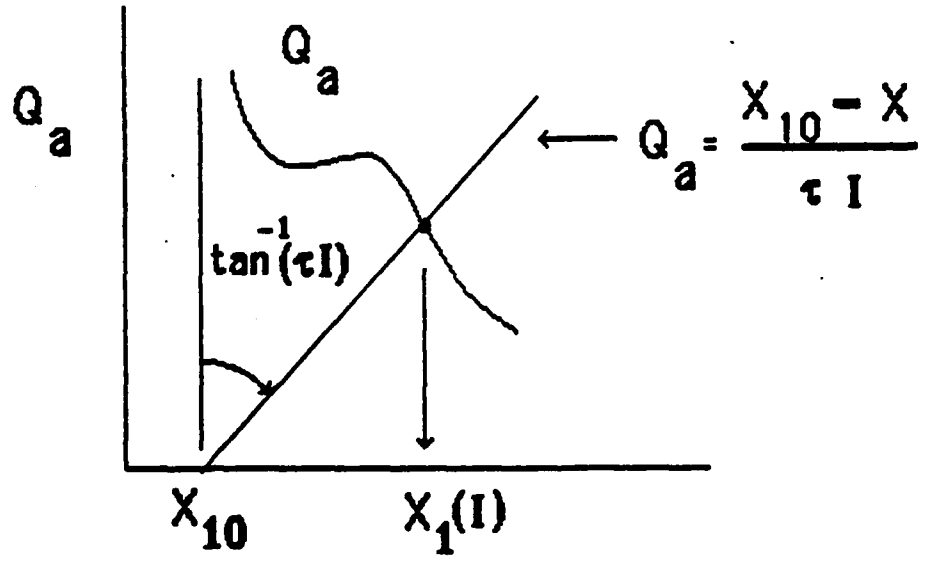

Fig. 2 Graphical scheme for simultaneous solution of Eqs. (1) and (2).

Figure 3 shows the results of an actual calculation on a particle of refractive index $1.38+10^{-5}i$ and for which the unperturbed radius is 4.828μ. The apparent Lorentzian response in Fig. 3a is due to the resonant stimulation of the g_{30} coefficient in Eq. (2) (a TM mode). The simulation was carried out for an intensity of 50W/cm^2 for which the particle size vs. absorption is depicted by the straight dashed lines. As one changes the wavelength of the laser by a few angstroms from $2\pi a_0/x_{10}$ to $2\pi a_{0z}/x_{20}$ we see that the number of solutions for absorption changes from 3 to 1. The multivaluedness of the absorption is most

apparent when the solutions are plotted against wavelength (Fig. 3b). The transitions shown in Fig. 3b correspond to the points of infinite slope. At these points catastrophes will take place. The abrupt changes seen in light scattering [3] may be calculated by mapping the various solutions at a given wavelength onto the scattering response (Fig. 3c). The overall light scattering response vs. wavelength is shown in Fig. 3d. With this scheme we have predicted a host of new phenomena including the observation of hidden resonances [16] and multistability [17]. In some sense one may consider the scheme depicted in Fig. 3 to be exact. However, it should be emphasized that no dynamics are included in this diagram and the particular problem is perhaps the simplest Mie bistability problems which one can imagine.

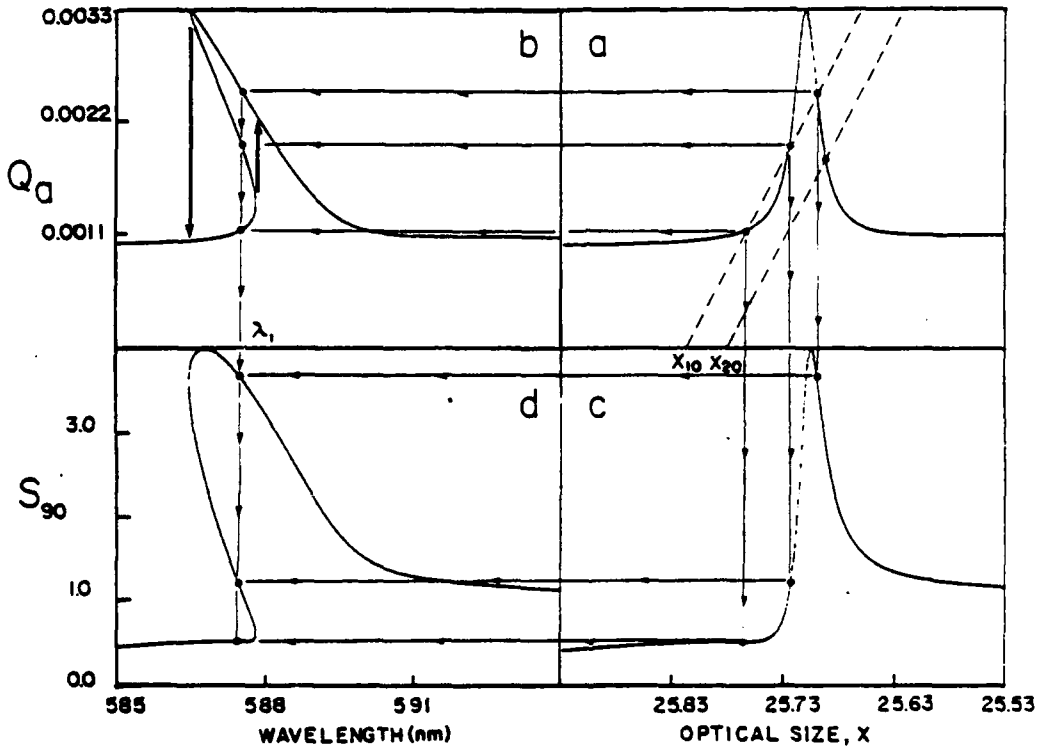

Fig. 3 The results of calculation on a cloud droplet particle of refractive index $1.38+10^{-5}i$ and for which the unperturbed radius is 4.828μ.

The next step is clearly to take a careful look at the Mie problem in the presence of a Kerr effect. Both experimental and theoretical work on this problem is currently underway.

4. REFERENCES

1. *Surface Enhanced Raman Scattering,* edited by R.K. Chang and T.E. Furtak Plenum, New York (1982).
2. A. Schmidt-Ott, P. Schurtenberger, and H.C. Siegman, Phys. Rev. Lett. 45, 1284 (1982).
3. S. Arnold, K.M. Leung and A.B. Pluchino, Opt. Lett. 11, 800 (1986).
4. K.M. Leung, Phys. Rev. A 33, 2461 (1986).
5. J.B. Snow, S.-X. Qian and R.K. Chang, Opt. News 12, 5 (1986).
6. See the review by D.S. Chemla, D.A.B. Miller and P.W. Smith, Opt. Eng. 24, 556 (1985).
7. D.S. Chemla and D.A.B. Miller, Opt. Lett. 11, 522 (1986).
8. K.M. Leung and He Ming-Guo, Submitted to J. of Wave Material Int.
9. D.S. Chemla, J.P. Heritage, P.F. Liao and E.D. Issac, Phys. Rev. B 21, 4553 (1983).
10. A. Ashkin and J.M. Dziedzic, Appl. Opt. 19, 660 (1980).
11. L.M. Folan, S. Arnold and S.D. Druger, Chem. Phys. Lett., 118, 322 (1985).
12. R. Thurn and W. Kiefer, Appl. Opt., 24, 1515 (1985).
13. S. Arnold, L.M. Folan and K.M. Leung, in preparation.
14. S. Arnold, E.K. Murphy and G. Sageev, Appl. Opt., 24, 1048 (1985).
15. S. Arnold, M. Neuman and A.B. Pluchino, Opt. Lett. 9, 4 (1984).
16. S. Arnold, L.M. Folan and T. Scalese, Bull. Am. Phys. Soc. 32, 566 (1987).
17. S. Arnold, in preparation.

C. DYNAMICAL AND NON-EQUILIBRIUM PROPERTIES OF SURFACE AND INTERFACES

Professors P.S. Riseborough, P. Hanggi and H.J. Juretschke

Unit SS7-3

1. OBJECTIVE(S)

To develop a theoretical and experimental understanding of some specific interactions of surfaces with electrons, phonons, atoms, and with each other, that govern the dynamical properties of surfaces and interfaces - the emerging crucial "missing link" between current surface science studies and the practical behavior of surfaces. Since no unified framework exists to attach the myriad of problems of probable importance, we will study three situations, representative of the range of questions that must be answered, that offer the greatest hope for fruitful analysis and potential impact in this new area. The general theme of phonon interactions, from microscopic to macroscopic time and length scales, couples the three target problem areas within the field of dynamical and nonequilibrium phenomena.

Under this common theme, the specific theoretical problems chosen address the relaxation mechanisms of hot electrons in very small structures and the dynamics of surface reactions with incoming atoms or molecules. Accompanying experiments will concentrate on developing second harmonic light generation in interface regions as a tool for studying time-dependent strains in those regions.

The emphasis of most current surface studies on the gross aspects of surfaces, such as their electronic properties or their average structural relaxation, has been very successful in understanding many of the major new features seen or expected there. However, at the next stage of detailed quantitative descriptions of particular phenomena, evidences of new complexities are accumulating that point to the need for re-examining critically the underlying theory in order to understand more fully the restrictions and new conditions, as well as the new degrees of freedom, imposed by the existence of a surface, and by its dynamical response. For example, electrons participating in current transport in a narrow surface region may encounter closely spaced barriers before being able to shed the excess energy gained in local regions of high field, and thus continue to remain "hot." Similarly, atoms colliding with a surface often do so in times so short that they do not allow for a full exchange of energy to reach thermalization. The common features of phenomena such as these are, first of all, that they deal with processes that start out far from, and may never reach, steady states close to thermal equilibrium; and, secondly, that because of the existence of the surface, or an interface, the importance of various relaxation mechanisms may differ markedly from their relative strengths in bulk material.

SECTION II: SOLID STATE

2. SUMMARY OF RECENT PROGRESS

A. Electron-Phonon Scattering by Hot Electrons in Quantum Well Microstructures

The research has focused on the mechanisms whereby optically excited electrons in the immediate vicinity of an interface relax towards lower energy states. We have developed a formalism that is capable of describing the scattering of electrons by interface optical phonons. Unlike previous formulations [14,15] the dynamical properties of the materials on both sides of the interface play important roles in the scattering processes. The equilibration of optically excited electrons proceeds mainly by intersubband scattering, since this dominates the rate of energy loss.

The rates of decay of electronic states have been calculated in the Born approximation. However, since the corresponding wave function renormalizations are unusually large, these results are not conclusive. The inclusion of higher order processes results in a significant change of the decay rates. Therefore, a strong electron-phonon coupling theory has been constructed to describe the electron (polaron) state formed at the interface.

3. STATE OF THE ART AND RESEARCH DETAILS

A. Electron-Phonon Scattering by Hot Electrons in Quantum Well Microstructures

The size of electronic components has decreased rapidly over the last decade, to such an extent that many of the classical concepts developed for bulk materials have become completely inappropriate for their description. An important consequence of the reduction of the size of electronic devices is that the internal electric fields become very large. Fields of the order of 10^3 V/cm are quite common in present day integrated circuits, while field strengths of the order of 10^5 V/cm can be found between the neighboring gates of charge coupled devices and in quantum well layered devices. At such large fields, the electrons are rapidly accelerated and acquire large kinetic energies. The net result is that the conducting electrons cannot be regarded as being in equilibrium with the rest of the microstructure, and the conduction process becomes extremely non-ohmic at room temperatures [2]. This regime is characterized by extremely nonequilibrium thermodynamics.

The manner in which the electron gas exchanges energy with the rest of the system becomes extremely important. As we shall outline later, there is considerable evidence that the dissipative process for these high energy electrons is completely different from the processes that usually occur for the electrons in thermal equilibrium. This is even more true for quantum well systems such as MOSFET's [3] or quantum well heterojunctions [4] in which the

saturation velocities of 10^6 cm/sec are considerably lower than the bulk values of 10^7 cm/sec [5]. The presence of the interfaces may be of crucial importance in the description of the nonequilibrium effects.

At room temperature, it is generally believed that the mobility is governed and limited by phonon scattering, and that most of the excess energies are transferred to the lattice via optical phonons. But, as Ando et al. [1] have pointed out in their recent review article, the theory of phonon scattering for the electronic mobility is quite unsatisfactory. The calculated mobility [6] is much larger than the experimental value. Even more distressing is that the one-phonon process leads to a mobility that is almost independent of the density of electrons in the inversion layer. The experiments show a $N_s^{1/3}$ dependence where N_s is the electron density.

At this time, therefore, a more general investigation of the processes through which an electron can emit or absorb phonons and equilibrate with the lattice is called for. In particular, it should take into account the specific nature of the phonon spectra near the interfaces, as well as the possibility that the energy exchange between the electrons and phonons may become a resonant process. This possibility is offered since the separations of the various subbands nearly match the bulk phonon energies in some systems [7]. In addition, the role of the effects of higher order phonon processes must be clarified. In bulk materials, such effects are usually negligible, as may be implied by Migdal's theorem [8]. However, in quantum well systems the theorem no longer applies, so the multiphonon processes could be of importance. The presence of these multiphonon events may strongly influence the hot electron relaxation rates, but may also be responsible for the discrepancy between the experimental data on mobilities in the ohmic regime and theoretical calculations that only consider single-phonon scattering events [1]. Other authors [1] have speculated that these discrepancies may be due to the effects of electron correlations in the final states, but apparently no one has investigated the possibility of the multiphonon processes that we suggest.

The optical properties of inversion layers show related anomalies, presumably also associated with the electron phonon scattering mechanisms. Kneschaurek and Koch [9] have studied the temperature dependence of the intersubband optical transitions. These and related experiments [10,11] show that the widths of the resonance lines present a problem at high temperatures in that the widths do not increase concomitantly with the increase in the phonon-induced relaxation rate inferred from transport properties. This raises the question of how well the transport scattering rate is correlated with the corresponding optical rate in the presence of multiphonon events. There are two obvious differences that come to mind. One is the weight of the factor $(1-\cos\theta)$ that usually enters into the momemtum scattering rate [12], and the other is the frequency dependence of the scattering rate [13]. The presence of important multiphonon processes [17] may be such that these relaxation rates become completely different from each other.

The research focuses on the properties of an electron gas at the interface between a semiconductor and another material where band bending effects

induced by the external field drive the conduction band below the fermi level in the vicinity of the surface. The electronic motion normal to the surface is confined by the electrostatic potential. The confinement within this narrow potential well causes the electronic energy levels to be quantized. The electrons remain free to move parallel to the surface. Thus, we consider the sequence of subbands with energy levels $E(n,k_{||})$ given by

$$E(n,k_{||}) = \Delta_n + \frac{\hbar^2 k_{||}^2}{2m^*} \tag{1}$$

where $k_{||}$ is a two-dimensional wave vector parallel to the surface, m^* is the electronic effective mass and Δ_n is the energy of the n^{th} subband at $k_{||} = 0$. The subband energies, Δ_n and the z-dependence of the wavefunctions $\psi_n(z)$ are found as the solution of the eigenvalue equation

$$\left[-\frac{\hbar^2}{2m}\frac{\partial^2}{\partial z^2} + eE_o z \right] \psi_n(z) = \Delta_n \psi_n(z) \tag{2}$$

which has the solutions

$$\psi_n(z) = Ai\left(\left(\frac{z - z_n}{d} \right) \right) \tag{3}$$

depicted in Figure 1. In (3),

$$d = \left(\frac{\hbar^2}{2m^* eE_o} \right)^{1/3}$$

is a measure of the thickness of the depletion layer, and $z_n = \Delta/eE_o$. The subband energy Δ_n is fixed by the boundary condition at $z = 0$, which requires that $Ai(-z_n/d)$ vanishes. Thus, we have

$$\Delta_n = eE_o\, x_n$$

where $x_1 = 2.338$, $x_2 = 4.087$, which are the zeros of the Airy function.

We have explored the influence of electron-phonon interactions on the properties of the electrons in these inversion layers, in particular the multiphonon processes.

We have generalized the electron-phonon interaction formulated by Evans and Mills [14] to the case of an interface. We have considered the scattering from both the bulk and interface phonons, since it has been noted [15,16] that

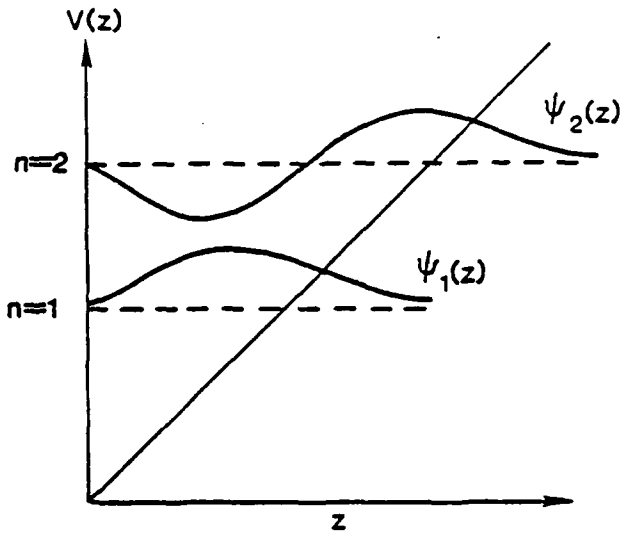

Figure 1 The z-dependence of the wave functions of the first and second lowest subbands.

at interfaces with large dielectric mismatch the optical phonons may have large energies (870 K).

Thus, the two frequencies of the interface/optical phonons are given by the condition

$$\epsilon_1(\omega_s) = -\epsilon_2(\omega_s) \tag{4}$$

in which $\epsilon_1(\omega)$ and $\epsilon_2(\omega)$ are the frequency-dependent dielectric functions for the materials on either side of the interface. The frequencies of the interface phonons are generally intermediate between the LO and TO phonon frequencies of each medium. The electrostatic potential set up by such phonons satisfies Laplace's equation, if one neglects the effects of retardation. Hence, the potential for an interface phonon with a wave vector $q_{||}$ parallel to the surface has the spatial dependence of

$$\exp\left[i\,\vec{q}_{||}\cdot\vec{x}_{||} - q_{||}\,|z|\right] \tag{5}$$

where z is the distance measured normal to the interface. Because of this z-dependence, we find that electrons trapped on one side of the interface should be appreciably scattered by the potential set up by both interface modes.

In contrast, the bulk phonons decrease rapidly in amplitude at the interface boundary, as can be seen by the following elementary argument. The bulk phonons of region 1 satisfy the condition $\nabla \cdot D = 0$, by virtue of $\epsilon_1(\omega_{LO_1}) = 0$. In region 2, if $\epsilon_2(\omega_{LO_1}) \neq 0$, we must have $\nabla^2 \phi_2 = 0$. Thus for $z < 0$, the potential is

$$\phi_2(z) = \phi_2^0 \exp\left[i \vec{q}_{||} \cdot \vec{x}_{||} + q_{||} z \right] \tag{6}$$

Continuity of ϕ at $z = 0$ requires $\phi_1^0 = \phi_2^0$. Continuity of D then gives $\phi_1(0) = \phi_2(0) = 0$, so that the potential ϕ_1 has the form

$$\phi_1(z) = \exp\left[i \vec{q}_{||} \cdot \vec{x}_{||} \right] \sin q_z z \tag{7}$$

which vanishes as z approaches zero. Thus, the potential due to the high frequency bulk LO phonons will not penetrate across the interface to where the electrons are located, while, as argued above, the interface phonons do.

The frequency of the interface optical phonons is given by ω_s where

$$\omega_s^2 = \frac{1}{2}\left[\frac{\epsilon_1(0)+\epsilon_2(\infty)}{\epsilon_1(\infty)+\epsilon_2(\infty)}\omega_1^2 + \frac{\epsilon_2(0)+\epsilon_1(\infty)}{\epsilon_2(\infty)+\epsilon_1(\infty)}\omega_2^2 \right.$$

$$\left. \pm \sqrt{\left\{ \left(\frac{\epsilon_1(0)+\epsilon_2(\infty)}{\epsilon_1(\infty)+\epsilon_2(\infty)} \right)\omega_1^2 - \left(\frac{\epsilon_2(0)+\epsilon_1(\infty)}{\epsilon_1(\infty)+\epsilon_2(\infty)} \right)\omega_2^2 \right\}^2 + 4\left\{ \frac{\epsilon_1(0)-\epsilon_1(\infty)}{\epsilon_1(\infty)+\epsilon_2(\infty)} \right\}\left\{ \frac{\epsilon_2(0)-\epsilon_2(\infty)}{\epsilon_1(\infty)+\epsilon_2(\infty)} \right\}} \right]$$

in which ω_1 and ω_2 are the transverse optical frequencies of the materials on either side of the interface. Likewise, $\epsilon_1(0)$, $\epsilon_2(0)$ and $\epsilon_1(\infty)$, $\epsilon_2(\infty)$ are the zero frequency and high frequency limits of the dielectric constants. Thus, electrons in material 1 can scatter with interface phonons, and the energy transfer can involve large frequencies, of the order of ω_2. By contrast, the bulk phonon scattering rate may only involve energies of the order $\hbar\omega_1$, which could be significantly smaller, as may be seen from Figure 2.

The lifetime of an electronic state can be analyzed from a study of the one-electron Green's function, defined by

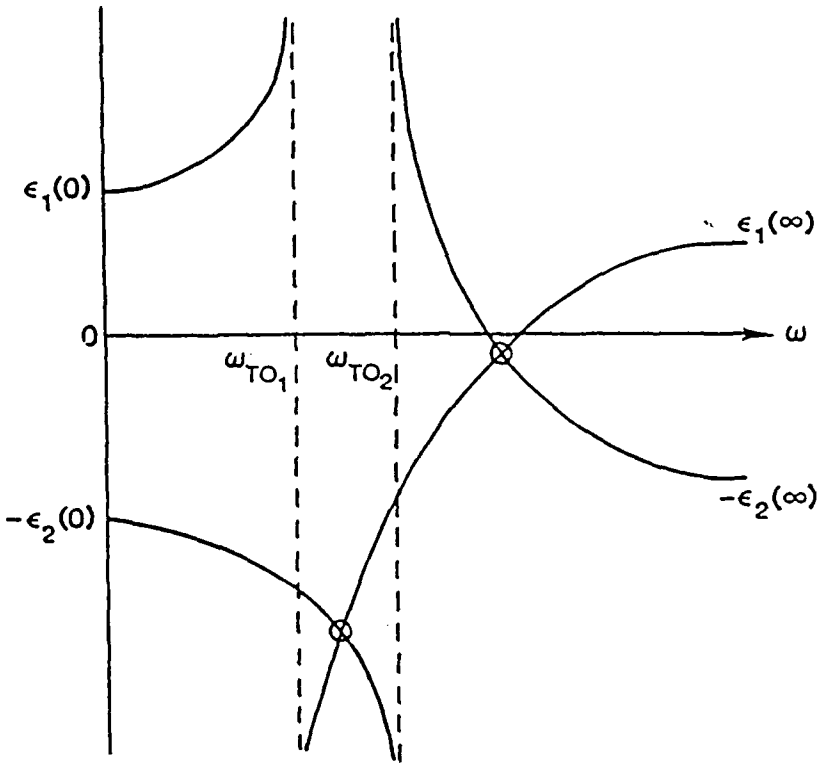

Figure 2 The graphical solution of the equation $\epsilon_1(\omega) = -\epsilon_2(\omega)$ for the frequency of the interface phonons.

$$G_{n,m}(\vec{k}_{\|},t) = 1\theta(t) \left\langle \left[a_{\vec{k}_{\|},n}(t),\ a^{+}_{\vec{k}_{\|}m}(0) \right]_t \right\rangle \qquad (8)$$

where $a_{\vec{k}_{\|},n}$ and $a^{+}_{\vec{k}_{\|},n}$ are the operators which annihilate and create electrons of wave vector $\vec{k}_{\|}$, in the subband n.

The Fourier transform, with respect to time, obeys the Dyson equation

$$\left[\omega - \Delta_n - \frac{\hbar^2\vec{k}_{||}^2}{2m}\right] G_{nn'}(\vec{k}_{||},\omega) \tag{9}$$

$$- \sum_{n''} \sum_{nn''} (\vec{k}_{||},\omega)\, G_{n''n'}(\vec{k}_{||},\omega) = \delta_{nn'}$$

which defines the self-energy $\sum_{nn''}(\vec{k}_{||},\omega)$. The lowest order contribution to the self-energy is given by

$$\sum_{nn'}(\vec{k}_{||},\omega) = \sum_{\vec{q}_{||},n''} M_{nn''}(\vec{q}_{||})\, M_{n''n'}(\vec{q}_{||}) \tag{10}$$

$$\times \left[\frac{1+N(\omega_s)-f_{n''}(\vec{k}_{||}-\vec{q}_{||})}{\omega-\Delta_{n''}-\frac{\hbar^2}{2m^2}(\vec{k}_{||}-\vec{q}_{||})^2-\omega_s-i\eta} + \frac{N(\omega_s)+f_{n''}(\vec{k}_{||}-\vec{q}_{||})}{\omega-\Delta_{n''}-\frac{\hbar^2}{2m^2}(\vec{k}_{||}-\vec{q}_{||})^2+\omega_s-i\eta}\right]$$

in which $N(x)$ and $f(x)$ are the Bose-Einstein and Fermi-Dirac distribution functions, respectively.

The imaginary part of the diagonal self-energy gives rise to the lifetime of the electronic state, as calculated in the Born approximation. The energy loss associated with single-phonon events, which scatter electrons from the state $(n,\vec{k}_{||})$, has been tabulated in [18]. Although these calculations are in reasonable qua.titative agreement with other, similar theoretical work, they are not to be relied upon. As Kawamoto, Kalia and Quinn [19] pointed out, the real part of the electronic self-energy represents a large fraction of the interband subspacings and it is strongly k-dependent. We find that it is also rapidly varying with ω, which strongly renormalizes the lifetime, through the wave function renormalization. For example, on approximating the self-energy by

$$\sum_{nn}^{eff}(\vec{k}_{||},\omega)$$

$$\simeq \sum_{nn}(\vec{k}_{||},\omega) - \sum_{1} \frac{\sum_{n,n'}(\vec{k}_{||},\omega)\, \sum_{n'n}(\vec{k}_{||},\omega)}{\omega-\Delta_{n'}-\frac{\hbar\vec{k}_{||}^2}{2m^*}-\sum_{mm}(\vec{k}_{||},\omega)} \tag{11}$$

the lifetime τ of the state $(\vec{k}_{||},n)$ is given by

$$\frac{\hbar}{2\tau} = \frac{\text{Im} \sum_{nn}^{eff} (\vec{k}_{||},\omega)}{1 - \frac{\partial}{\partial\omega} \text{Re} \sum_{nn}^{eff} (\vec{k}_{||},\omega)} \tag{12a}$$

which is to be evaluated at the frequency ω, given by the solution of the equation

$$\omega - \Delta_n - \frac{\hbar^2 \vec{k}_{||}^2}{2m^*} = \sum_{nn}^{eff} (\vec{k}_{||},\omega) \tag{12b}$$

The rapid variation of $\text{Re} \sum_{nn}^{eff}(\vec{k}_{||},\omega)$ may result in an enhancement of 1/2 by up to an order of magnitude greater than the Born approximation value. Inclusion of higher order processes significantly changes these results. As a consequence of these strong manybody effects, we have adopted a multiphonon approach to the calculation of the lifetimes.

The interface phonons are treated by performing two canonical transformations

$$\hat{H}' = D_2^+ D_1^+ \hat{H} D_1 D_2$$

where

$$D_1 = \exp\left[\frac{i}{\hbar}\left(\vec{k}_{||} - \sum_{q_{||}} \vec{q}_{||}\, b_{q_{||}}^+ b_{q_{||}}\right) \cdot \vec{r}_{||}\right]$$

and

$$D_2 = \exp\left[\sum_{q_{||}} \frac{\lambda\, e^{-q_{||}z}\,(b_{q_{||}}^+ - b_{q_{||}})}{\sqrt{q_{||}\left(q_{||}^2 + (\frac{2m\omega_s}{\hbar})^2\right)}}\right]$$

and λ is a coupling constant.

This transformation complicates the kinetic energy terms of the Hamiltonian, but does yield a z-dependent Franck-Condon-like shift. This yields part of the image potential at the interface. One finds that if $\epsilon_{\infty_2} > \epsilon_{\infty_1}$ the electrons

are attracted to the interface while, if $\epsilon_{\infty_1} > \epsilon_{\infty_2}$, the electrons are repelled.

The image potential does result in a change in the z dependence of the electronic wavefunctions, but only the lowest states are appreciably effected. The states with higher principle quantum numbers, n, when evaluated with the W.K.B. approximation do not significantly deviate from the corresponding W.K.B. approximation for the Airy functions. As a result of these changes, the matrix changes involved in the thermalization process of higher energy electrons, do not change by an order of magnitude, one might infer from the exponential dependence of the interface phonon amplitudes. The variation is limited to a factor of 2 or 3, for reasonable values of the parameters. This results in a change of the electronic lifetimes by a factor of 9. This is of the right order of magnitude needed to reconcile the theory and experimental data.

4. REFERENCES

A. Electron-Phonon Scattering by Hot Electrons in Quantum Well Microstructures

1. T. Ando, A. Fowler and F. Stern, "Electronic properties of two-dimensional systems," Reviews of Mod. Phys., 54, 437-672 (1982).

2. E.M. Conwell, *High Field Transport in Semiconductors,* Academic Press (New York, 1960).

3. E. Nicollian and J. Brews, *MOS Physics and Technology,* Wiley Publishing (New York, 1982).

4. K. Ploog, H. Kunzel, J. Knecht, A. Fisher and G. Dohler, "Simultaneous modulation of electron and hole conductivity in new periodic GaAs doping multilayer structures," Appl. Phys. Lett., 38, 870-872 (1981).

5. C. Canali, G. Manni, R. Minder and G. Ottavani, "Electron hole drift velocity measurements ir silicon and their empirical relation to electric field and temperature," IEEE Trans. Electron Devices, ED22, 1045-1047 (1975).

6. H. Ezawa, "Inversion layer mobility with intersubband scattering," Surface Science, 58, 25-32 (1971).

7. G. Abstreiter and K. Ploog, "Inelastic light scattering from a quasi two-dimensional electron system in GaAS/$Al_2Ga_{1-2}As$ heterojunctions," Phys. Rev. Lett., 42, 1308-1311 (1979).

8. A.B. Migdal, Sov. Phys., JETP 7, 996 (1958).

9. P. Kneschaurek and J.F. Koch, "Temperature dependence of the electron intersubband resonance on (100) Si surfaces," Phys. Rev., B16, 1590-1596 (1976).

10. A. Kamgar, "Temperature dependence on manybody effects in Si accumulation layers: an experimental observation," Solid State Commun., 29, 719-722 (1979).

11. F. Schaffler and F. Koch, "Subband spectroscopy at room temperature," Solid State Commun., 37, 365-368 (1981).

12. J.M. Ziman, *Electrons and Phonons: The Theory of Transport Phenomena in Solids*, Clarendon Press (Oxford, 1960).

13. P.S. Riseborough, "Spin-fluctuation contribution to the high frequency electrical conducting of nearly magnetic transition metals," Phys. Rev., B27, 5775-5783 (1983).

14. E. Evans and D. Mills, "Interactions of slow electrons with the surface of a model dielectric: theory of surface polarons," Phys. Rev., B8, 4004-4018 (1973).

15. K. Hess and P. Vogl, "Remote polar phonon scattering in Si inversion layers, " Solid State Commun., 30, 807-809 (1979).

16. B.T. Moore and D.K. Ferry, "Remote polar phonon scattering in Si inversion layers," J. Appl. Phys., 51, 2603-2605 (1980).

17. T. Holstein, "Studies of polaron motion: the small polaron," Annals of Physics, 8, 343 (New York, 1959); P.S. Riseborough, Annals of Physics, 153, 1 (1984).

18. P.S. Riseborough, "Electron energy loss in the vicinity of an interface" (to be submitted).

19. G. Kawamoto, R. Kalia and J. Quinn, Surface Science, 98, 589 (1980).

D. INFRARED-LASER-INDUCED MOCVD

Professor D.M. Schleich

Unit SS7-4

1. OBJECTIVE(S)

Standard CVD methods for the growth of silicon films require that the substrate be heated to temperatures that cause the decomposition of silane ($Ts > 600°C$). Unfortunately, these high temperatures limit the incorporation of hydrogen in the film. This is detrimental to the electronic properties of the amorphous films. A high concentration of unpaired spins, a consequence of low [H], pins the Fermi level. However, with incorporation of sufficient hydrogen the defect concentration can be lowered enough to allow the Fermi level to be adjusted by substitutional doping. Therefore, the uncoupling of the gas temperature from substrate temperature, to allow for a lowering of the nucleation temperature, has been of great interest in the growth of silicon. In the growth of III-V and II-VI compound semiconductors there are temperature problems associated with substrate decomposition (InSb, InP), film breakdown (HgCdTe) and dopant migration.

Two methods that have been widely used to separate growth temperature from gas phase chemistry have been plasma assisted CVD and UV photolysis CVD. Both techniques have inherent drawbacks; for example a plasma can cause sputtering damage to the film, and UV sources exhibit both high cost and low efficiencies. However, cw CO_2 lasers offer an inexpensive and efficient source of photons which could be used to lower the substrate temperatures . It had been reported in the literature that continuous vibrational excitation of silane gas above a heated substrate would lower the temperature necessary for amorphous silicon deposition [1-4]. We felt that if it were possible to lower the temperature of deposition by vibrationally exciting gas phase molecules, that we would be able to isolate the substrate requirements for many reactions that have temperature limitations. In addition, we felt that it would be important to have a better understanding of what role the vibrational excitation played in the chemical reactions occurring in the deposition process.

We thought that the best system to begin our studies was on the simple decomposition of silane to silicon. This system has been widely studied by classical CVD and is an important technological area. In addition, since silane does not undergo an electronic transition until the vacuum ultraviolet, the CO_2 laser appears to be the best choice for excitation of the gas species.

2. SUMMARY OF RECENT PROGRESS

We have studied in detail the irradiation of silane with energy supplied by a cw CO_2 laser. We have determined that vibrationally excited silane rapidly transfers its energy to the surrounding molecules and heats the gas phase. Therefore, contrary to previous results, we have shown that vibrationally excited silane molecules do not deposit films at temperatures lower than those necessary for classical CVD. In addition, we have shown that using proper conditions, the CO_2 laser can increase the temperature of the gas to temperatures where homogeneous gas phase chemistry occurs with silane. The most likely initial step is the formation of SiH_2 which reacts readily with the surrounding gas molecules. In a system containing a high concentration of silane, polysilanes are formed in the gas phase. These polysilanes can travel long distances within the reactor (> 1 cm) and deposit amorphous silicon films at temperatures as low as 200°C. In systems containing other reactive species, for example ammonia or nitrous oxide, the SiH_2 can form gaseous intermediates capable of forming silicon nitride or oxide films at similar low temperature.

3. STATE OF THE ART AND RESEARCH DETAILS

All experiments were performed in a CVD reactor equipped with ZnSe windows for the introduction and monitoring of the ir laser light.

In initial experiments we attempted to decompose silane using an unfocused laser beam (the laser operated in multi-line TEM_{00} mode). The laser beam traversed the chamber 1 cm above the substrate. The substrate was held to a temperature below 700° K. Neither film growth nor powder generation was observed for laser intensities up to 100 watts cm^{-2} and silane pressures from 1 to 6 torr. The addition of 5 torr of argon gas to reduce the thermal conductivity of the reactor gas caused no noticeable change. We proceeded to assess the effects of increased power densities on the decomposition process. The laser beam was focused with a 20 cm F.L. front surface spherical mirror before its entry into the reaction zone. The beam waist within this zone was calculated to be ≈ 0.3 mm in radius. With power densities up to 17 kw cm^{-2} no decomposition or deposition was observed. The beam path was then altered so that it impinged on the leading edge of the substrate Fig. 1 to produce a small incandescent spot. The substrate temperature thus decreased with circular symmetry away from this spot.

REACTOR CONFIGURATION FOR THE CREATION OF GROWTH RINGS

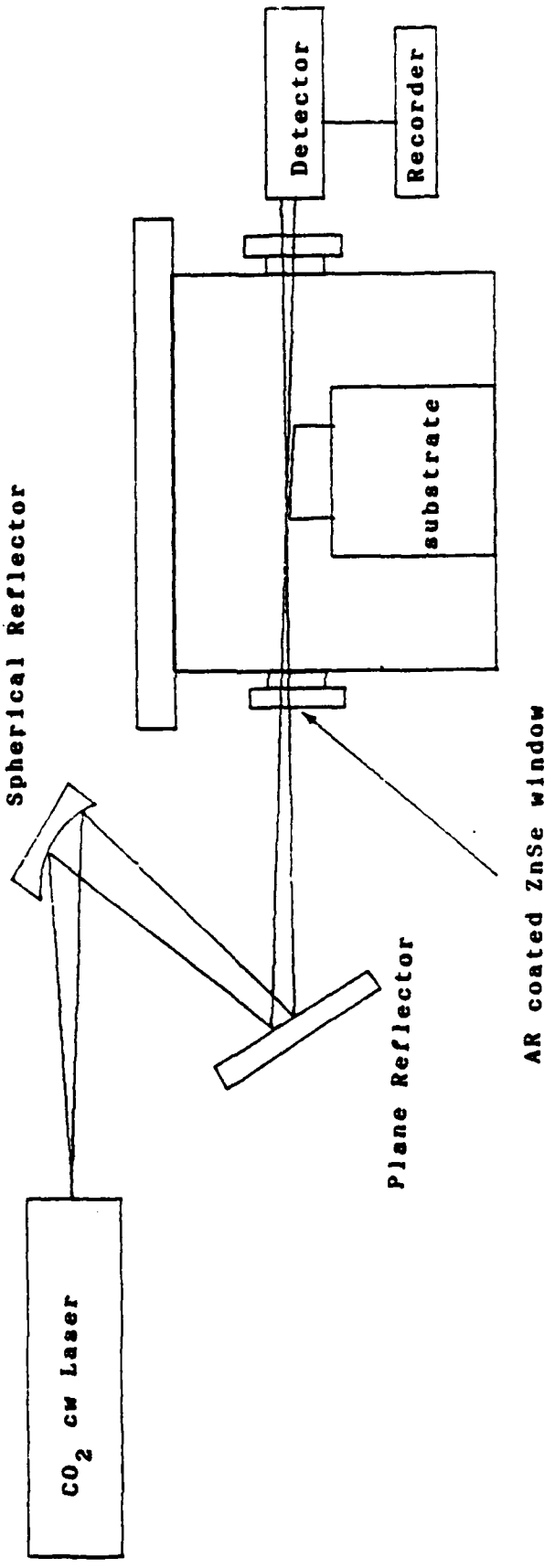

Fig.1

The resulting growth rings Fig. 2 were semicircular with no perturbation to the ring uniformity in the regions just below the passing laser beam. This result indicated that a grazing incidence laser beam neither promoted growth where the substrate was too cold nor altered the growth rate where the substrate temperature was sufficient for normal cvd. Although there had been reports in the literature that vibrationally excited silane could decompose at a low substrate temperature, probably the surface substrate temperature had been raised beyond that indicated [1-4]. Under the conditions within the reactor, similar to those previously reported, the mean free path will be very short (less than 1 micron) and collisions with gas molecules will cause energy transfer and general heating of the gas. The hot gas can then exchange heat very rapidly upon collision with the substrate causing a rise in the surface temperature. These initial experiments led us to believe that in order for pure gas phase modifications to occur we would have to induce homogeneous chemical reactions in the gas phase, and that the new gas phase species could react at different substrate temperatures. We performed a series of experiments to determine if, and under what conditions of gas composition, pressure, and laser intensity silane homogeneous reactions would occur.

Visually detectable decomposition, noted by the formation of a light yellow film on a silica substrate, occured with a focused 50 w laser beam at 10.5 torr of silane and with a focused 40 w laser beam at 7 torr of silane and 20 torr of argon. The addition of the argon served to lower the thermal conductivity of the gas within the reactor and in turn lead to the lowering of the power required for the threshold of detectable deposition. We proceeded to perform another series of runs with argon in excess at a pressure of 100 torr, varying the silane pressure and incident laser power until film formation was detected.

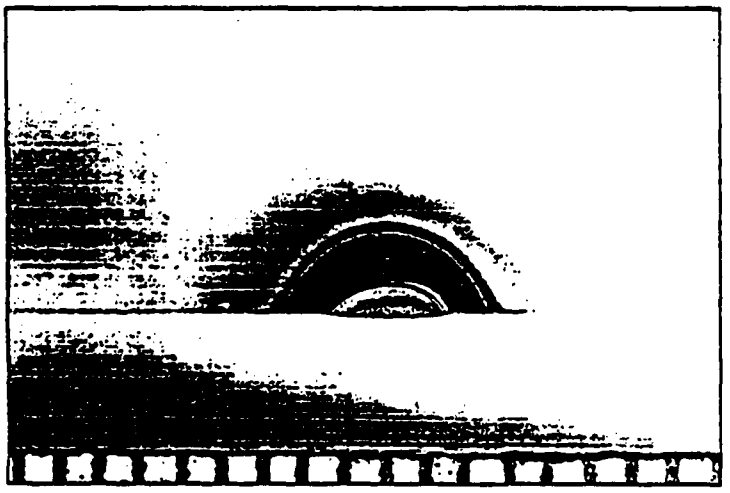

Figure 2. Growth rings showing regular deposition

These experiments were performed to aid in the calculation of the gas phase decomposition temperature. To perform this calculation a boundary condition was required. This was supplied by a silica substrate (2.5 cm i.d. 6 cm length) held coaxial with the laser beam. It is important to note the importance of the position of the beam focus along the line connecting the input and output ZnSe

windows of the reactor. If the focus fell towards the rear of the reactor the silane gas attenuated the incident laser beam too strongly for the power densities required for decomposition to be reached. In our configuration the focus fell ≈3cm from the front window. The silica tube was set in a cradle and the cradle was adjusted so that its midpoint coincided with the position of the focus. The temperature of the silica tube was measured by a thermocouple attached to a silica hook formed on the tube and held in intimate thermal contact by gallium metal Fig. 3. It was found that noticeable film production took place when the substrate reached a temperature ≈ 100°C above reactor ambient. This value was used as the boundary condition for the subsequent gas decomposition temperature calculations. The following are the set of conditions for silane pressure and laser power that lead to a noticeable rate of film growth at the previously determined boundary condition.

Silane Pressure (torr)	Laser Power (watts)
9.8	16
8	20
6.7	28
6.2	34

At these conditions we immediately observed disilane and trisilane, in the gas phase, by quadrupole mass spectrometry. If the laser power was increased, the higher resultant gas temperatures lead to the rapid formation of powder deposits on the substrate and on the reactor walls. Infrared spectroscopy of these deposits showed strong SiH_2 and SiH_3 peaks indicative of polysilane. When the laser power was slightly reduced, and the substrate temperature raised, it was possible to grow films at a substrate temperature as low as 200°C. These films could be grown even when the laser beam was more than a centimeter from the substrate. These distances are far greater than those possible for the transfer of energetically excited species, but rather correspond to the diffusion of a reasonably stable chemical species created at the laser focus.

4. CALCULATION:

We chose to approximate the system as an infinite cylinder ignoring the z dependence in the heat equation, since the horizontal extent of the substrate was several times as great as its radius. This is similar to the case of an infinite cylinder with a central uniformly heated core. The equation governing our model then reduces to that of the steady state heat equation in r:

$$d2T/dr2 + 1/r(dT/dr) + q/K = 0$$

q = heat source strength per unit volume per unit time

K = thermal conductivity

A Pascal program was written which numerically integrated the heat equation subject to the condition that at r = R, the radius of the tube, the

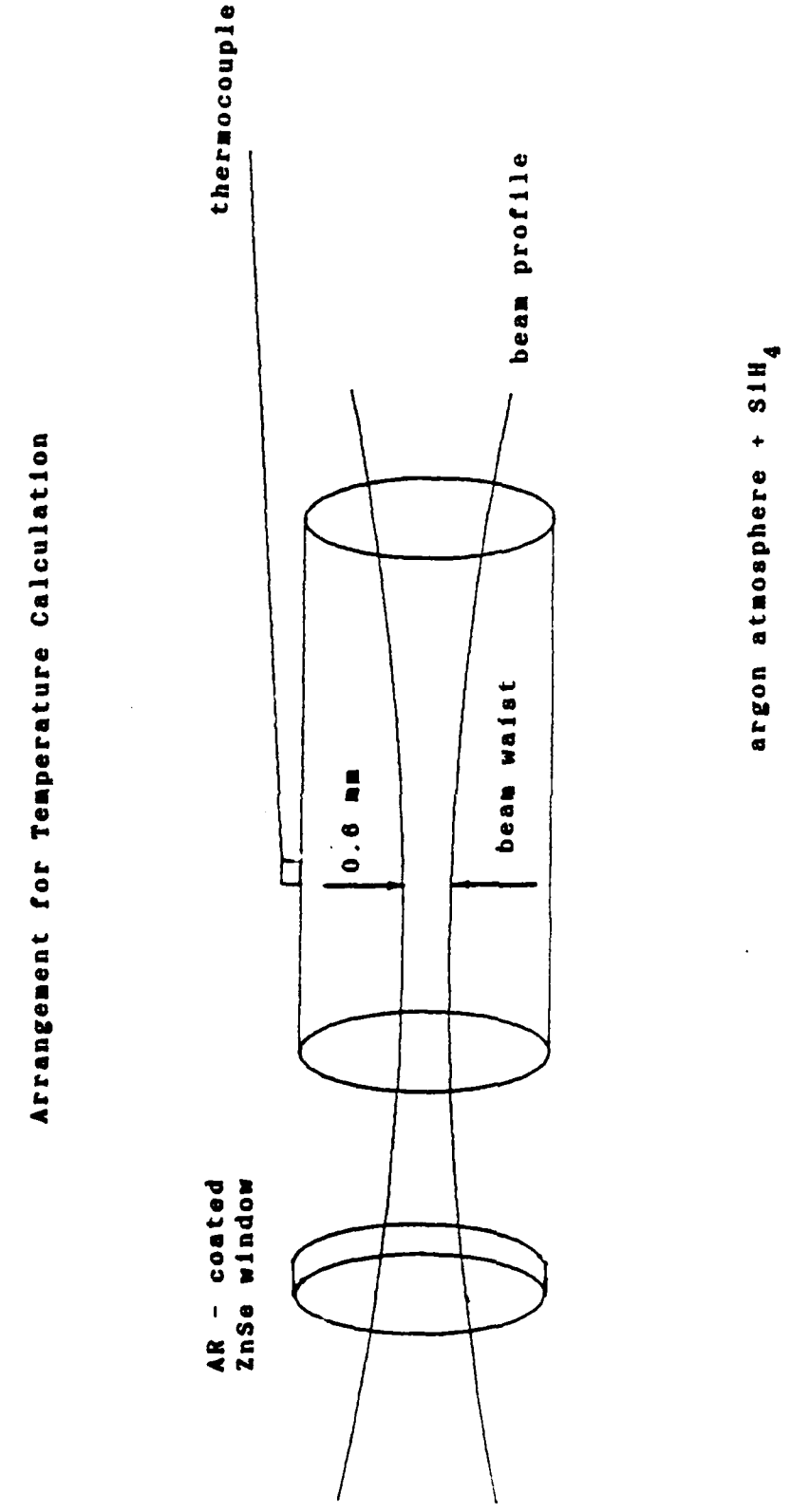
Arrangement for Temperature Calculation
thermocouple
beam profile
argon atmosphere + SiH_4
0.6 mm
beam waist
AR - coated
ZnSe window

Fig.3

temperature converges to that given by the boundary condition. A total of 500 integration steps were performed along the radius extending from the theoretical beam waist to r = R. The attenuation coefficient, which was required for the determination of power loss within a unit length of the beam path, was taken from curves previously published for the pressure dependent absorption coefficient for silane [3]. Its value was estimated to be $\approx 4.9 \times 10^{-4}$ /cm^{-1}torr^{-1} a moderately strong absorption. Since we were working in dilute solution with argon gas we could use the thermal conductivity of argon (1.75×10^{-4} watts/(cm^2)(°C/cm). Corrections were performed for the affects of temperature on the values of the thermal conductivity and attenuation coefficient. Further, local temperature changes along 1 cm increments of the tube's major axis were used to correct each elements thermal conductivity and in turn its attenuation coefficient. This lead to a more realistic value for the actual power loss in the element coinciding with the position of the focus. The correction made to the thermal conductivity is given by:

$$K = K_o(T_{local}/To)^{0.5}$$

where K_o = the thermal conductivity at 20°C. the correction for the attenuation coefficient is given by:

$$\beta = \beta o(To/T_{local})$$

where β_o = derived attenuation coefficient at 20°C where we assume a Charles' Law affect on the concentration of absorbing species.

The program ran up the beam power in increments of 0.1 watts up to the powers listed above. This allowed the continuous correction of the affects of the rise in temperature and the determination of the temperature at the focus as a function of input power. A plot of the calculations is shown in Fig. 4. The results of our calculations for the various experiments performed are consistent with an average decomposition temperature for the gas equal to ≈1130K.

5. DISCUSSION:

We believe that a strictly pyrolytic process is taking place when a sufficiently intense cw ir laser beam interacts with a silane gas mixture allowing for a rise in gas temperature above ≈1100K. The direct photolysis of silane by UV photolysis is very difficult because of the far UV character of the absorption. Photolysis can occur with an ArF excimer laser (photon energy 6.4 eV); however, the indications are that this is either a multiphoton process or a multistep process with the creation of polysilanes and subsequent decomposition via combination with silane [5]. In the case of ir laser excitation, a single P(20) ir photon (≈.1eV) is far to low in energy to cause photolysis. In order for decomposition to occur it would be necessary to have the rapid absorption of many photons. Previous studies have shown that intramolecular relaxation of vibrational energy to an excited distribution of states is very rapid [6]. Therefore it is unlikely that sufficient energy can be

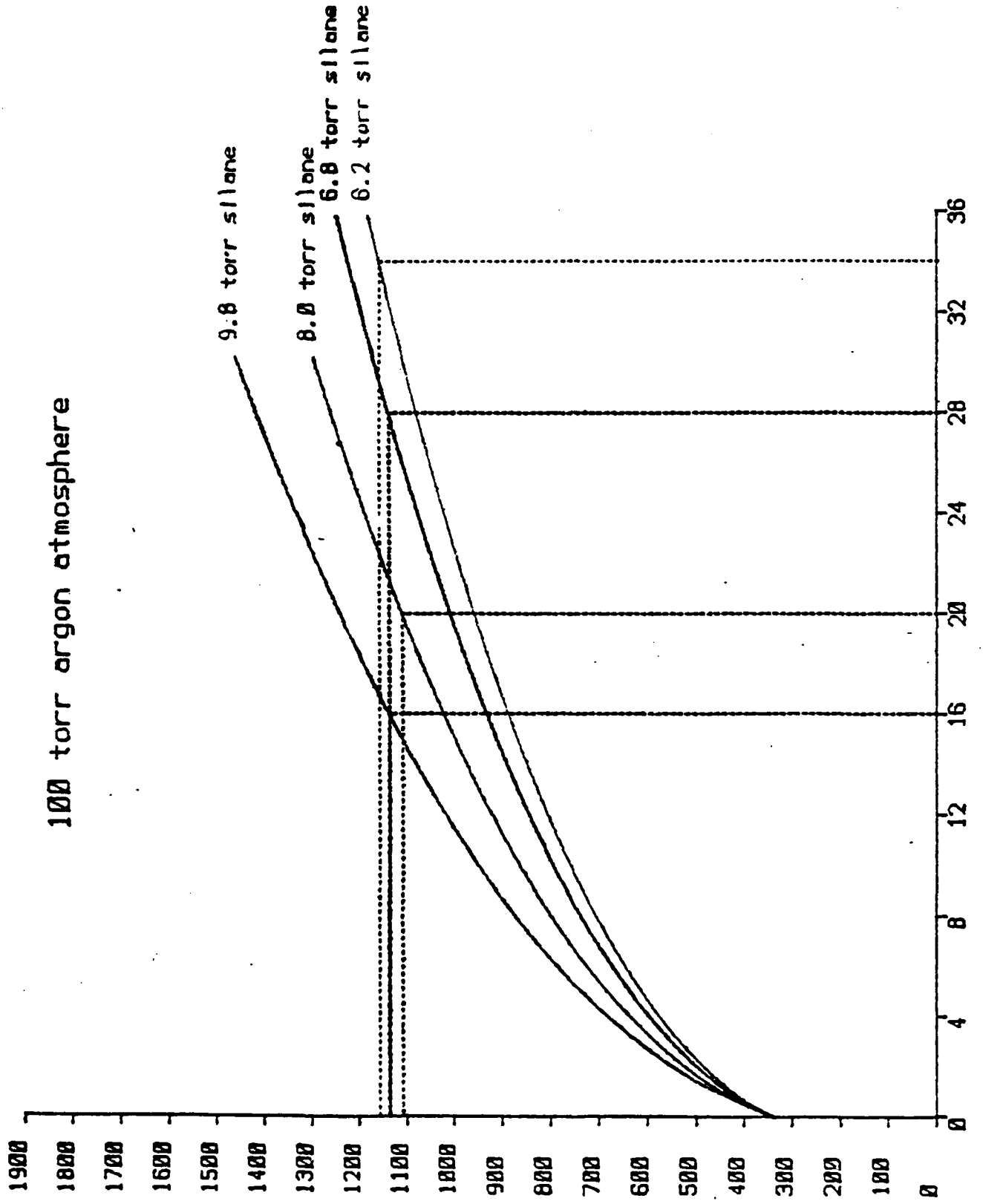
100 torr argon atmosphere
9.8 torr silane
8.0 torr silane
6.8 torr silane
6.2 torr silane
GAS TEMP. (DEGREES K)
1900
1800
1700
1600
1500
1400
1300
1200
1100
1000
900
800
700
600
500
400
300
200
100
0
0
4
8
12
16
20
24
28
32
36
Power (watts)

Fig. 4

deposited by a cw laser and collected in the state necessary for bond fission, before it is transferred by collision to a bath molecule. Further, it is not clear that the required resonance absorption condition still exists for the absorption to the $v > 2$ vibrational states. Purely photolytic processes have been observed for silane using and ir CO_2 laser source but these have involved collisionless multiphoton dissociations using a TEA laser [7]. In this case the intense photon bombardment creates a quasi continuum where subsequent photon absorptions lead to dissociation.

Our results indicate that at gas temperatures below some critical value ($T_g = 1100K$) there is no evidence of rapid decomposition sufficient of realistic film growth. Previous researchers have shown this to be true in the case of the less stable disilane molecule [8]. Under reactor pressures of between 1 and 10 torr the mean free path for the excited silane molecule is $\approx$1 to 10 microns. Therefore, the energy absorbed by the silane molecule will be equilibrated after traveling <1 mm. However, if the substrate cannot dissipate the heat gained from the gas phase, its temperature could rise substantially allowing for deposition at the surface. We believe that the relatively volatile and stable disilane and trisilane, observed in the gas phase, and perhaps higher order polysilanes are responsible for the formation of amorphous silicon films at a reduced substrate temperature.

6. CONCLUSION AND FUTURE DIRECTIONS

It seems most likely that the first stage in the laser pyrolysis is to create the highly reactive SiH2 species:

$$SiH_4 \rightarrow SiH_2 + H_2$$

In a system with only silane and inert gas, polysilanes will be rapidly formed due to collision with SiH_4. If other gas species are present, then different intermediates will be formed and new materials can be deposited on the substrate at a low temperature. In order to verify this hypothesis we have started work on the low temperature growth of silicon nitride. Since the thermal conductivity of ammonia is very close to argon, no additional dilution is necessary to reach the cracking temperature for the creation of active silicon species. Using laser power and gas pressure conditions similar to those for pure silane we were able to deposit either a transparent film or white powder from the NH_3/SiH_4 mixture when the ratio is $\approx$10 or greater. FTIR measurements on the sample show that materials grown at substrate temperatures of 200°C or less contains Si_xN_y. The Si-N stretch is the major feature of the spectrum; however, there is observable hydrogen, primarily detected as a N-H stretch. This was expected since it is very difficult to to remove the last traces of hydrogen from nitrides.

It has been shown that by exciting gas phase silane with a CO_2 laser we are able to create active gas phase species which can prepare low temperature materials. There are many areas of this research to be explored both from a

fundamental perspective as well as a technological one:

(a) Careful characterization of the films grown;

(b) In situ detection of gas phase species (ideally FTIR);

(c) Testing with additional species either as dopants or main reactants with silane; and

(d) Expansion to III-V materials, ideal because of the access to excitation of the group V hydrides with the CO2 laser.

7. REFERENCES

1. M. Meunier, T.R. Gattuso, D. Adler, and J.S. Haggerty, Appl. Phys. Lett. 43(3), 273 (1983).

2. M. Meunier, J. H. Flint, D. Adler and J. S. Haggerty, J. Non Cryst. Sol. 59 & 60, 699 (1983).

3. T. R. Gattuso, M. Meunier, D. Adler, and J.S. Haggerty, Mat. Res. Soc. Symp. Proc. Vol. 17, (1983).

4. R. Bilenchi, I. Gianinoni and M. Musci, Nat. Res. Soc. Proc., Vol. 17 (1983).

5. T. Taguchi, M. Morikawa, Y. Hiratsuka, and K. Toyoda, Appl. Phys. Lett. 49 (15),971 (1986).

6. P. L. Houston, A. V. Nowak, and J.I. Steinfeld, J. Chem. Phys. 58 (8), 3373 (1973).

7. T. F. Deutsch, J. Chem. Phys. 70 (3), 1187 (1979).

8. T. Iwanaga and M. Hanabusa, Jpn. J. Appl. Phys. 23 (7), 473 (1984).

Work Supported by this Grant:

1. Ph.D. Dissertation, Polytechnic University, Dr. John Carter Jan. 1988.

2. J. Carter, D.J. Dunstan, F.Lai, and D.M. Schleich Abstract # 257, Vol. 87-1, Spring Meeting, Electrochemical Soc., Philadelphia, Pa., May 10-15. 1987.

3. D.M. Schleich, W.Y.F. Lai and A. Lam, in "The Design, Activation and Transformation of Organometallics into Common and Exotic Materials, Ed. R. Laine. 1987.

4. D.M. Schleich, W.Y.F. Lai, A. Lam, NATO Advanced Research Workshop, September 1986, Montpellier, France.

5. Due to the work performed in our laboratory supported by JSEP we have been invited by Dr. K. Jones, Chief of Electronic Materials, Fort Monmouth to participate in a industrial-government-academic consortium on MOCVD.

6. We have received industrial support for MOCVD and CVD work on III-V's and Si-Ge-B alloys from AT&T Bell Labs and Grumman Aerospace.

82 Blank

E. RESONANT INTERACTIONS IN CRYSTALS AT X-RAY WAVELENGTH SURFACES

Professors G. Schaefer and E.E. Kunhardt

Unit SS7-5

1. OBJECTIVE(S)

The objective of this project is to investigate concepts for obtaining a non-divergent beam of x-ray radiation with enhanced coherence from the interaction of Ewald modes and active oscillators in a crystal.

2. SUMMARY OF RECENT PROGRESS

In general, there are two ways to enhance the coherence properties of radiation emitted by atomic oscillators: (1) to alter the properties of spontaneous emission through the interaction of the oscillators with a resonant cavity; and (2) to utilize induced emission. We have developed a new concept for obtaining a non-divergent beam of x-ray radiation with enhanced coherence properties. The approach utilizes the interaction of active oscillators and Ewald modes in a crystal. Using the high Q that can be achieved in a crystal, the x-ray emission can be channeled into a limited number of allowed modes (Kossel modes); this increases the lifetime of the oscillators and thus enhances the coherence of the radiation. We have been investigating various methods for enhancing the Q factor of the crystal cavity and for extracting the radiation from the crystal. These issues will be discussed in the next section.

3. STATE OF THE ART AND PROGRESS DETAILS

In recent years, the concept of inhibited or enhanced spontaneous emission in cavities, first outlined by Purcell [1] at Radio Frequencies, has been extended by Stehle [2] and Kleppner [3] to the near IR and visible spectral regime. This concept has been verified by several experiments [4-8].

The basic quantity describing the interaction between an individual atomic transition, (n-m), and electromagnetic radiation of the frequency $\nu=(E_n-E_m)/h$, is the Einstein coefficient B_{mn} for absorption or induced emission. The Einstein coefficient for spontaneous emission, A, in addition depends on the availability of states for the electromagnetic radiation of the frequency ν expressed as the density of photon states, $\rho(\nu)$:

$$A_{nm} = \rho(\nu)(h\nu)B_{mn}$$

The values for A, usually used to characterize the transition probability of a specific transition, are based on the availability of states in free space for dipole radiation $\rho_s=8\pi\nu^2/c^3$:

$$A_s = \frac{8\pi\nu^2}{c^3} h\nu B$$

The density of states in a cavity, $\rho_c(\nu)$, is quite different. If the cavity is tuned with its lowest order mode to the frequency ν of the atomic transition and the quality factor of the cavity is Q, then the density of states is $\rho_c=8\pi\nu^2 Q/c^3$ and the transition probability in the cavity, A_c, is enhanced:

$$A_c = Q\frac{8\pi\nu^2}{c^3} h\nu B = QA_s$$

If the cavity dimensions are small compared to half the wavelength of the atomic radiation then the transition probability is decreased.

The same effect is observed if the atomic system is placed inside a waveguide so that the frequency of the atomic transition, ν, is close to the cutoff frequency, ν_c, of the waveguide. At the cutoff frequency the waveguide acts as a resonator with quality factor Q and the transition probability in the guide A_g becomes:

$$A_g(\nu=\nu_{co}) = Q_o A_s$$

Below cutoff the transition probability approaches:

$$A_g(\nu<\nu_{co}) = \frac{1}{Q_o} A_s$$

and above cutoff the transition probability decreases with ν:

$$A_g(\nu>\nu_{co}) \propto \frac{\nu}{(\nu^2-\nu_{co}^2)^{1/2}} A_s$$

up to the cutoff frequency for the next higher order mode ν_{c1}, at which the waveguide again acts as a cavity with the quality factor Q_1 for this mode. Once a larger number of modes can be excited, the resonance effect for the individual mode becomes less pronounced, and finally, the density of modes approaches the value for free space.

The concept of inhibited and enhanced spontaneous emission can also be applied to the emission of x-ray radiation inside a crystal lattice. Such radiation (Kossel radiation) is only emitted as specific modes of propagation, the Borrmann modes. Although the basic features of the Borrmann effect are well known, they are briefly reviewed here [9-16]. They are as follows: a parallel-sided, monocrystal slab with lattice planes perpendicular to the slab faces is illuminated by a beam of x-radiation at an angle θ with respect to the planes.

The field distribution inside the crystal excited by the incident beam can be described as a superposition of what we shall denote as Ewald modes. These are the sets of modes that are permitted in a system consisting of a periodic array of oscillators. (See [11] for a discussion of the dispersion surfaces corresponding to these modes.) In general, these modes have a complex wave vector, and they are strongly attenuated, so that the energy in the incident beam is quickly absorbed. When the angle of incidence, θ, is set to the Bragg angle, one of the modes has an almost real wave vector. This mode, the Borrmann mode, may be considered as the superposition of the incident and diffracted beams, with corresponding propagation vectors, K_O and K_H that are directed to reciprocal lattice points (rℓps) O and H on the surface of the Ewald sphere [11]. For this angle of incidence, these beams have essentially the same amplitude and wavelength. The resulting wave (the two beam Borrmann mode) has a standing wave pattern, with the periodicity of the lattice, in the direction perpendicular to the lattice planes, and propagates in a direction parallel to the lattice planes. The minimum field-planes are coincident with the lattice planes, which explains why the mode suffers little absorption (almost real wavenumber). Thus, the wave (mode) propagates through the crystal and emerges at a point parallel to where the incident beam struck the crystal. Again, note that this is a *traveling* mode in the direction parallel to the lattice planes.

Increasing the number of rℓps on the surface of the sphere to $n > 2$ results in the n-beam Borrmann mode. In such cases, the diffracted beams are highly collimated, as well as monochromatic, and their phases are displayed in the form of asymmetries of the diffracted intensity profiles [13]. The absorption coefficients of selected modes of propagation can be reduced to values much smaller than those attainable in the 2-beam case [14]. Calculations indicate [15] that, for transmission of CuKα radiation through Ge crystals, the absorption coefficients of four of the twelve modes of propagation in a 6-beam interaction can be reduced from the average of 352 cm^{-1} to values smaller than one cm^{-1}. Calculated values of the excitations of all twelve modes of propagation of x-rays and the corresponding absorption coefficients are listed in Table I.

Quantitative experimental verification has not yet been reported, but qualitative photographic results, described in [15], are in reasonable agreement with the above calculations. Detailed verification of the latter will make possible x-ray investigations of highly absorbing materials using relatively long wavelengths, as well as the more general class of experiments which involve long paths of x-ray beams within crystals.

In the analysis of Ewald modes, a plane wave description is normally used and the oscillators are assumed to be passive [11]. The plane wave assumption was removed in the analysis of Kato, [17] who instead assumed spherical wave fronts for the incident radiation. This resulted in a better description of the experimental conditions which invariably involve beams of finite width and non-zero divergence. A Gaussian incident beam profile would be more realistic.

Table I

μ's and excitations at the exact 6-beam pt.
for CuKα_1 radiation

Mode	μcm^{-1}	Excitation	
1	0.02	1/12	
2	0.16	1/18	
3	0.16	1/9	1/3
4	0.48	1/12	
5	38.72	1/18	
6	38.72	1/9	
7	60.02	1/18	1/3
8	60.02	1/9	
9	85.43	1/12	
10	1,186.16	1/12	
11	1,377.79	1/18	1/3
12	1,377.79	1/9	

$\mu_{ave} = 352.12$

To our knowledge, none of the descriptions of the propagation of Ewald modes in a crystal takes into account the possibility that the oscillators may be active. That is, they may exist in a number of different states whose population, to a certain extent, can be entirely controlled (by excitation with an electron beam, or x-rays of shorter wavelength, for example). Moreover, some of the oscillator transitions may be resonant with the incident radiation (Ewald modes).

From the above description, it is evident that for K_α radiation, the crystal lattice acts as a system of waveguides with, in general, a large number of allowed modes. The number of waveguides for which the cutoff frequency of the lowest order modes is below the frequency of the x-ray radiation of course depends on the lattice constant and the energy levels of the emitting atom. The frequency of K_α radiation is, to the first order, proportional to Z^2 where Z is the atomic number. For crystals composed of only one kind of atom there is only little choice for the right combination of wavelength and lattice constant. which means that only one or a few waveguides exist with $\nu_c < \nu$. Some crystals of low Z materials, in fact, do not have any allowed Borrmann modes. Compound crystals, doped crystals, and doped compound crystals, however, provide a large variety of combinations of lattice constants and wavelength so that a combination can be found for which the x-ray frequency is little above the cutoff frequency of a low order allowed mode. Of special interest, of course, are modes with extremely low absorption coefficients as shown in Table I (modes 11 and 12). These are the modes which, at cutoff, correspond to a

very high quality factor Q.

There are also methods to provide some fine adjustment of the lattice constant. A method used during fabrication would be to adjust the doping density of some doping material (not necessarily the atoms used for x-ray emission). Fine-tuning during the experiment may be accomplished through temperature or pressure changes.

Another method to obtain high Q factors is to generate a cavity which means to provide a coupling mechanism between a Borrmann mode and the equivalent mode with opposite direction of propagation. Assuming that one finds a combination of emitter and lattice so that the frequency $\nu > \nu_c$ is only fairly close to the cutoff frequency, ν_c, of a low loss Borrmann mode. In this case, the wavelength of the guided wave, λ_g, is much larger than the wavelength, λ, of the x-ray radiation. A periodic structure with periodicity $d = \lambda_g/2$ and planes perpendicular to the propagation direction of the Borrmann mode would then create a cavity for the x-ray radiation. Such a periodic structure could, for example, be generated through a super lattice.

Another way to provide feedback between the Borrmann modes with opposite direction of propagation is x-ray-phonon scattering. If we select a combination of lattice constant and x-ray wavelength such that the lattice constant is only slightly larger than half the wavelength $a=(1+\epsilon)\frac{\lambda}{2}$ with $(\epsilon << 1)$ then the propagation constant of the propagating Borrmann mode becomes very small and can be the same order of magnitude as the propagation constant of phonons. In this case, it is possible to launch an acoustic wave with the right frequency in the opposite direction to the Borrmann mode such that 180° back scattering of the propagating Borrmann mode occurs. A standing wave pattern (two acoustic waves in opposite directions in combination with a low loss Borrmann mode (see Table I) in a crystal close to cut-off, therefore, provides an x-ray cavity with a very high quality factor Q. It should be mentioned here that Rivlin [18] estimates the quality factor of Bragg modes in a perfect crystal to approach 10^8.

There are two important consequences resulting from the interaction of x-ray emitters with resonant cavities which allow oscillation of only a few modes.

1. First, the cavity provides a channeling of the x-ray radiation into the mode of the cavity, and

2. Second, the external observable lifetime of the radiation becomes dominated by the radiating decay of the cavity rather than the lifetime of the atomic state. The interaction of Borrmann mode based cavities in crystals with the active oscillators, therefore, provides an efficient method to generate beams of characteristic x-ray radiation with improved spatial and temporal coherence.

4. REFERENCES

1. E.M. Purcell, Phys. Rev., 69, 681 (1946).
2. P. Stehle, Phys. Rev. A, 2, 102 (1970).
3. D. Kleppner, Phys. Rev. Lett., 47, 233 (1981).
4. G. Gabrielse and H. Dehmelt, Phys. Rev. Lett., 55, 67 (1985).
5. R.G. Hulet, E.S. Hilfes and D. Kleppner, Phys. Rev. Lett., 55,
6. A. Anderson et al., IQEC Digest of Technical Papers, ThAA1 (1987).
7. D.J. Heinzen et al., IQEC Digest of Technical Papers, ThAA2 (1987).
8. F. DeMasrtini et al., IQEC Digest of Technical Papers, ThAA3 (1987).
9. G. Borrmann, Z. Physik 42, 157 (1941); Z. Physik 127, 297 (1950).
10. P.P. Ewald, Rev. of Mod. Phys., 37, 46 (1965).
11. B.W. Batterman and H. Cole, Rev. Mod. Phys., 36, 681 (1964).
12. R.W. James, Solid State Phys., 15, 53 (1963).
13. B. Post, Acta Cryst., A35, 17-21 (1979).
    B. Post, Acta Cryst., A39, 711-718 (1983).
14. T. Joko and A. Fukuhara, J. Phys. Soc. Japan, 22, 597-604 (1967).
15. T.C. Huang, M.H. Tillinger and B. Post, Z. Naturforschung, 28a, 600-603, (1973).
16. Z.G. Pinsker, *Dynamical Scattering of X-Rays in Crystals*, Springer Series in Solid State Sciences, Vol. 3 (Springer Veriag, New York, 1978), Chap. VII.
17. N. Kato, Acta Cryst., 13, 349 (1960).
18. L.A. Rivlin, Sov. J. Quantum Electron., 7, 380 (1977).

SECTION III:
INFORMATION ELECTRONICS

SECTION III: INFORMATION ELECTONICS

A. ROBUST AND NONLINEAR FILTERING, DETECTION AND ESTIMATION IN TELECOMMUNICATIONS, RADAR AND SONAR PROBLEMS

Professor L. Kurz

Unit IE7-1

1. OBJECTIVE(S)

In recent years the general area of robust detection and estimation has received considerable attention. In this context, "robustness" was meant to signify insensitivity to small deviations from the assumptions about the noise model. Frequently, a robust method was described as being a procedure with uniformly good behavior within a family of contaminated distributions [1-9]. However, the exact meaning of "uniformly good behavior" and "contaminated family," though defined in distinct mathematical terms of a give situation, becomes in effect ambiguous for the data processor to which the input is a stream of observables with unknown and/or slowly time-varying statistics.

To alleviate this vagueness, further research efforts were concentrated on the stability of various stochastic distances [10-15] to give these properties a qualitative as well as quantitative measure. Nevertheless, the stability does not always imply good performance in terms of the expected value of a cost functional; moreover, these stochastic distances are usually too abstract to be easily related to the system design.

To bypass the problems associated with the differences generated between theoretical and practical conceptualizations of robustness, one of the major objectives of the present research effort was to introduce descriptors of robustness which leas naturally to the design of practical detectors and estimators. A *major breakthrough* in the theory of robust detection and estimation was also achieved [31,32]. Specifically, two approaches to robust procedures which include *dependent sampling* were developed.

It was recognized by Chadwick and Kurz [16] that in low signal-to-noise ratio (SNR) environments, nonparametric detectors should operate in a sequential mode to insure an increase in the information rate while maintaining a constant error rate. Brownstein and Kurz [17] demonstrated that group rather than sample-by-sample updating of the data is necessary for efficient operation of detectors in a sequential mode. They also demonstrated that stochastic approximation algorithms represent a useful tool for an efficient operation of adaptive detectors [18,18-22]. The natural objective of the ongoing research is to investigate the use of variable threshold sequential detectors as practical and efficient means of truncation of the decision process. Also, a class of sequential partition detectors that include stationary and quasi-stationary Markov processes was studied in detail. Applications to detection of underwater sounding data were stressed [31].

AD-A193 072 BASIC RESEARCH IN ELECTRONICS (JSEP) JOINT SERVICES ELECTRONICS PROGRAM..(U) POLYTECHNIC UNIV FARMINGDALE NY WEBER RESEARCH INST A A OLINER ET AL. 31 DEC 87 2/2

UNCLASSIFIED POLY-WRI-1533-88 AFOSR-TR-88-0275 F/G 9/1 NL

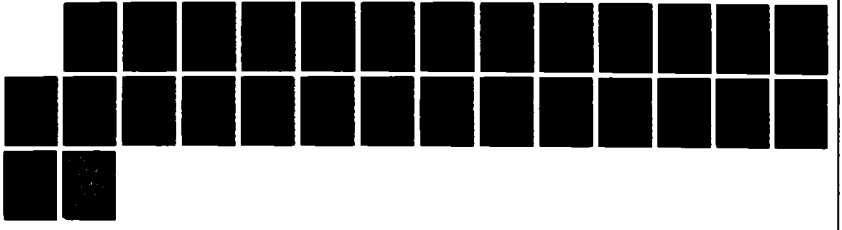

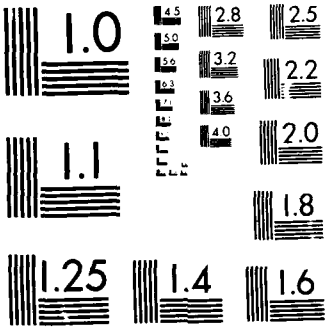

SECTION III: INFORMATION ELECTONICS

With the advent of satellite communications, the problem of data transmission through satellite channels became particularly important [23-26]. Some of the techniques used in robust detection lead naturally to procedures which suppress interference owing to the nonlinear nature of satellite transponders. In general, optimization and evaluation of various modulation schemes used in satellite data transmission were among the objectives of the present research effort. Various form of nonlinear filtering and equalization were also investigated [29,33].

2. SUMMARY OF RECENT PROGRESS

In the last year, several significant contributions to the theory of partition detection and estimation were introduced. Specifically, a class of 8 sequential adaptive detectors for underwater non-gaussian noise environments were considered.[34] A new approach was developed which permits the design of non-linear robust detectors and estimators for efficient operation in dependent noise.[35]

In addition, further contributions were made to the problem of optimization of satellite channels to insure improved data transmission.[36,37]

Finally, detailed study of performance of differentially coherent QPSK systems in slowly fading Rician channels was completed.[38]

3. STATE OF THE ART AND PROGRESS DETAILS

A. Sequential Adaptive Detectors for Underwater Non-Gaussian Noise Environments [34]

The problem of sequential signal detection in the presence of slowly varying not necessarily Gaussian noise was treated by introducing the sequential generalized linear tests (SGLT) and the sequential generalized quantiles statistic T_i^*. Detectors based on these tests combine the good qualities of order and partitioning statistics: robustness, increased efficiency, and ease of implementation. In particular, the sequential T_i^* detector (STi*D) was analyzed in detail. It was shown that the same detector structure is needed for fixed-sample and sequential optimum operation, that the STi*D is asymptotically optimum and more efficient than the corresponding sequential partition detector, and that its transmission rate is up to four times that of its fixed-sample-size counterpart.

Furthermore, some truncated and curved boundary decision rules in sequential operation of the detector were introduced to improve the efficiency even in extremely low signal-to-noise-ratio (SNR) environments, which are often encountered in underwater acoustics. These decision rules also eliminate the influence of occasionally unbounded sample sequences which are an integral

part of sequential detectors operating in severe noise. On the other hand, asymptotic measures of performance were evaluated under relatively high SNR operation of the detector, encountered in some practical situations, such as active sonar, and their performance was compared to the exact and computer simulated results.

B. Non-Linear Robust Detection and Estimation in Dependent Noise [35]

Adaptive optimal detection and estimation algorithms were considered. The algorithms are generally non-linear. The development is more general than most previous treatments of non-linear detection and estimation in that it is permitted for the noise to be dependent, subject only to a mixing condition.

Optimal detection procedures depend on knowledge of the noise probability density function (pdf); therefore, a methodology for estimation of pdf's. The approach permits estimation based on dependent samples, and was extended to estimation of conditional pdf's. The latter are required for optimal detection in dependent noise.

The methodology adopted to the problem of estimation of pdf's--piecewise polynomial approximation--requires knowledge of quantiles and truncated moments of the density to be estimated. This led to the consideration of estimation of these quantities; the Robbins-Monro Stochastic Approximation (RMSA) algorithm was employed for this. A proof of convergence of the RMSA algorithm with a dependent input sequence is given under the assumption that the sequence is mixing. This is an important generalization of the available theory.

Adaptive non-linear filtering and prediction algorithms were also presented. These are based on piecewise approximation to a regression function involving only estimated partition moments and quantiles. All of the algorithms are simple enough to be adaptively implemented in real time, and several illustrations of performance were presented.

C. Nonlinear Equalization in Satellite Data Transmission Systems [36,37]

The problem of designing and evaluating the performance of a minimum mean-square error equalizer (MMSEE) for binary PSK transmission over band-limited nonlinear satellite channels was considered. The effect of inter-symbol interference followed by AM/AM and AM/PM conversions were taken into account while optimizing the performance in the presence of the downlink white Gaussian noise. In analyzing the problem, the decision was made on a typical signal in a received sequence taking into account past and future interfering signals, i.e., ISI.

As an illustrative example of the receiver, a typical channel model was considered in detail. Based on the analysis, an alternative receiver structure

which is more suitable for implementation was introduced. The taps gain coefficients for minimum mean-square error between the received sample and the actual transmitted bit, were obtained using numerical methods. The performance of the equalizer using computer simulation techniques and it was shown that significant performance improvement over the single-sample sign detector can be obtained.

The results of reference 36 were then generalized to a satellite transmission systems using quadrature phase shift keyed (QPSK) signals.[37]

D. Performance of Differentially Coherent QPSK Systems in Slowly Fading Rician Channels [38]

A detailed analytical approach to the evaluation of the error rate performance of a differentially coherent QPSK system with linear diversity in a frequency selective slow fading channels with Rician distributed signal envelopes was presented.

First, a real-time channel parameter estimation technique was introduced, followed by the error probability evaluation using linear diversity in a Rician fading environment. Gaussian and exponential delay autocorrelation functions were assumed, and the intersymbol interference for one- and two-symbols adjacent to decision intervals, various data rates and phases, SNR, as well as the ratio of the direct signal component power to the multipath power were taken into account and evaluated.

Extensive simulation results suggest that if the normalized data rate, d, is less than .2, the system is insignificantly affected by intersymbol interference. If the diversity order $L = 2$, $d > 0.4$ or if $L = 4$, $d > 0.6$, the second symbols on either side of the detection interval start generating about twenty per cent intersymbol interference as compared to the first pair. It is also interesting to note that below these rates the high SNR can counteract the loss in a fading environment. But for a high data rate, the fading generates the dominant metric probability of error for various detected phases. This is a result not observed in linear channels. Typical performance results are shown in Figures 1 and 2.

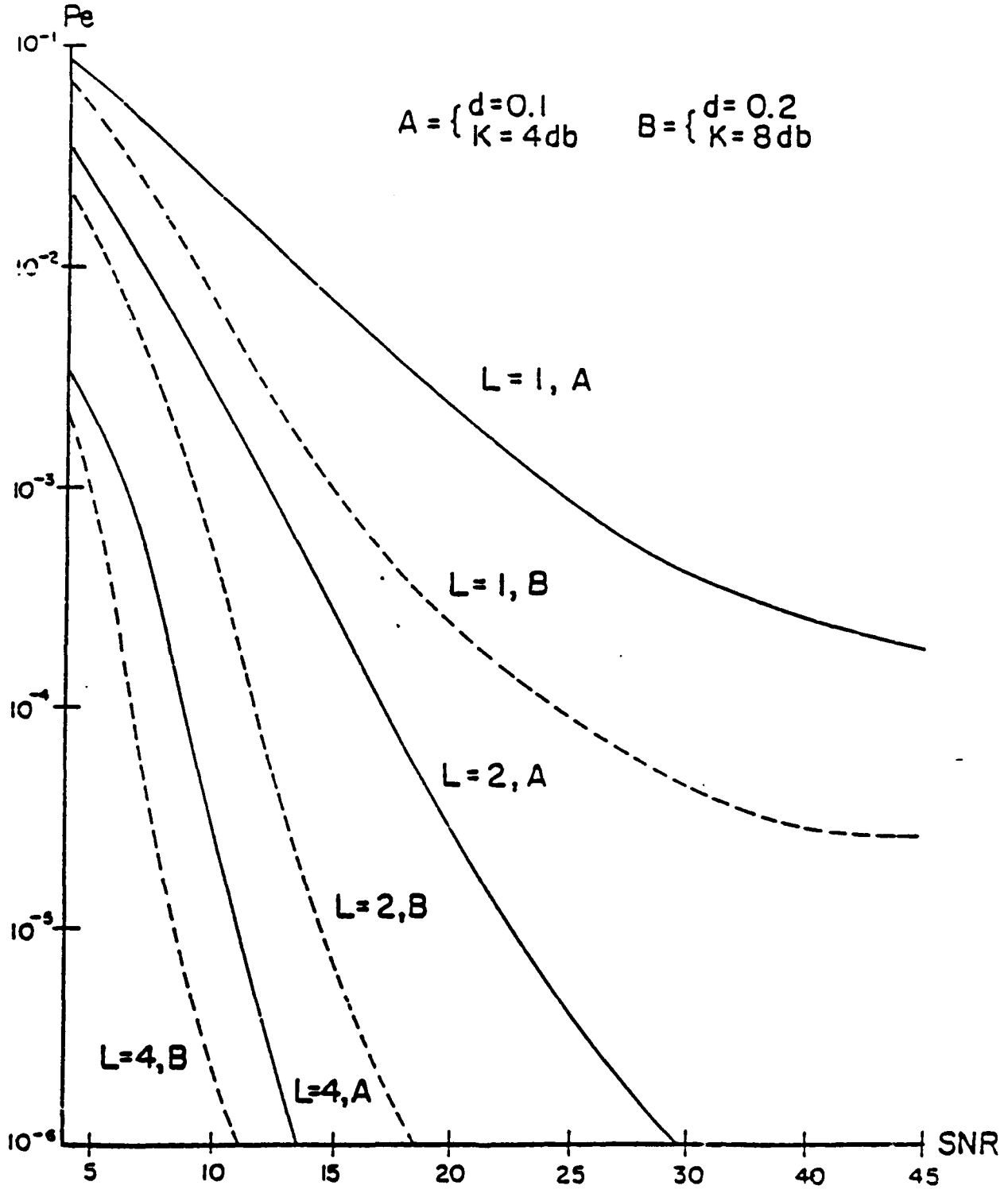

Fig. 1 Probability of Error Vs. Diversity Order Gaussian Delay Spectrum Case

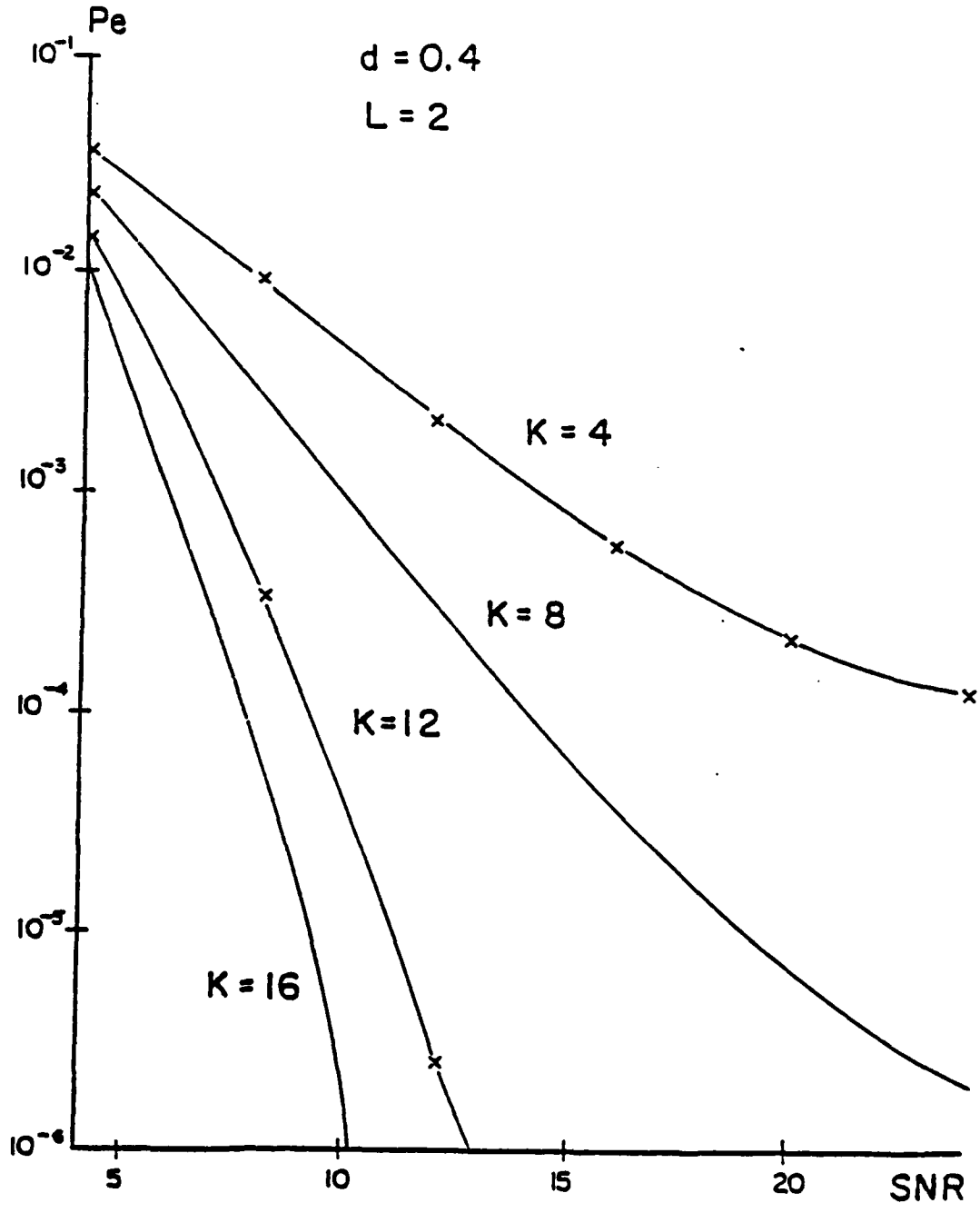

Fig. 2 Probability of Error Vs. Propagation SNR Gaussian Delay Spectrum Case

4. REFERENCES

1. P.J. Huber, "Robust estimation of a location parameter," Ann. Math. Stat., vol. 35, pp. 73-101, 1964.

2. R.D. Martin, "Robust estimation of signal amplitude," IEEE Trans. on Inform. Theory, vol. IT-18, 1972.

3. R.D. Martin and C.J. Masreliez, "Robust estimation via stochastic approximation," IEEE Trans. on Inform. Theory, vol. IT-21, 1975.

4. A.D. Spaulding and D. Middleton, "Optimum reception in an impulsive interface environment, Part I: Coherent detection," IEEE Trans. on Comm., vol. COM-25, pp. 910-923.

5. A.D. Spaulding and D. Middleton, "Optimum reception in an impulsive interface environment, Part II: Incoherent detection," IEEE Trans. on Comm., pp. 924-934, 1977.

6. J. Saks and D. Ylvisaker, "A note on Huber's robust estimation of a location parameter," Ann. Math. Stat., vol. 43, pp. 1068-1075, 1972.

7. R.D. Martin and S.C. Schwartz, "Robust detection of a known signal in nearly Gaussian noise," IEEE Trans. on Inform. Theory, vol. IT-17, pp. 50-56, 1971.

8. J.M. Morris and V.D. VandLinde, "Robust quantization of discrete time signals with independent samples," IEEE Trans. on Comm. vol. COM-22, pp. 1987-1902, 1974.

9. J.M. morris, "The performance of quantizers for a class of noise-corrupted signal source," IEEE Trans. on Comm., vol. COM-24, pp. 184-189, 1976.

10. P. Papantoni-Kazakos, "Robustness in parameter estimation," IEEE Trans. on Inform. Theory, vol. IT-23, pp. 223-231, 1977.

11. F.R. Hampel, "A general qualitative definition of robustness," Ann. Math. Stat., vol. 42, pp. 1887-1896, 1971.

12. P. Papantoni-Kazakos, "The Vasershtein distances as the stability criterion in robust estimation," IEEE Trans. on Inform. Theory, vol. IT-26, pp. 620-625, 1980.

13. H.V. Poor, "Robust decision design using a distance criterion," IEEE Trans. on Inform. Theory, vol. IT-26, pp. 575-587, 1980.

14. M.V. Poor and D. Alexandrou, "A general relationship between two quantizer design criterions," IEEE Trans. on Inform. Theory, vol. IT-26, pp. 210-212, 1980.

15. M.V. Poor and J.B. Thomas, "Application of Ali-Silvey distance measures in the design of generalized quantizers in binary decision systems," IEEE Trans. on Comm., vol. COM-25, pp. 893-900, 1977.

16. M.D. Chadwick and L. Kurz, "Two sequential nonparametric detection procedures," Information and Control, vol. 12, No. 5, pp. 403-428, November 1968.

17. H. Brownstein and L. Kurz, "Parametric and nonparametric detectors based on sequential sample median test," Information and Control, vol. 17, No. 5, pp. 417-435, December 1970.

18. E. Voudouri and L. Kurz, "Sequential robust m-interval polynomial approximation (MIPA) partition detectors, Proc. IEEE Intr. Conf. Acoustics, Speech and Signaling, pp. 611-614, April 1983.

20. R.D. Dwyer and L. Kurz, "Sequential partition detectors with dependent sampling," Journ. of Cybernetics, vol. 10, pp. 211-232, 1980.

21. R.D. Dwyer and L. Kurz, "Sequential partition detectors in large signal and impulsive noise," Proc. 1980 Conf. on Infor. Sc. and Syst., Princeton U., pp. 507-512, March 1980.

22. E. Voudouri and L. Kurz, "Generalized sequential linear rank and partition tests, "Proc. IEEE Int. Conf. on Comm., pp. 1597-1602, June 1983.

23. A. Elrafaie and L. Kurz, "A recursive approach to detection of BPSK in the presence of nonlinearities and Gaussian noise," Proc. Glob. Comm., pp. 1029-1043, November 1983.

24. S. Bendetto and E. Biglieri, "Nonlinear equalization for digital satellite channels," IEEE Journ. Select. Topics in Comm., vol. SAC-1, pp. 46-57, January 1983.

25. T.C. Huang, J.K. Omura and W.C. Lindsey, "Analysis of coherent satellite communication systems in the presence of interference and noise," IEEE Trans. on Comm., vol. COM-29, May 1981.

26. G.F. Herrmann, "Performance of maximum likelihood receiver in the non-linear satellite channel," IEEE Trans. on Comm., vol. COM-25, pp. 633-643, July 1977.

27. E. Voudouri and L. Kurz, "Sequential partially ordered partition detectors," Proc. Glob. Comm., pp. 764-768, November 1984.

28. E. Voudouri and L. Kurz, "Robust sequential m-interval polynomial approximation detectors with dependent sampling," Proc. 19th Annual Conf. on Info. Sciences and Syst., pp. 132-137, March 1985.

29. A. Elrafaie and L. Kurz, "A minimum mean square error equalizer for nonlinear satellite channels", Proc. Glob. Comm. November 1986, also to appear in IEEE Trans. on Comm.

30. D. Malhotra, "Equalization in digital satellite communication systems using robust Kalman filtering," Ph.D. Dissertation, Polytechnic Institute of New York, June 1985.

31. R.F. Dwyer and L. Kurz, "Characterizing partition detectors with stationary and quasi-stationary Markov dependent data," IEEE Trans. on Info. Theory, vol. 32, pp. 471-83, July 1983.

32. B. Jaroszewicz. "M-internal orthogonal polynomial estimators with applications," Ph.D. Dissertation, Polytechnic University, January 1986.

33. T.S. Yoo, "Optimum recursive equalizers for digital satellite channels," Ph.D. Dissertation, Polytechnic University, June 1986.

34. E. Voudouri and L. Kurz, "A class of sequential adaptive detectors for underwater non-gaussian noise environments," IEEE Journal of Oceanic Engineering, Vol. OE-12, No. 1, pp. 38-46, January 1987.

35. G.R. Lomp, "Non-linear robust detection and estimation in dependent noise," Ph.D. Dissertation, Polytechnic University, June 1987.

36. A.F. Elrafaie and L. Kurz, "A minimum mean-square error equalizer for nonlinear satellite channels," IEEE Trans. on Communication, Vol. Com-35, No. 5, pp. 556-560, May 1987.

37. A. Said, A.F. Elrafaie and L. Kurz, "Equalization for QPSK signals over non-linear channels," Proc. Glob. Comm. November 1987. An improved version accepted for publication in the International Journal on Satellite Communications.

38. Kuong-I. Shu, "Performance of Differentially Coherent QPSK systems in Slowly Fading Rician Channels," Ph.D. Dissertation, Polytechnic University, June 1987.

B. A RAISED POWER TEST AND SOME OF ITS APPLICATIONS IN ARRAY SIGNAL PROCESSING

Professor S. Unnikrishna Pillai

Unit IE7-2

1. OBJECTIVES

The problem of estimating the number of systematic (signal) components in data obtained by a collection of spatially deployed sensors, simultaneously exposed to spatially white noise is considered here. A method heretofore proposed, based on the ratio of arithmetic mean to geometric mean of the sample covariance matrix eigenvalues, is reviewed and an alternative based on the higher powers of the eigenvalues is developed. The latter test is found to be applicable in cases where the conditions for the former are not met. Specifically this is used to analyze the performance of a modified spectrum estimator utilizing a covariance matrix raised to a higher power.

2. SUMMARY OF RECENT PROGRESS

One of the important problems in sonar, radar and geological acoustic data processing is that of resolving an unknown number of closely spaced sources from information collected at a set of sensor elements. Several approaches have been reported for solving this and related problems [1-6]. In particular determination of the unknown number of signals, when the additive noise is element to element uncorrelated and of equal variance has been formulated as a sequential hypothesis testing problem [6-8]. Under suitable preprocessing such as spatial smoothing, this test has also been extended to coherent cases [9,10]. A crucial assumption in all these cases is that the number of unknown sources present in the scene is strictly less than the total number of sensor elements used to collect the data. When this is not the case this test would always indicate the number of sources present to be the same as the number of sensor elements, thus making the results meaningless. In

what follows we review this situation and derive an alternate test to estimate the number of sources in that situation. This is made possible by deriving the asymptotic distribution of this new test criterion.

The usefulness of this test to estimate the number of unknown arrivals, is illustrated in section 4. There it is shown that if the source scene is apriori known to consist of point sources in uncorrelated noise of equal variance, then by a 'raised power technique' on the array output covariance matrix, one can achieve the same type of performance as in the case of the so called Multiple Signal Classification (MUSIC) technique developed by Schmidt [4,8]. The advantage here is that this 'raised power technique' avoids the determination of the eigenvectors of the array output covariance matrix and their further partitioning into signal and noise subspaces, thereby eliminating the associated decision errors. The raised power test developed in section 3.1 is used to determine the penalty for raising the covariance matrix to a higher power in this new technique. It is shown that the number of samples used in estimating the covariances have to be increased, as the power to which the matrix is raised is increased. Simulation results are presented to support these conclusions.

3. STATE OF THE ART AND PROGRESS DETAILS

We consider the problem of estimating the number of "systematic" (signal) components present in the data which is measured as an M-component random vector $\underline{x}(t_n); n = 1, 2, \ldots N$. In general the observed data $\underline{x}(t_n)$ have two unobservable random parts.

$$\underline{x}(t_n) = \underline{u}(t_n) + \underline{v}(t_n); \; n = 1, 2, \ldots N \tag{1}$$

Here $\underline{u}(t_n)$ and $\underline{v}(t_n)$ are random vectors with zero mean and covariances given by

$$E[\underline{u}^*(t)\underline{u}^T(t)] = \Sigma \tag{2}$$

and

$$E[\underline{v}^*(t)\underline{v}^T(t)] = \sigma^2 I \tag{3}$$

Usually $\underline{v}(t)$ can be interpreted as composed of errors of measurement: uncorrelated components with equal variances. In those cases where data is received at a set of M sensors, this would correspond to spatially white noise inducing an uncorrelated random component in each sensor of variance σ^2. Similarly $\underline{u}(t)$ can be interpreted as made up of useful signal parts and is supposed to be in a space of dimension K less than M. As a result Σ is of rank K, and the observable covariance matrix $R = \Sigma + \sigma^2 I$, has an eigenvalue σ^2 with multiplicity (M-K).

Many practical situations can be attributed to this model. One of its uses is in exploratory studies, where the observer is interested in reducing the vast amount of available measurements. Another interesting area of application is in modern radar and sonar problems where a set of sensors is used to collect data from spatially distributed targets. There, the above model would correspond to the situation where M sensor elements are used to receive signals from K not totally coherent point sources in the presence of spatially uncorrelated noise of equal variance σ^2.

In applications where one makes use of eigenvectors associated with the systematic part (unequal eigenvalue part) and the noise part (those corresponding to the equal eigenvalue σ^2) separately, it is necessary to partition the eigenvectors, and hence the eigenvalues, into two groups: those belonging to the systematic or unequal part and those belonging to the equal one. This partitioning is trivial, given the ensemble-averaged covariance matrix R. However, when only an estimate $\hat{R}$ of R such as

$$\hat{R} = \frac{1}{N}\sum_{n=1}^{N} \underline{x}^*(t_n)\underline{x}^T(t_n) \tag{4}$$

is available, this is no longer a trivial problem since with probability 1, none of its eigenvalues will be equal [11]. Statistical tests, based on the asymptotic multivariate Gaussian

nature of the eigenvalues, have been devised for the real case by Anderson [12], Lawley [13], and others [14], to estimate the number of equal eigenvalues with a certain confidence level. Similar results for the complex case are reported in [15, 16]. Specifically with $\underline{u}(t)$ and $\underline{v}(t)$ as complex Gaussian random processes and $\hat{R}$ as in (4), its eigenvalue-decomposition would give

$$\hat{R} = \hat{U}\hat{\Lambda}\hat{U}^{\dagger} \tag{5}$$

where ($\dagger$ stands for complex conjugate transpose)

$$\hat{U} = [\underline{\hat{u}}_1, \underline{\hat{u}}_2, \ldots \underline{\hat{u}}_M] \tag{6}$$

and

$$\hat{\Lambda} = \begin{bmatrix} \ell_1 & 0 & \ldots & 0 \\ 0 & \ell_2 & \ldots & 0 \\ \vdots & \vdots & \ddots & \vdots \\ 0 & 0 & \ldots & \ell_M \end{bmatrix} \tag{7}$$

Here $\underline{\hat{u}}_1, \underline{\hat{u}}_2, \ldots \underline{\hat{u}}_M$, are the M orthonormal eigenvectors and $\ell_1, \ell_2, \ldots \ell_M$, are the corresponding real eigenvalues of $\hat{R}$. A test criterion for the equality of the (M-K) lowest eigenvalues in the complex case has been shown to be [16]

$$\delta_K(\underline{\ell}) = \left(\frac{1}{M-K}\sum_{i=K+1}^{M} \ell_i\right) \Big/ \left(\prod_{i=K+1}^{M} \ell_i\right)^{\frac{1}{M-K}} \tag{8}$$

which is the ratio of the arithmetic mean to the geometric mean of the corresponding sample eigenvalues. Using an asymptotic analysis, it can be shown that

$$N(M-K)\ell n\delta_K(\underline{\ell}) \sim \chi^2(d) \tag{9}$$

where

$$d = (M-K)^2 - 1 \tag{10}$$

represents the degrees of freedom associated with the χ^2 random variable in (9). This will allow one to examine the equality of the lowest (M-K) eigenvalues by computing

$2N(M-K)\ell n\delta_K(\underline{\ell})$ and accepting the hypothesis if it is less than the upper-tail significance point of the appropriate χ^2 distribution for some suitable significance level α. The test will proceed with K=1,2,... and the first value of K for which the test succeeds is taken as the estimate for K[7,8,9]. Clearly the test is meaningful only if $K < M$, i,e; so long as the number of targets is less than the number of sensor elements.

In what follows we derive an alternate test based on higher powers of the eigenvalues and derive its asymptotic distribution. The usefulness of this test is briefly discussed in section 4 for a specific application where the conventional test based on (9) turns out to be inappropriate.

A. A Raised Power Test and Its Statistics

With symbols as defined above and $\lambda_1, \lambda_2, \ldots \lambda_M$ representing the roots of R, the hypothesis H_K under test is $\lambda_{K+1} = \lambda_{K+2} = \ldots = \lambda_M$. The required criterion for the equality of the (M-K) lowest eigenvalues of $\hat{R}$, based on their p^{th} powers would be

$$\begin{aligned}\Delta_K(\underline{\ell}, p) &= \left[\left(\frac{1}{M-K}\sum_{i=K+1}^{M}\ell_i^p\right)\Big/\left(\prod_{i=K+1}^{M}\ell_i^p\right)^{\frac{1}{M-K}}\right]^{\frac{1}{p}} \\ &= \left(\frac{1}{M-K}\sum_{i=K+1}^{M}\ell_i^p\right)^{\frac{1}{p}}\Big/\left(\prod_{i=K+1}^{M}\ell_i\right)^{\frac{1}{M-K}}\end{aligned} \tag{11}$$

We will show that

$$\frac{2N(M-K)}{p}\ell n\Delta_K(\underline{\ell}, p) \sim \chi^2(d) \tag{12}$$

where d is as defined in (10).

Proof

Following Anderson [17], define

$$d_i = \sqrt{N}(\ell_i - \lambda_{K+1})\ ;\ i = K+1, \ldots M \tag{13}$$

This gives

$$\ell_i = N^{-1/2}d_i + \lambda_{K+1} \tag{14}$$

With (11) and (14) in (12) we have

$$\frac{2N(M-K)}{p}\ell n\Delta_K(\underline{\ell},p) = \frac{N}{p}\left[\frac{(M-K)}{p}\ell n\left\{\frac{1}{M-K}\sum_{i=K+1}^{M}\left(1+\frac{N^{-1/2}d_i}{\lambda_{K+1}}\right)^p\right\}\right.$$
$$\left. - \sum_{i=K+1}^{K}\ell n\left(1+\frac{N^{-1/2}d_i}{\lambda_{K+1}}\right)\right]$$
$$\doteq \frac{N}{p}\left[\frac{(M-K)}{p}\ell n\left\{\frac{1}{M-K}\sum_{i=K+1}^{M}\left(1+\frac{pd_i}{N^{1/2}\lambda_{K+1}}+\frac{p(p-1)d_i^2}{2N\lambda_{K+1}^2}+\ldots\right)\right\}\right.$$
$$\left. - \sum_{i=K+1}^{M}\left(\frac{d_i}{N^{1/2}\lambda_{K+1}}-\frac{d_i^2}{2N\lambda_{K+1}^2}+\ldots\right)\right]$$
$$= \frac{N}{p}\left[\frac{(M-K)}{p}\ell n\left\{1+\left(\frac{p\sum d_i}{N^{1/2}(M-K)\lambda_{K+1}}+\frac{p(p-1)\sum d_i^2}{2N(M-K)\lambda_{K+1}^2}+\ldots\right)\right\}\right.$$
$$\left. - \frac{\sum d_i}{N^{1/2}\lambda_{K+1}}+\frac{\sum d_i^2}{2N\lambda_{K+1}^2}+\ldots\right]$$
$$= \frac{N}{p}\left[\frac{(M-K)}{p}\left(\frac{p\sum d_i}{N^{1/2}(M-K)\lambda_{K+1}}+\frac{p(p-1)\sum d_i^2}{2N(M-K)\lambda_{K+1}^2}\right.\right.$$
$$\left.\left. - \frac{p^2(\sum d_i)^2}{2N(M-K)^2\lambda_{K+1}^2}+\ldots\right)-\frac{\sum d_i}{N^{1/2}\lambda_{K+1}}+\frac{\sum d_i^2}{2N\lambda_{K+1}^2}+\ldots\right]$$
$$= \frac{1}{\lambda_{K+1}^2}\left[\sum_{i=K+1}^{M}d_i^2-\left(\frac{1}{M-K}\right)\left(\sum_{i=K+1}^{M}d_i\right)^2\right]+O_p(1) \qquad (15)$$

It can be shown that the limiting distribution of $d_{K+1}, d_{K+2}, \ldots d_M$, is the same as the distribution of the eigenvalues of a hermitian matrix $U_{22} = (u_{ij}), i,j = K+1, K+2, \ldots M$. Further, for circular Gaussian data [18] elements of U_{22} are asymptotically independent, identically distributed, zero mean random variables with common variance λ_{K+1}^2. Then it follows that (15) has the limiting distribution of

$$= \frac{1}{\lambda_{K+1}^2}\left[tr(U_{22}^2) - \left(\frac{1}{M-K}\right)\left(tr(U_{22})\right)^2\right]$$
$$= \frac{1}{\lambda_{K+1}^2}\left[tr\left(U_{22}U_{22}^{\dagger}\right) - \left(\frac{1}{M-K}\right)\left(tr(U_{22})\right)^2\right]$$
$$= \frac{1}{\lambda_{K+1}^2}\left[\left(\sum_{i\neq j}|u_{ij}|^2 + \sum_{i=K+1}^{M} u_{ii}^2\right) - \left(\frac{1}{M-K}\right)\left(\sum_{i=K+1}^{M} u_{ii}\right)^2\right]$$
$$= \frac{1}{\lambda_{K+1}^2}\sum_{i\neq j}|u_{ij}|^2 + \frac{1}{\lambda_{K+1}^2}\left[\sum_{i=K+1}^{M} u_{ii}^2 - \left(\frac{1}{M-K}\right)\left(\sum_{i=K+1}^{M} u_{ii}\right)^2\right] \qquad (16)$$

Thus $(\sum_{i\neq j}|u_{ij}|^2)/\lambda_{K+1}^2$ is asymptotically χ^2 with (M-K)(M-K-1) degrees of freedom; independently, $[\sum_i u_{ii}^2 - (\sum_i u_{ii})^2/(M-K)]/\lambda_{K+1}^2$ is asymptotically χ^2 with (M-K-1) degrees of freedom. Thus (15) has a limiting χ^2 distribution with $[(M-K)^2-1]$ degrees of freedom and hence

$$\frac{2N(M-K)}{p}\ell n\Delta_K(\underline{\ell}, p) \sim \chi^2(d) \qquad (17)$$

where d is as in (10). This completes the proof. On comparing (8) and (17) it now follows that the effect of raising the eigenvalues to a higher power p is to reduce the effective number of samples by a factor of p.

4. AN APPLICATION FROM ARRAY SIGNAL PROCESSING

We illustrate the usefulness of the above test with an example from sensor array signal processing [19]. The objective in array signal processing is to estimate the number of targets and their associated parameters such as angles of arrival, power levels etc. by making use of the data available at the sensor element outputs. The Maximum Likelihood Method (MLM) of spatial spectrum estimation is one of the earliest superresolution techniques proposed [20], and is still today an important tool for estimating directions of multiple signal arrivals. The MLM requires the inverse of the matrix of covariances obtained between all array element pairs. This is then scanned by a pointing vector to give an estimate of power vs. pointing angle. The maxima of this function are then used as estimates of arrival angles. More recently, elegant techniques based on a vector space decomposition of

the covariance matrix have been developed [4,8] which give results superior to those of the MLM. In particular, the resolution capability of the MLM deteriorates with decreasing signal to noise ratios (SNR). Furthermore, estimates of arrival angle for sources closely spaced in angle tend to be more biased under such conditions, even when obtained with a perfectly estimated covariance matrix. On the other hand, with a perfectly estimated covariance matrix, the vector space methods always give unbiased estimates even when the source directions are only infinitesimally apart and have superior resolvability compared to the MLM-estimator.

To understand the superior performance of the vector space spectral estimators, consider the array processing problem described above where an M element array located at $\underline{d}_1, \underline{d}_2, \ldots \underline{d}_M$, with respect to some frame of reference, receives signals from K narrowband sources which arrive as plane waves with wave vectors $\underline{\nu}_1, \underline{\nu}_2, \ldots \underline{\nu}_K$ in that frame. Let the k^{th} arrival at the origin be denoted $s_k(t); k = 1, 2, \ldots K$. Then the i^{th} element output $x_i(t)$ at time t can be written as [8]

$$x_i(t) = \sum_{k=1}^{K} s_k(t)\ e^{-j(\underline{d}_i \cdot \underline{\nu}_k / c)} + n_i(t) \tag{18}$$

where c represents the speed of propagation in the medium and $n_i(t)$ stands for additive noise which we will take to be uncorrelated from element to element and of equal variance, N_0. In vector form (18) becomes

$$\underline{x}(t) = A^{\bullet}\ \underline{s}(t) + \underline{n}(t) \tag{19}$$

where

$$\underline{x}(t) = [x_1(t),\ x_2(t), \ldots\ x_M(t)]^T \tag{20.a}$$

$$\underline{s}(t) = [s_1(t),\ s_2(t), \ldots\ s_K(t)]^T \tag{20.b}$$

and

$$\underline{n}(t) = [n_1(t),\ n_2(t), \ldots\ n_M(t)]^T \tag{20.c}$$

Here T stands for the transpose and * represents complex conjugation. Further,

$$A = [\underline{S}(\underline{\nu}_1),\ \underline{S}(\underline{\nu}_2), \ldots\ \underline{S}(\underline{\nu}_K)] \tag{21}$$

is an MxK matrix consisting of signal direction vectors given by

$$\underline{S}(\underline{\nu}_k) = [e^{j(\underline{d}_1 \cdot \underline{\nu}_k/c)}, e^{j(\underline{d}_2 \cdot \underline{\nu}_k/c)}, \ldots,\ e^{j(\underline{d}_M \cdot \underline{\nu}_k/c)}]^T \tag{22}$$

The correlation matrix of the received signal vector $\underline{x}(t)$ is then an MxM matrix,

$$R = E[\underline{x}^*(t)\underline{x}^T(t)] = AR_{SS}A^\dagger + N_0 I \tag{23}$$

where $R_{SS} = E[\underline{s}^*(t)\underline{s}^T(t)]$ represents the KxK source correlation matrix and † denotes complex conjugate transpose.

When the sources are not completely correlated, $AR_{SS}A^\dagger$ will be of rank K and hence the lowest eigenvalue of R, which will equal N_0 will repeat (M-K) times. Letting $\underline{e}_i$, $i = K+1,\ K+2,\ \ldots M$, represent the normalized eigenvectors, corresponding to the (M-K) repeated eigenvalue, we get

$$R\underline{e}_i = (AR_{SS}A^\dagger + N_0 I)\underline{e}_i = N_0\underline{e}_i \tag{24.a}$$

which implies

$$A^\dagger \underline{e}_i = 0 \tag{24.b}$$

or equivalently

$$\underline{S}^\dagger(\underline{\nu}_k)\underline{e}_i = 0;\ \text{for all i } = K+1, K+2, \ldots M \text{ and } k = 1, 2, \ldots K \tag{25}$$

Thus the K signal direction vectors are orthogonal to the subspace spanned by the noise eigenvectors. This is the basis for the MUSIC estimator $P_{MU}(\underline{\nu})$ proposed by Schmidt [21] where

$$P_{MU}(\underline{\nu}) = \frac{1}{|[\underline{e}_{K+1},\ \underline{e}_{K+2}, \cdots\ \underline{e}_M]^\dagger\ \underline{S}(\underline{\nu})|^2} \tag{26}$$

This however can be rewritten as

$$\frac{1}{P_{MU}(\underline{\nu})} = (U^{\dagger}\underline{S}(\underline{\nu}))^{\dagger} \begin{bmatrix} 0 & & & \underline{0} \\ & \ddots & & \\ & & 0 & \\ & & & 1 \\ \underline{0} & & & \ddots \\ & & & & 1 \end{bmatrix} U^{\dagger}\underline{S}(\underline{\nu}) \tag{27}$$

where U is the modal matrix of R. Using (24) and (25) we see that $U^{\dagger}\underline{S}(\underline{\nu})$ results in a set of new direction vectors, which for true directions of arrival $\underline{\nu}_k; k = 1, 2 \ldots K$, would span the same subspace as the one spanned by the eigenvectors corresponding to the K largest eigenvalues (signal subspace eigenvectors) and from this it follows that $1/P_{MU}(\underline{\nu})$ given by (27) equals zero iff $\underline{\nu} \in \{\underline{\nu}_1, \underline{\nu}_2 \ldots \underline{\nu}_K\}$.

Within this framework the Maximum Likelihood spectrum estimator of Capon can be written as [20]

$$P(\underline{\nu}) = \frac{1}{\underline{S}^{\dagger}(\underline{\nu})R^{-1}\underline{S}(\underline{\nu})} \tag{28}$$

Using similar manipulations as in (27) we have

$$\frac{1}{P(\underline{\nu})} = \frac{(U^{\dagger}\underline{S}(\underline{\nu}))^{\dagger}}{N_0} \begin{bmatrix} \mu_1 & & & \underline{0} \\ & \mu_2 & & \\ & & \ddots & \\ & & & \mu_K \\ & & & & 1 \\ \underline{0} & & & & \ddots \\ & & & & & 1 \end{bmatrix} U^{\dagger}\underline{S}(\underline{\nu}) \tag{29}$$

where

$$\mu_k = \frac{1}{1 + \lambda_k/N_0} > 0; \quad k = 1, 2, \ldots K \tag{30}$$

As before U is the modal matrix of R (or $AR_{SS}A^{\dagger}$) and λ_i is the i^{th} non zero-eigenvalue of the noiseless part ($AR_{SS}A^{\dagger}$) of R. Note that positive definiteness of the signal correlation matrix implies that $\lambda_i > 0$ and hence $\mu_i < 1$ for all $i = 1, 2, \ldots K$.

The improvement in performance in terms of resolution for the MLM spectrum estimator will increase in SNR is well known [21,22]. To see this, note that the reason for the inferior resolvability for MLM($\underline{\nu}$), as compared to $P_{MU}(\underline{\nu})$, is because of the full rank diagonal matrix in (29). The quantity of interest there (as a function of SNR) is μ_k as given by (30). As increases in the SNR would result in increased values of the $\lambda_k s$, the μ_k's would, in turn, decrease. For large SNR's, $\mu_k \to 0$, $k = 1, 2, \ldots K$, and from (27) and (29) it follows that MLM spectrum approaches the one obtained by MUSIC method.

This, however, raises the following question:

In the presence of a multiple-source scenario, can the MLM spectral estimator be modified, without sacrificing its simplicity, such that the modified spectral estimator would tend to attain the superior properties of the vector space spectral estimators such as MUSIC? A comparison between (27) and (29) shows that, they differ (barring N_0) only because of the nonzero values of μ_k, $k = 1, 2, \ldots K$, appearing in (29). Thus for true direction vectors, whereas MUSIC is able to satisfy the requirement of zero norm in the quadratic product (27) exactly, the MLM is only able to do this approximately. Hence the degradation in performance for MLM due to the nonzero values of μ_k can be eliminated by suitably modifying it so as to drive the equivalent $\mu_k' s$ to zero. This can, in fact be achieved by modifying the MLM estimator as

$$P_p(\underline{\nu}) = \frac{1}{\underline{S}^\dagger(\underline{\nu}) R^{-p} \underline{S}(\underline{\nu})} \tag{31}$$

where p is some positive number greater than one. As in (29) it can be shown that

$$\frac{1}{P_p(\underline{\nu})} = N_0^{-p} (U^\dagger \underline{S}(\underline{\nu}))^\dagger \begin{bmatrix} \mu_1^p & & & & & \\ & \mu_2^p & & & \underline{0} & \\ & & \ddots & & & \\ & & & \mu_K^p & & \\ & & & & 1 & \\ \underline{0} & & & & & \ddots \\ & & & & & & 1 \end{bmatrix} U^\dagger \underline{S}(\underline{\nu}) \tag{32}$$

Since $0 < \mu_k < 1$ for all $k = 1, 2, \ldots K$, $\mu_k^p \rightarrow 0$ as $p \rightarrow \infty$ for all k. Thus asymptotically, the modified spectral estimator given by (31) would approach (26) and hence would have all the desirable properties of the vector space spectral estimators. We note that this result is independent of SNR and hence, in particular, is true at low SNRs also.

We remark that the modification suggested here is different from that introduced by Pisarenko in connection with estimating spectra by means of nonlinear functions of the covariance matrix [23]. He proves that for a spatially stationary field, $\tilde{P}_N(\underline{\nu})$, given by

$$\tilde{P}_N(\underline{\nu}) = (\underline{S}^\dagger(\underline{\nu}) R^N \underline{S}(\underline{\nu}))^{1/N} \tag{33}$$

converges in probability to the true spectra under some mild conditions (See corollary after remark 4 in [23]). This also follows from a general result known in spectral theory (See Th.3.3.3 in Kadison and Ringrose [24]), which states that for a bounded operator A

$$\text{As } N \rightarrow \infty, \quad ||A^N||^{1/N} \quad \textit{has a limit.} \tag{34.a}$$

This limit is known as the spectral radius. Note that (33) follows from (34.a) by defining the norm of A to be

$$||A|| = \underline{S}^\dagger(\underline{\nu}) A \underline{S}(\underline{\nu}) \tag{34.b}$$

and substituting R for A in (34.b).

However the modification suggested in (31) discretizes the spectrum and is valid even for spatially nonstationary situations such as correlated arrivals. To see this note that as $p \rightarrow \infty$, equation (32) represents the length of the direction vector $\underline{S}(\underline{\nu})$ projected onto the subspace spanned by the minimal eigenvector(s) (corresponding to the lowest eigenvalue). Using (24) and (25), this length (after projection) will be zero only for those distinct direction vectors corresponding to actual targets whose total number is less than the number of array elements. As a result the limiting spectrum in (31) will consist of a set of impulses representing those distinct direction vectors. Further from the arguments following (32), it is clear that the spectrum so obtained corresponds to the true spectrum

only when the data itself represents point sources and thus the modified MLM estimator in (31) is asymptotically optimal for a point source scenario.

When the ensemble averaged values of covariances are known, the value of p to which the covariance matrix R is raised can be arbitrarily large. In that case p has the same effect on all (M-K) diagonal entries in (32) corresponding to the noise subspace part and hence can take any value. However, when only an estimate $\hat{R}$ of the covariance matrix is known, as mentioned before, the probability of any two of its eigenvalues being equal is zero [11], and as a result p will have a different effect on those entries corresponding to the noise subspace part.

The question about the choice for the value of p to which the matrix $\hat{R}$ may be raised can however be readily answered by making use of the asymptotic result developed in section 3. It is shown there that, when $\hat{R}$ is estimated using N samples, the result of raising its eigenvalues to a higher power p in an algorithm is to reduce the effective number of samples in averaging to N/p. Since $\hat{R}$ is hermitian, the effect of raising it to a higher power p is identical to replacing its eigenvalues $l_1, l_2, \ldots l_M$, by $l_1^p, l_2^p, \ldots l_M^p$, and hence from the above discussion it now follows that when $\hat{R}$ is made use of in a spectrum estimation algorithm, as in (31), it is necessary to increase the number of samples used in averaging by a factor of p.

This observation is also supported by simulation results shown in Fig. 1 and Fig. 2. There a four element aperiodic array receives signals from two sources located along 85° and 94° with respect to the line of the array. The SNR in each case is taken to be 7.5 dB and 6 dB respectively. Fig. 1.a shows the spectrum obtained by the MUSIC method where 25 samples are used in averaging $\hat{R}$. The corresponding MLM spectrum is shown in Fig. 1.b. The same covariance matrix is raised to the fourth power to compute the modified MLM spectrum given by (31) and this is shown in Fig. 2.b. As before the targets are barely resolvable here. As required by the asymptotic result in section 3, the number of samples used in averaging $\hat{R}$ is increased to 100 for performance comparable to the MUSIC

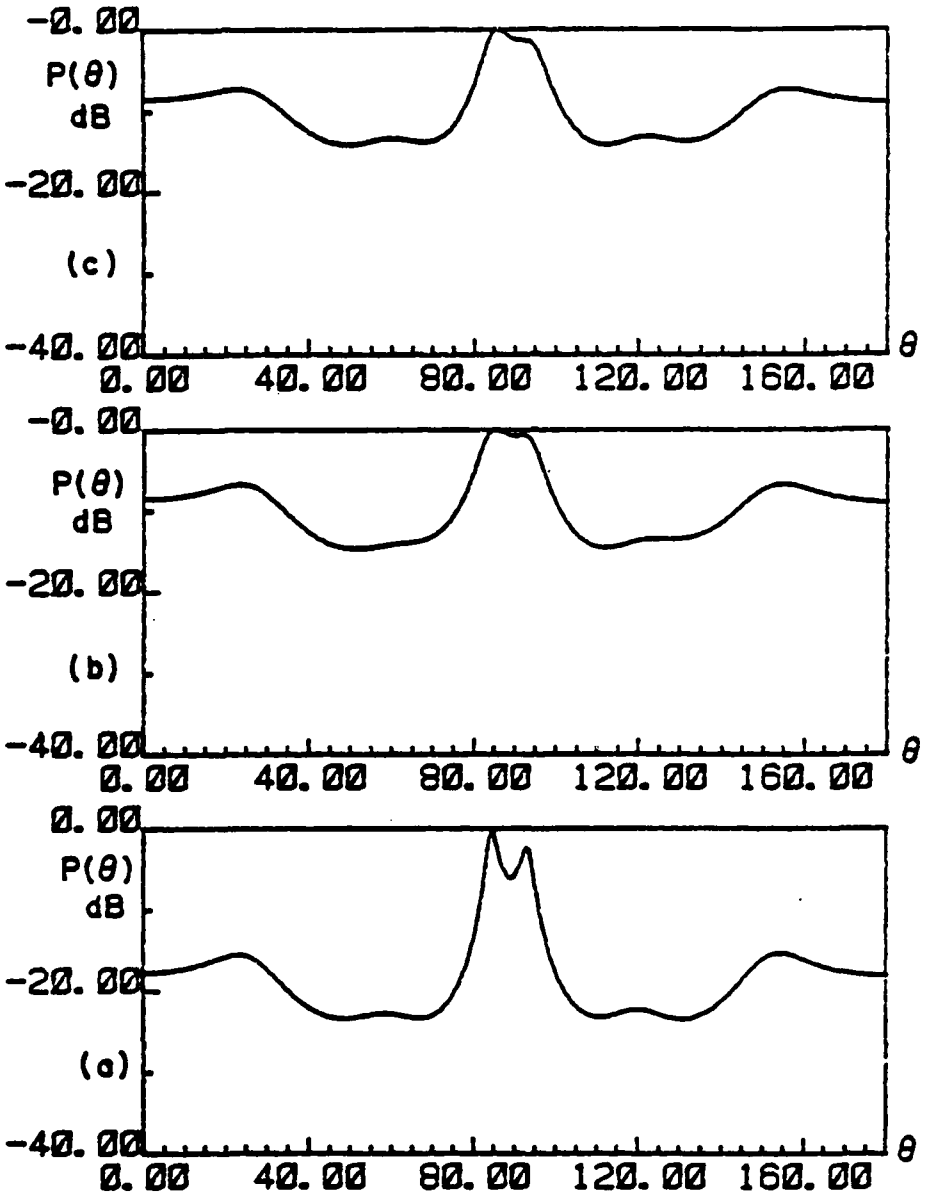

Fig.1 Effect of the number of samples used in averaging on the Spatial Spectrum. A four element aperiodic array with element locations 0,2.1,4.3 and 5.8 (half wavelenghts) receives signals from two sources located along 85° and 94° with SNRs 7.5 dB, 6dB respectively. (a) The MUSIC estimator using 25 samples in averaging $\hat{R}$. (b) The Capon estimator with 25 samples. (c) The Capon estimator with 100 samples.

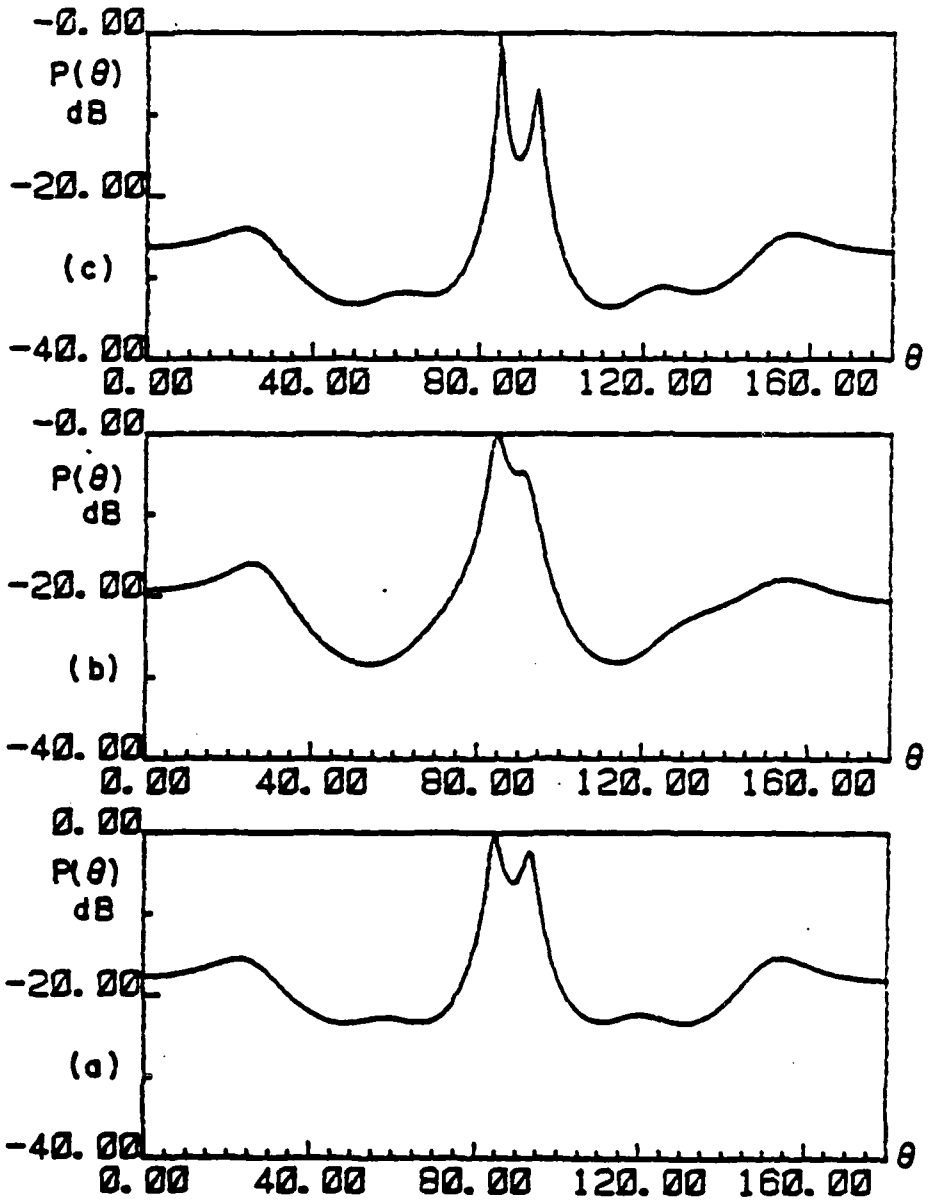

Fig.2 Effect of raising the sample covariance matrix to a higher power on the spatial spectrum. Details are as in Fig.1. (a) The MUSIC estimator with 25 samples. (b) The Modified Capon estimator with 25 samples and p = 4 (See (31)). (c) The Modified Capon estimator with 100 samples and p = 4.

estimator and the spectrum recomputed using (31) is shown in Fig. 2.c. The improvement in performance, obtained with increasing the number of samples used in averaging and then raising the covariance matrix to a higher power prior to computing the spectrum can be seen by comparing Fig. 1.c and Fig. 2.c.

We have seen that by raising the covariance matrix to a higher power it is possible to realize spectrum estimators with performance levels comparable to those that make use of eigenvectors of the covariance matrix in their algorithm. Although there is an advantage in not performing such an eigenvalue-eigenvector analysis here, the disadvantage lies in the larger number of actual samples required in estimating the covariances.

In the context of estimating the number of signal (systematic) components from noisy observations at an array of sensor elements, a new test, that is based on higher powers of the eigenvalues of the array output sample covariance matrix is developed. This is then used in analyzing the degradation in performance of a modified spectrum estimator which makes use of higher powers of the covariance matrix in estimating the arrival angles of the point sources in the scene. For comparable performance as in the conventional method, the modified method is shown to require larger number of data samples in estimating the interelement correlations.

5. REFERENCES

1. M. Wax and T. Kailath, "Optimum Localization of Multiple Sources by Passive Arrays," *IEEE Trans. Acoust., Speech, Signal Processing*, vol. ASSP-31, pp. 1210-1218, Oct. 1983.

2. R.N McDonough, "Application of the Maximum-Likelihood Method and the Maximum-Entropy Method to Array Processing," in *Nonlinear Methods of Spectral Analysis*. S. Haykin, Ed., Springer-Verlag, 1983, Ch. 6.

3. S.W. Lang and J.H. McClellan, "Frequency Estimation with Maximum Entropy Spectral Estimators," *IEEE Trans. Acoust., Speech, Signal Processing*, vol. ASSP-28, pp. 716-724, 1980.

4. R.O. Schmidt, "Multiple Emitter Location and Signal Parameter Estimation," in *Proc. RADC Spectrum Estimation Workshop*, pp. 243-258, Oct. 1979.

5. D.H. Johnson, "The Application of Spectral Estimation Methods to Bearing Estimation Problems," *Proc. IEEE*, vol. 70, no. 9, pp. 1018-1028, 1982.

6. D.W. Tufts and R.Kumaresan, "Estimation of Frequencies of Multiple Sinusoids: Making Linear Prediction Perform Like Maximum Likelihood," *Proc. IEEE*, vol. 70, no. 9, pp. 975-989, 1982.

7. D.N. Simkins, "Multichannel Angle of Arrival Estimation," *Ph.D. Dissertation*, Stanford University, Stanford, CA, 1980.

8. R.O. Schmidt, "A Signal Subspace Approach to Emitter Location and Spectral Estimation," *Ph.D. Dissertation*, Stanford University, California, Nov. 1981.

9. G. Bienvenu and L. Kopp, "Optimality of High Resolution Array Processing Using the Eigensystem Approach," *IEEE Trans. Acoust., Speech, Signal Processing*, vol. ASSP-31, pp. 1235-1248, Oct. 1983.

10. A.M. Bruckstein, T.J. Shan and T. Kailath, "The Resolution of Overlapping Echos," *IEEE Trans. Acoust., Speech, Signal Processing*, vol. ASSP-33, no. 6, pp. 1357-1367, Dec. 1985.

11. M. Okamato, "Distinctness of the Eigenvalues of a Quadratic Form in a Multivariate Sample," *Annals of Statistics*, 1, pp. 763-765, 1973.

12. T. W. Anderson, "Asymptotic Theory for Principal Component Analysis," *Ann. Math. Stat.* 34, pp. 122-148, 1963.

13. D.N. Lawley, "Estimation in Fact Analysis under Various Initial Assumptions," *British Journal of Statistical Psychology*, II, pp. 1-12, 1958.

14. S.N. Roy, *Some Aspects of Multivariate Analysis.* John Wiley and Sons, New York, 1957.

15. D.R. Cox and D.V. Hinkley, *Theoretical Statistics.* Chapman and Hall, London, England, 1974.

16. K.V. Mardia, J.T. Kent and J.M. Bibby, *Multivariate Analysis.* Academic Press, 1979.

17. T.W. Anderson, *An Introduction to Multivariate Statistical Arrays.* John Wiley and Sons, 1976.

18. I.S. Reed, "On a Moment Theorem for Complex Gaussian Processes," IRE Trans. Inform. Theory, pp. 194-195, Apr. 1962.

19. R.A. Monzingo and T.W. Miller, *Introduction to Adaptive Arrays.* John Wiley and Sons, 1976.

20. J. Capon, "High Resolution Frequency Wavenumber Spectrum Analysis," *Proc. IEEE*, vol. 57, no. 8, pp. 1408-1418, 1969.

21. S.M. Kay and S.L. Marple, Jr., "Spectrum Analysis - A Modern Perspective," *Proc. IEEE*, vol. 69, no. 11, pp. 1380-1419, 1981.

22. R.T. Lacoss, "Data Adaptive Spectral Analysis Methods," *Geophysics*, vol. 36, pp. 661-675, Aug. 1971.

23. V.F. Pisarenko, "On the Estimation of Spectra by Means of Nonlinear Functions of the Covariance Matrix," *Geophys. J. Roy. Astronomical Soc.*, vol. 28, pp. 511-531, 1972.

24. R.V. Kadison and J.R. Ringrose, *Fundamentals of the Theory of Operator Algebras.* vol. 1, Ch. 2, pp. 85-87, Academic Press, 1983.

END

DATE

FILMED

9-88

DTIC